UNIVERSITY OF SASSARI

PH.D. SCHOOL IN NATURAL SCIENCE

Dissertation for the Degree of Doctor of Philosophy in
Science and Technology of minerals and rocks of industrial interest
presented at Sassari University in 2012

XXV CYCLE

Integrated Geophysical Methods applied to some Archaeological sites of north Sardinia

DIRECTOR: PROF. MARCO CURINI GALLETTI

COORDINATOR: PROF. GIACOMO OGGIANO

TUTOR:
DR. PAOLA MAMELI

PH.D. STUDENT:
DR. VALERIA TESTONE

INDEX

Abstract

This study deals with the employment of a multimethod geophysical survey, electrical (Electrical Resistivity Tomography) and electromagnetical (Ground Penetrating Radar) carried out on two archaeological sites near shore archaeological sites.

For this purpose the settlements of Sant'Imbenia (Alghero, SS) and Santa Filitica (Sorso, SS), two Roman villas located in northern Sardinia were considered.

The focus of the paper is to assess as the geophysical response of different instruments might be impacted by different moisture conditions and archaeological contexts.

The electromagnetic surveys were conducted in reflection mode, using a monostatic GPR, working simultaneously by two transmitters (frequency of 200 and 600 MHz) and two receivers, while the electrical surveying was conducted with a Terrameter SAS 1000 device combined with ES 10-64 electrode selector.

The 2D and 3D high-resolution models revealed a distribution of shallow anomalies that indicate the presence of buried structures (walls and filled cavities) in the surveyed areas.

A comparison of the results was made, checking the relative merits and demerits of the different techniques in the two coastal archaeological sites.

The integration of geophysical methods has provided useful information to design a more efficient plan for further archaeological excavations.

Key Words: Archaelogical site, Electrical Resistivity Tomography, Ground Penetrating Radar, Sant'Imbenia Roman villa, Santa Filitica archaeological complex.

Riassunto

Questo studio tratta i risultati di un indagine geofisica multimetodo, elettrica (Tomografie Elettriche di Resistività) ed elettromagnetica (Ground Penetrating Radar) condotta in due siti archeologici prossimi alla costa.

Per questo scopo sono state considerati gli insediamenti di Sant'Imbenia (Alghero, SS) e Santa Filitica (Sorso, SS), due ville Romane localizzate nella Sardegna settentrionale.

In particolare, lo scopo di questo lavoro è valutare come la risposta geofisica di differenti strumenti può essere influenzata da differenti condizioni di saturazione oltre che dal contesto archeologico.

Le indagini elettromagnetiche sono state condotte in modalità di riflessione utilizzando un GPR monostatico, operante simultaneamente mediante due trasmettitori (frequenza da 200 e 600 MHz) e due ricevitori, mentre l'indagine geoelettrica è stata eseguita con un georesistivimetro Terrameter SAS 1000 combinato con un selezionatore di elettrodi ES 10-64.

I modelli 2D e 3D ad alta risoluzione hanno rivelato una distribuzione di anomalie superficiali che indicano la presenza di differenti tipi di strutture sepolte (muri e cavità riempite) nelle aree investigate.

I risultati sono stati comparati, verificando le potenzialità e i limiti delle tecniche nei due differenti siti archeologici costieri.

L'integrazione dei metodi geofisici ha fornito utili informazioni per la progettazione di un efficiente piano per ulteriori scavi archeologici.

Parole chiave: Sito archeologico, Tomografie di resistività elettrica, Ground Penetrating Radar, villa Romana di Sant'Imbenia, complesso archeologico di Santa Filitica.

Introduction

Fast and effective methods for studying the physical characteristics of subsoil are particularly helped in detecting natural or artificial bodies and buried structures, to assess the lithological variation in horizontal and vertical directions and to monitor the variations, as a function of time, of the subsoil parameters.

The archaeological research a preliminary knowledge of sites worthy of investigations according to the information of the archaeologists is essential for correct planning of the investigations.

In fact the geophysical techniques, by offering a non-invasive high-resolution survey, provide great benefits in terms of reduction of costs, time and the risk associated with direct and destructive investigations such as excavation and masonry coring.

Geophysical methods can be applied as a fundamental tool in a wide range of archaeological prospections, and are fully included in the new "Archaeometric" cultural trend: "Archaeological emergency" and "no-dig archaeology.

The particular problems encountered in archaeology led to the development of a sub-discipline now called "archaeological geophysics".

The use and theoretical study of new electrode arrangements, particularly suitable for buried archaeological features and fast area coverage (Aspinall and Lynam, 1968), and the automatic logging of data (Kelly et al., 1984) boosted the use of this technique. While improvements are still ongoing, earth resistance surveying has established itself as one of the key methods for geophysical prospecting in archaeology.

Using a proton magnetometer, Martin Aitken started in 1958 the development of another successful technique, the magnetometer surveying.

Interest in the technique was spurred by the discovery that not only fired kilns and ferrous objects would show magnetic anomalies but also soil features such as ditches and pits. Irwin Scollar used the differential sensor configuration for large-scale surveys since 1963, and in 1966 he began with automatic digital recording on punched paper tape. Also in the 1960s, John Alldred and Frank Philpot have introduced the fluxgate magnetometers which has enabled continuous measurements thanks to the increase of the recording speed.

Then, limitations of sensitivity have led to the development of Alkaline vapour magnetometers (sensitivities of 0.01nT) by Beth Ralph, Helmut Becker and Peter Melichar in the 1970s.

Since then, these instruments have been improved and it is now possible to investigate large-area with high-resolution surveys (Eder-Hinterleitner et al., 1996; Powlesland, 2009).

At the end of 1980, the software and the instruments have become increasingly powerful and opportunities for exploration have become increasingly more.

Nowadays, the methodology for portable devices is extremely efficient, with 1–2 ha covered in a single day.

Active electromagnetic methods are increasingly used for the investigation of archaeological features. Most notably, Ground Penetrating Radar (GPR) is a well-established tool that combines high sensitivity and spatial resolution. Initially greeted enthusiastically (Stove and Addyman, 1989), it was used under unsuitable conditions (wet clay soils) and acquired a bad reputation amongst archaeologists in Britain. Once better understood the technique and its limitations, GPR is now successfully used on many sites (Conyers, 2010).

The study deals with the application of two geophysical methods, electrical (Electrical Resistivity Tomography) and electromagnetic (GPR), to characterize two archaeological sites near the shore in Northern Sardinia: the Sant'Imbenia Roman villa (Alghero, SS) and the settlement of Santa Filitica (Sorso, SS), a roman villa reoccupied until the IX century A.D.

The aim of these surveys is to demonstrate the advantages of combining geophysical methods and their effectiveness to detect, map and characterize different type of buried man-made structures in coastal archaeological contest where the intrusion of the marine water in shallow aquifer could reduce the efficacy of some geophysical method such as GPR.

The thesis includes few theoretical descriptions in the form of some geophysical basis and principal methodologies and has no ambition of a complete coverage here, but the basic relations and references to appropriate methods are being provided.

The **chapter 1** examines the theoretical basis of the electrical resistivity method and the main array employed for the archaeological prospecting, with particular reference to the Dipole-Dipole array. Furthermore the Abem Terrameter SAS 1000 device, combined with ES 10-64 electrode selector and RES2DINV - RES3DINV inversion softwares were described.

The **chapter 2** offers a description of the GPR methodology, from the theoretical basis, to its application in archaeological research.

This chapter contains also a brief description of the monostatic GPR IDS model "RIS_MF_HiMod" and of the main options used during the data processing.

The **chapters 3 and 4** present the result obtained with the employment of multimethod approach in the studied archaeological sites: the Sant'Imbenia Roman villa and the monumental complex of Santa Filitica respectively.

For each case study, after a brief description of the geological setting and archaeological features, the result of GPR and ERT surveys are reported.

References

ASPINALL, A., AND LYNAM, J., 1968. *Induced polarization as a technique for archaeological surveying.* Prospezioni Archeologiche, 3, 91-93.

CONYERS, L.B., 2010. *Ground-penetrating radar for anthropological research.* Antiquity, 84, 323, 175-184

EDER-HINTERLEITNER, A., NEUBAUER, W., AND MELICHAR, P., 1996. *Restoring magnetic anomalies.* Archaeological Prospection*,* 3, 4, 185-197.

KELLY, M.A., DALE, P., AND HAIGH, J.G.B., 1984. *A microcomputer system for data logging in geophysical surveying.* Archaeometry, 26, 183-191.

POWLESLAND, D., 2009. *Why bother? Large scale geomagnetic survey and the quest for "Real Archaeology"'.* In S. Campana and S. Piro (eds) Seeing the Unseen. Geophysics and Landscape Archaeology, London: Taylor & Francis Group, 167-182.

SCOLLAR, I., 1968. *A program package for the interpretation of magnetometer data.* Prospezioni Archeologiche, 3, 9–18.

STOVE, G. C., AND ADDYMAN, P.V., 1989. *Ground probing impulse radar: an experiment in archaeological remote sensing at York.* Antiquity, 63, 337-342.

Chap.1 - The electrical resistivity method: application to archaeological research

The electrical resistivity method is one of the geophysical methods which exploit the flow of a steady current in the ground, either direct or sinusoidal.

It is a practical technique with a relatively recent development of multi-electrode resistivity surveying instruments and fast computer inversion software (Mutzaza et al., 2012).

In archaeological research framework, the resistivity imaging technique has been successfully used to detect buried relics (mostly adobe walls), delimit these, find their characteristics and study the presence of collapse structures (De La Vega et al., 2005).

This method helps in detecting potential archaeological findings, produced by the buried artifacts with high-contrast resistivity.

The resistivity of the soil is almost entirely dependent on the amount and distribution of moisture within it, and the buried archaeological structures are affected from this distribution.

1.1 - Fundamental resistivity theory

The fundamental physical law used in resistivity survey is Ohm's Law that governs the flow of current in the ground.

In 1827, Georg Simon Ohm derived empirical relationship between the resistance (**R**) of a resistor in a simple series circuit, the current passing through the resistor (**I**), and the corresponding change in potential (**ΔV**):

$$\Delta V = R \cdot I \tag{1.1}$$

The units of **R**, **V**, and **I** are Ohms [Ω], Volts [V], and Amperes [A] respectively.

A simple series circuit that consists of a battery connected to a resistor (cylindrical-shaped body with uniform resistivity) by a wire demonstrates this relationship.

By using Ohm's Law, the value of resistance (**R**) can easily be calculated by plugging values of voltage (**ΔV**) and current (**I**) in the equation. The last two values are given because they can be measured.

The electrical resistance is defined as "the opposite offered by a body or substance to the passage through it of a steady electric current".

The electrical resistivity method concept is based on this empirical relation (1.1), with the assumption that the resistor in the circuit is the Earth.

There is another relationship that defined resistance (**R**) as a function of geometry of a resistor and the resistivity of the cylindrical-shaped body:

$$R = \frac{\rho \cdot L}{A} \tag{1.2}$$

For a given material, the resistance is inversely proportional to the cross-sectional area (**A**) [m^2] and is proportional to the length (**L**) [m] of element.

A factor that defines the ease for electrical current to flow through the media is known as resistivity (***ρ***).

By rearranging Equation (1.2) the resistivity can be expressed as:

$$\rho = \frac{R \cdot A}{L} \tag{1.3}$$

The electrical resistivity is an internal parameter of the material and the unit is Ohm-meter [Ω·m]; it quantifies how strongly the material opposes the flow of electric current.

High values of resistivity imply that the material making up the wire is very resistant to the flow of electricity. Low values of resistivity show that the material making up the wire transmits electrical current very easily (Muchaidze, 2008).

Less frequently, in geophysical investigations, the parameter of conductivity (**σ**) is measured. The conductivity is the inverse of resistivity (**1/ρ**), it has unit of Siemens/meter [S/m].

The estimation of the apparent resistivity of the Earth is relatively simple if several assumptions are made. The first assumption is that a model Earth is uniform and homogeneous, thus it possesses constant resistivity throughout the entire Earth.

The second assumption is that the Earth is a hemispherical resistor in a simple circuit consisting of a battery and two electrodes (the source and the sink electrodes) pounded into the ground (fig. 1.1).

The battery generates direct electrical current that enters the Earth at the source electrode connected to the positive portal of the battery.

The current exits at the sink electrode coupled to the negative portal of the battery (Muchaidze, 2008).

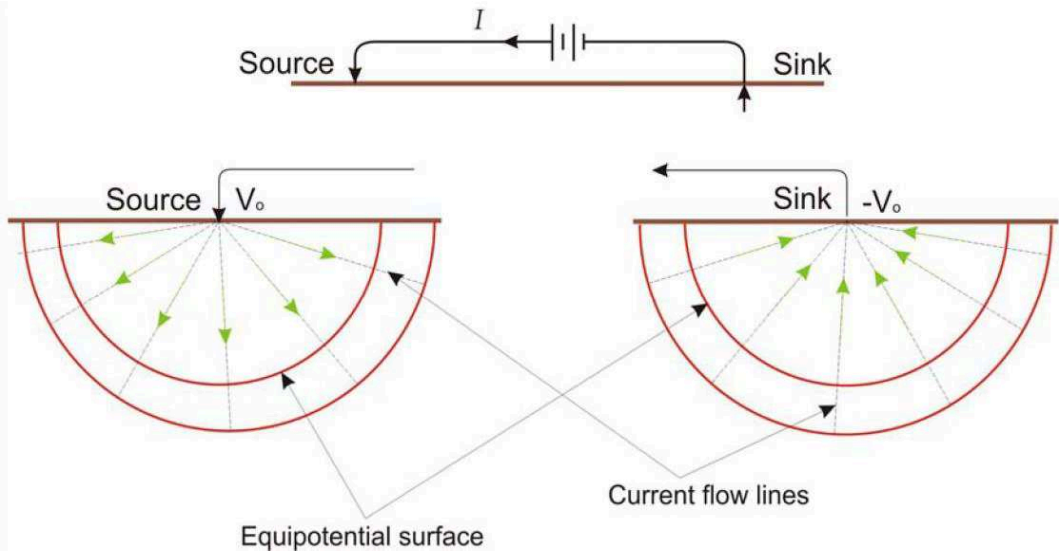

Fig. 1.1 - Current lines radiating from the source electrode and converging on the sink (Edwin and Coruh, 1988).

When current with I intensity is introduced to the ground , it is compelled to mode outward from the source electrode. Since we assume that the Earth is homogeneous, the current spreads in all directions from the electrode, and at each moment of time, the current front will move through a hemispherical zone (equipotential surface).

The area of such hemispherical zone can be found from the relationship:

$$A = 2\pi r^2 \tag{1.4}$$

where *r* is the distance from the source electrode to the point on the hemisphere surface.

By substituting equation (1.4) into equation (1.3), we can obtain an expression that defines resistance of the media at a point separated from the source by distance ***r***:

$$R = \frac{\rho}{2\pi r} \tag{1.5}$$

Combining Ohm's Law expressed by equation (1.1) and equation (1.5) the potential difference resulting from the flow of current through the hemispherical resistor can be found:

$$\Delta V = \frac{I \cdot \rho}{2\pi r} \tag{1.6}$$

with:

$$\Delta V = V_0 - V_r \tag{1.7}$$

where $\mathbf{V_0}$ is the potential at the source electrode;

$\mathbf{V_r}$ is the potential at the surface of the hemisphere with radius r.

Since the potential ($\mathbf{V_0}$) at source electrode is 0, the potential for a point located at the surface of the hemisphere with radius ***r*** is:

$$V_r = \frac{I \cdot \rho}{2\pi r} \tag{1.8}$$

This equation demonstrates, that for any point located at the hemispherical surface with radius ***r***, the potential difference between this point and source electrode is the same.
In other words, the potential difference between a source and any point on the equipotential surface has the same numerical value.

1.1.1 - The four-electrode array and apparent resistivity

In the field, two electrodes are required in order to pass an electric current into the ground. The current electrodes are commonly referred to as C_1 and C_2. Other two electrodes are connected to a voltmeter and are used to measure a potential difference between two points on the surface. These are called potential electrodes and referred to as P1 and P2. This concept of a four-electrode array is show in figure 1.2:

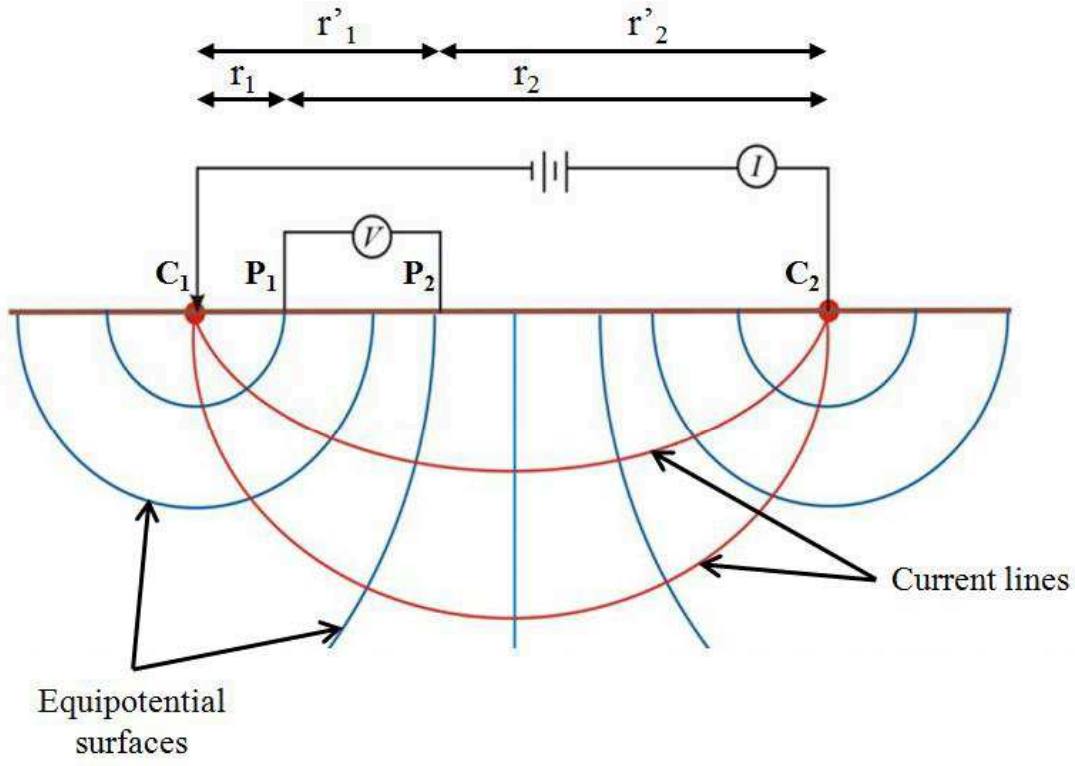

Fig. 1.2 - Scheme of four-electrode array with the interelectrode relative distances.

Since the distance between the current electrodes is necessarily finite, the potential at any surface point nearby will be affected by both.

The potential due to C_1 and C_2 observed at a potential electrode P_1 is obtained by:

$$V_{P1} = \frac{I \cdot \rho}{2\pi} * \left(\frac{1}{r_1} - \frac{1}{r_2}\right) \tag{1.9}$$

Likewise the potential due to C_1 and C_2 observed at a potential electrode P_2 is obtained by:

$$V_{P2} = \frac{I \cdot \rho}{2\pi} * \left(\frac{1}{r'_1} - \frac{1}{r'_2}\right) \tag{1.10}$$

Therefore, the potential difference (or voltage) observed between P_1 and P_2 is then given by the superposition of the individual potentials:

$$\Delta V_{P1P2} = \frac{I \cdot \rho}{2\pi} * \left[\left(\frac{1}{r_1} - \frac{1}{r_2}\right) - \left(\frac{1}{r'_1} - \frac{1}{r'_2}\right)\right] \tag{1.11}$$

For a homogeneous isotropic subsurface, the potential difference ΔV can be measured for an array of known geometry and a know injection current.

In reality, the sub-surface ground does not conform to a homogeneous and isotropic medium and thus the resistivity obtained is no longer the "true" resistivity but the "apparent" resistivity ($\boldsymbol{\rho_a}$).

The apparent resistivity of a half-space is given by solving (1.11) for $\boldsymbol{\rho}$, that is:

$$\rho_a = K \frac{\Delta V}{I} \tag{1.12}$$

where the term $\boldsymbol{k}$ is given by:

$$K = \frac{2\pi}{\left[\frac{1}{r_1} - \frac{1}{r_2} - \frac{1}{r'_1} + \frac{1}{r'_2}\right]} \tag{1.13}$$

and denotes the *geometric factor* which depends on the specific configuration of current and potential electrodes.

The relationship between the "apparent" resistivity and the "true" resistivity is very complex and to determine the true resistivity from the apparent resistivity values, must be solved the "inversion" problem (Loke, 2010).

Consequently, all field resistivity data are apparent resistivity while those obtained by interpretation techniques are "true" resistivity.

1.2 - The main array types used for archeological prospecting

For archaeological prospecting, the choice of the best array depends on the type of structure to be mapped (horizontal floor, vertical walls, etc.).

Among the characteristics of an array that should be considered are: i) the sensitivity of the array to vertical and horizontal changes in the subsurface resistivity; ii) the horizontal data coverage; iii) the signal strength (critical when the sites show a high background noise level); iv) the depth of investigation (usually the archeological feature are found in the shallow subsurface).

In the field, the different electrode arrays differ from each other according to the mutual arrangement of the pairs of current and potential electrodes.

The main array types used for subsurface prospecting are: (a) Wenner, (b) Wenner-Schlumberger, (c) Dipole-Dipole, (d) Pole-Pole and (e) Polo-Dipole (fig. 1.3).

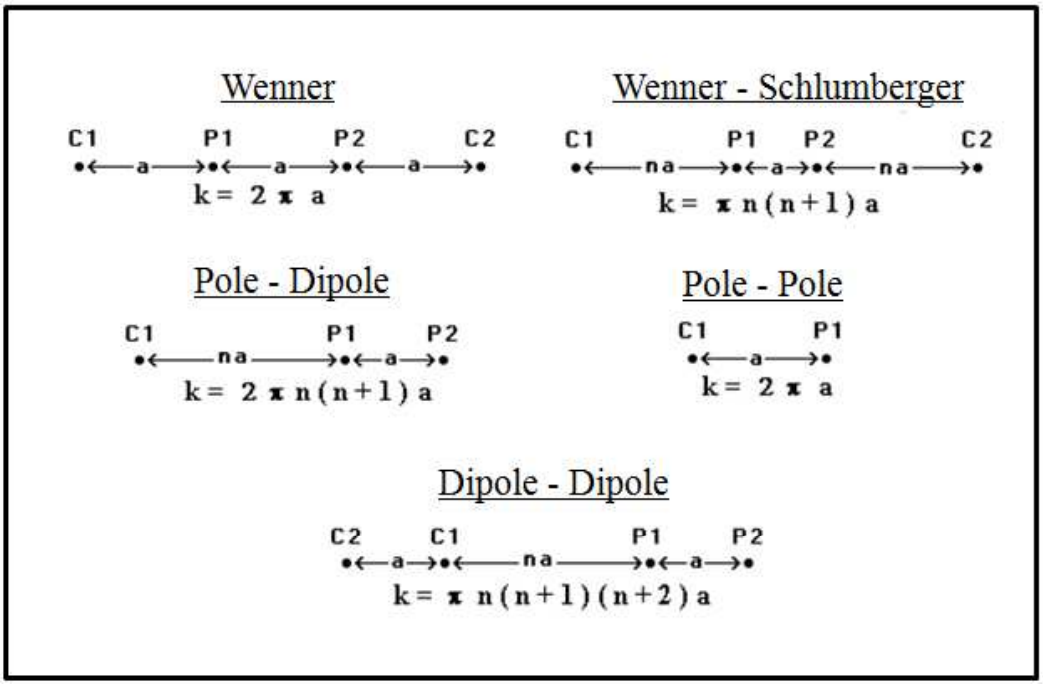

Fig. 1.3 - Common arrays used in resistivity surveys for archeological prospection and their geometrics factor.

In an array the electrodic distance determines the depth of investigation and allows to identify objects or structures of different size.

Small interelectrode distances are used to display small size objects.

Due to its characteristics, the main array used for archaeological investigations, and for acquisitions in this thesis, is the Dipole-Dipole array, whose arrangement of electrodes is shown in figure 1.4.

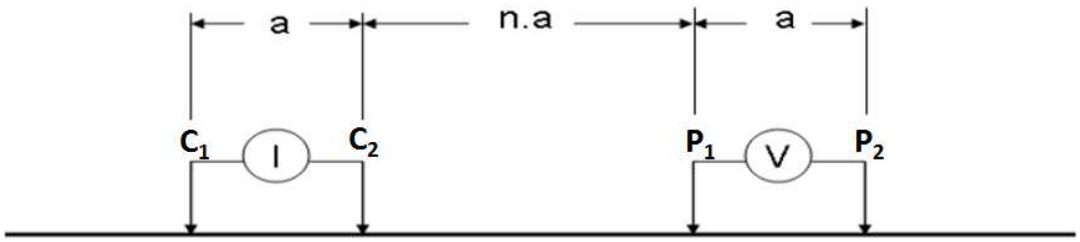

Fig. 1.4 - Dipole-Dipole array scheme.

The spacing between the current electrodes pair, C2 - C1, is given as **"a"** which is the same as the distance between the potential electrodes pair P1 - P2. This array has another factor marked as **"n"**, that is the ratio of the distance between the C1 and P1 electrodes and the C2 - C1 (or P1 - P2) dipole length **"a"**.

The geometric factor is: $K = \pi n(n+1)(n+2)a$, therefore the voltage is inversely proportional to cube of the **"n"** factor. For the same current, the voltage measured by the resistivity meter drops by about 56 times when **"n"** is increased from 1 to 6.

One method to overcome this problem is to increase the **"a"** spacing between the C1-C2 (and P1-P2) dipole pair to reduce the drop in the potential when the overall length of the array is increased to increase the depth of investigation.

Figure 1.5 shows two different arrangements for the dipole-dipole array with the same array length and different **"a"** and **"n"** factors. The signal strength of the array with the smaller **"n"** factor is about 28 times stronger than the one with the larger **"n"** factor.

The median depth of investigation of this array depends on both the **"a"** spacing and the **"n"** factor and, in general, this array has a shallower depth of investigation compared to the Wenner array.

The good horizontal data coverage of this array, can be an important advantage when the number of nodes available with the multi-electrode system is small.

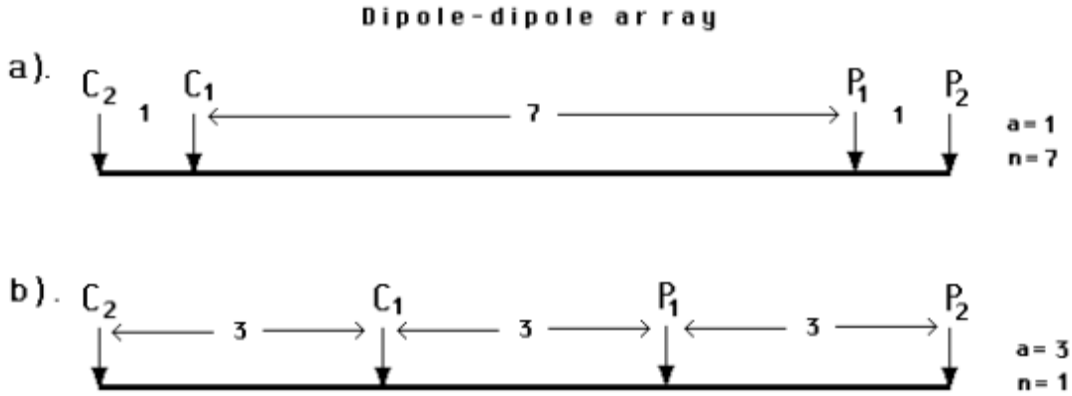

Fig. 1.5- Two possible different arrangements for a dipole-dipole array measurement. The two arrangements have the same array length but different "a" and "n" factors resulting in very different signal strengths (Loke, 2010).

The dipole-dipole array is very sensitivity to horizontal changes in resistivity, thus it is good in mapping vertical structures like walls, cavities, wells. This array is relatively insensitive to vertical changes in the resistivity and is not suitable to mapping horizontal structures such sedimentary layer or horizontal discontinuities.

1.3 - Electrical resistivity imaging (2-D multi-electrode survey)

Classical Direct Current (DC) electrical resistivity surveys are carried out with simple equipment consisting of a high voltage battery pack as the source of current, four metal stakes as electrodes, a volt–meter, and four reels of insulated cable. However a problem in such surveys is the practical difficulty of moving electrodes with large spreads of wire attached.
Moreover the classical survey technique is limited to simple 1D subsurface resistivity model interpretation as a resistivity profiles and vertical sounding.
The resistivity profiling involves the lateral movement of an electrode array of fixed size, i.e. with a constant electrode separation. If a progression is along a single line, the result is a profile of apparent resistivity with distance.
Vertical Electrical Sounding (VES) is employed if variations of resistivity with depth are of interest and the measurements are taken with gradually increasing distances of the electrodes.
As the distance between current probes increases, there is an increase in the depth of investigation. In this way, an estimate of the vertical resistivity distribution below the centre of the array is determined
The result of a VES survey is a curve of apparent resistivity as a function of depth.

A 2D subsurface resistivity model provides more accurate subsurface imaging. The resistivity varies in both the vertical direction and the horizontal direction along the survey line.

In the 2D case, it is assumed that subsurface resistivity does not change in the direction perpendicular to the survey line. In theory, a fully 3D resistivity survey and interpretation should be even more accurate. However, 2D surveys are the most practical and economic compromise between obtaining accurate images and keeping the survey costs down (Dahlin, 1996).

The construction of 2D and 3D images of the subsurface from resistivity data is commonly known as Electrical Resistivity Tomography (ERT).

ERT surveys are nowadays conducted with multiplex computer-controlled systems using a large number of electrodes connected to multicore cables at regular spacing (Barker, 1981; Griffiths and Turnbull, 1985; Griffiths et al., 1990).

Data acquisition is then entirely automatic with a computer-controlled switching unit collecting data from a predefined sequence of electrode arrays with varying geometries.

If resistivity data are acquired using multiple array separations on the same profile, the resulting dataset contains information about both lateral and vertical variations of resistivity.

Measurements are carried out between current electrodes pairs and potential electrode pairs. An increase in the distance between two electrode pairs gives the apparent resistivity data at greater depth. The usual form of display is then to plot apparent resistivity on a section of profile distance versus depth (fig.1.6).

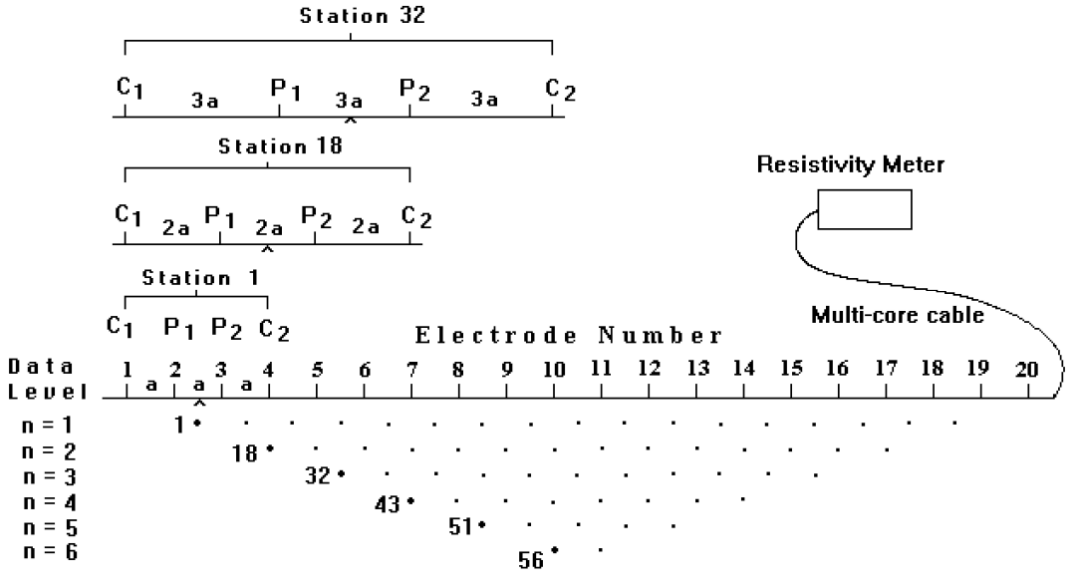

Fig. 1.6 - The arrangement of electrodes for a 2-D electrical survey and the sequences of measurements used to build up a pseudosection (Loke and Barker, 1996).

This is referred to as a pseudosection since it is indicative of resistivity variations with distance and depth, but does not necessarily correspond to the true distribution of resistivity in the form of a cross-section.

To plot the data from a 2D imaging survey, the pseudosection contouring method is normally used. Generally, the horizontal location of the point is placed at the mid-point of the set of electrodes used to make that measurement. The vertical location of the plotting point is placed at a distance that is proportional to the separation between the electrodes (Loke, 2010).

Just for the dipole-dipole array, apparent resistivity data are plotted at the intersection of the two lines drawn at a 45° angle to the horizon from the center of the current (C_1-C_2) and the potential (P_1-P_2) dipole pairs (fig. 1.7).

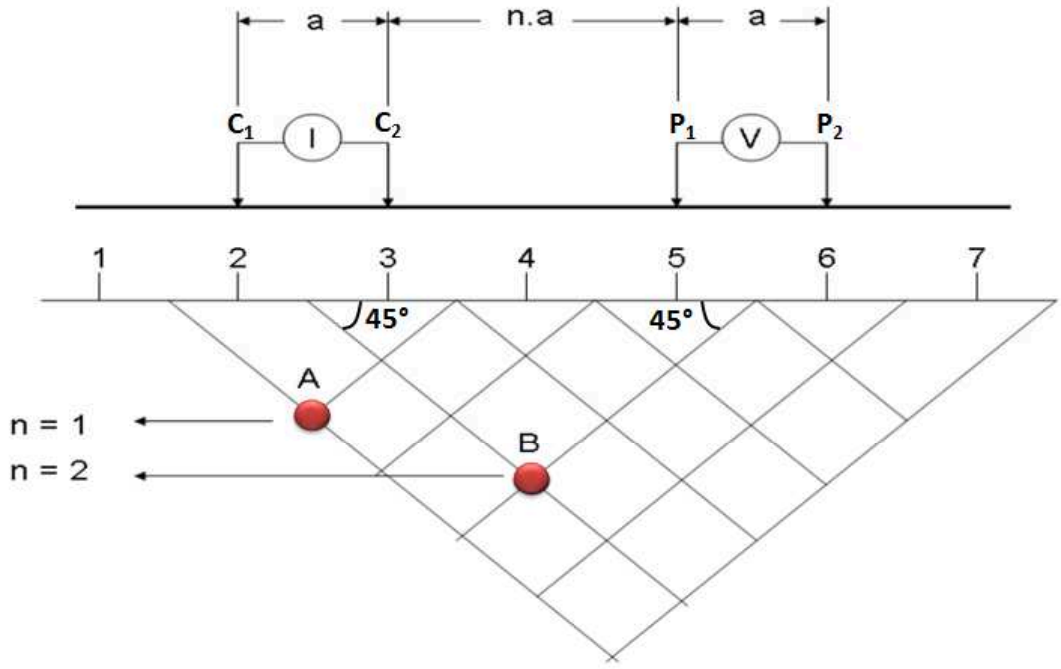

Fig. 1.7 - Classical method of plotting dipole-dipole data on a pseudosection. (A) plot for Dipole 1-2 and Dipole 3-4 measurement. (B) plot for Dipole 2-3 and Dipole 5-6 measurement.

It is important to emphasize that this is merely a plotting convention, and it does not imply the current flow or isopotential lines have a 45°angle with the surface in an inhomogeneous a Earth model (Loke, 2010).

Since the subsurface structures are 3D nature, a fully 3D resistivity survey using a 3D interpretation model should, in theory give, the most accurate results.

In this thesis, to display a more accurate resistivity anomalies in the archeological sites of interest, 2D resistivity data have been integrated to built 3D models.

The 3D data sets are constructed from a number of parallel 2D survey lines (fig. 1.8) according to the category 4 of Loke (2010).

For this type of data set, a series of 2D inversions is usually first carried out. The 3D inversion is then used on a combined data set with the data from all the survey lines in an attempt to gleam new information out of old data.

The success of the 3D inversion partly depends on the spacing between the lines and the type of array used. Ideally the distance between the lines should be about the same as the distance between adjacent electrodes in each line. However, in most cases, the distance between the lines can be two or more times larger than the inter-electrode spacing along the lines (Loke, 2010).

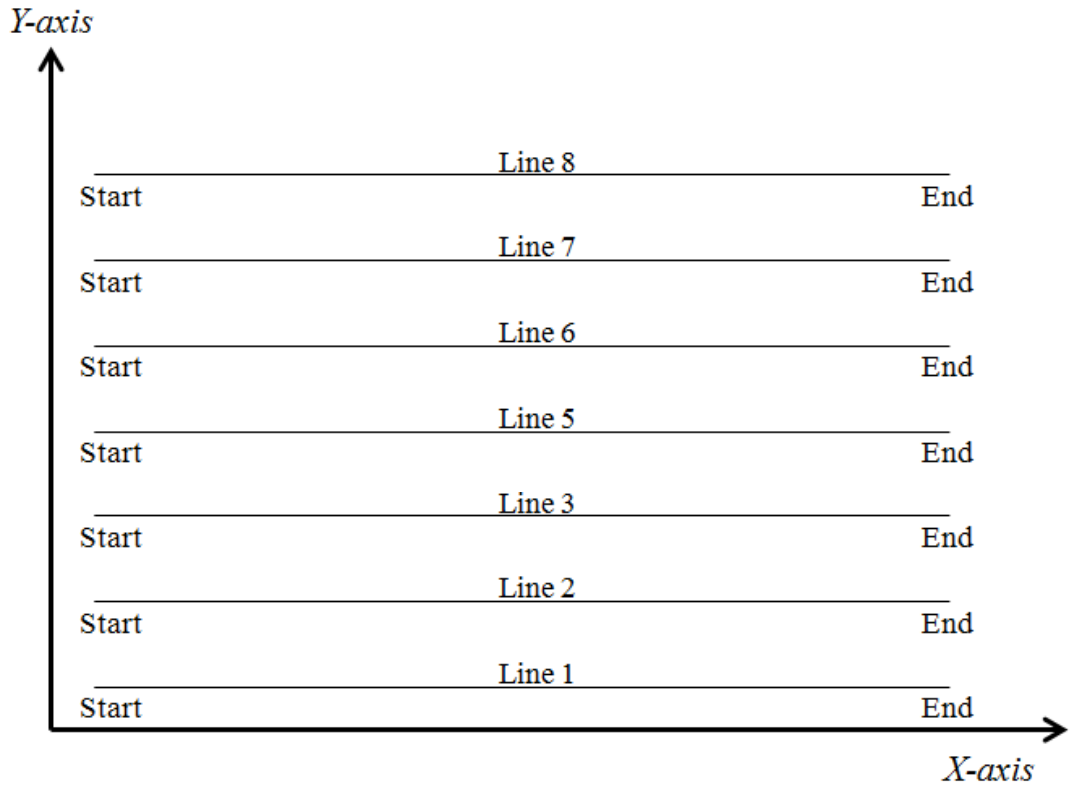

Fig. 1.8 - 2D survey lines used to construct the 3D data set.

1.4 - Equipment for multi-electrode survey: Abem Terrameter SAS1000

The geoelectrical surveys were carried out by a Terrameter SAS 1000 device, a single-channel georesistivimeter developed by ABEM Instruments (Sweden), based on the use of metal electrodes for galvanic coupling.

This device allows to get a complete set of geoelectrical measurement: SEV, resistivity profiles, 2D and 3D electrical resistivity tomography, measurement of induced polarization (IP) and self potential (SP).

The control unit Terrameter SAS1000 encloses both the energizing unit than the receiver. The electrically isolated transmitter sends out well-defined and regulated signal currents, it can be set to values from 1 mA up to 1000 mA. The maximum voltage at the current electrodes is 400V.

The receiver measures the response voltage signal at discrete time intervals and discriminates noise and measures voltage correlated with transmitted signal current.

The SAS 1000 is combined to LUND system which consist of Electrode Selector ES10-64 and multi-conductor cables (fig. 1.9).

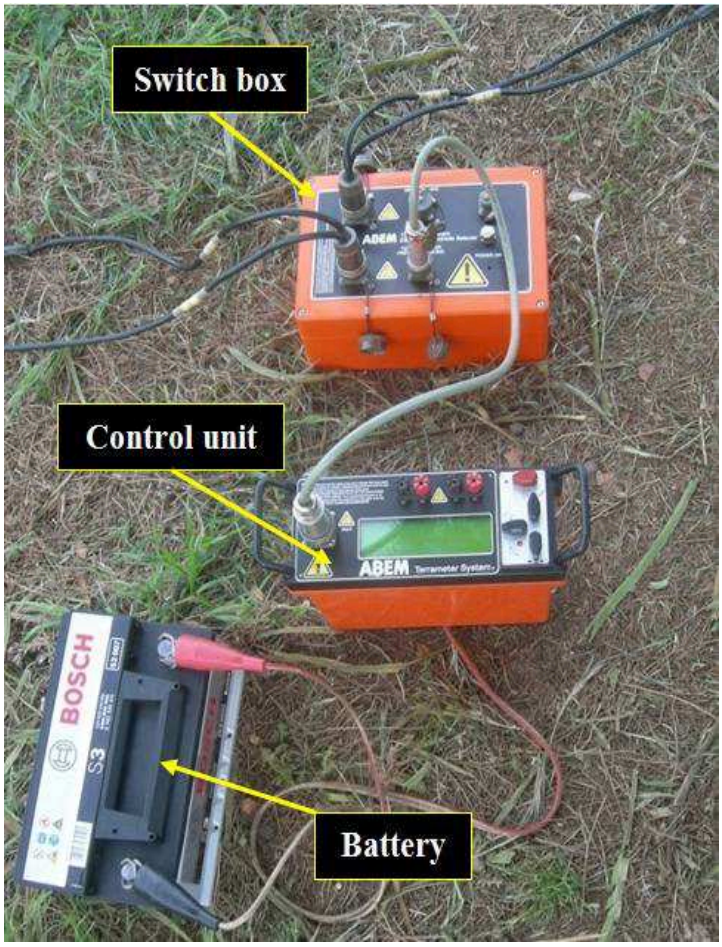

Fig. 1.9 - Arrangement for data acquisition with Abem Terrameter SAS1000 and Lund 2D multi - electrode resistivity survey.

The ES 10-64 is a multi-channel relay matrix switch for high-resolution 2D and 3D resistivity surveys which allows the automatic control of the electrode arrays.

Field system uses a multicore cable to which 64 electrodes are connected at takeouts at predetermined equal intervals (fig. 1.10).

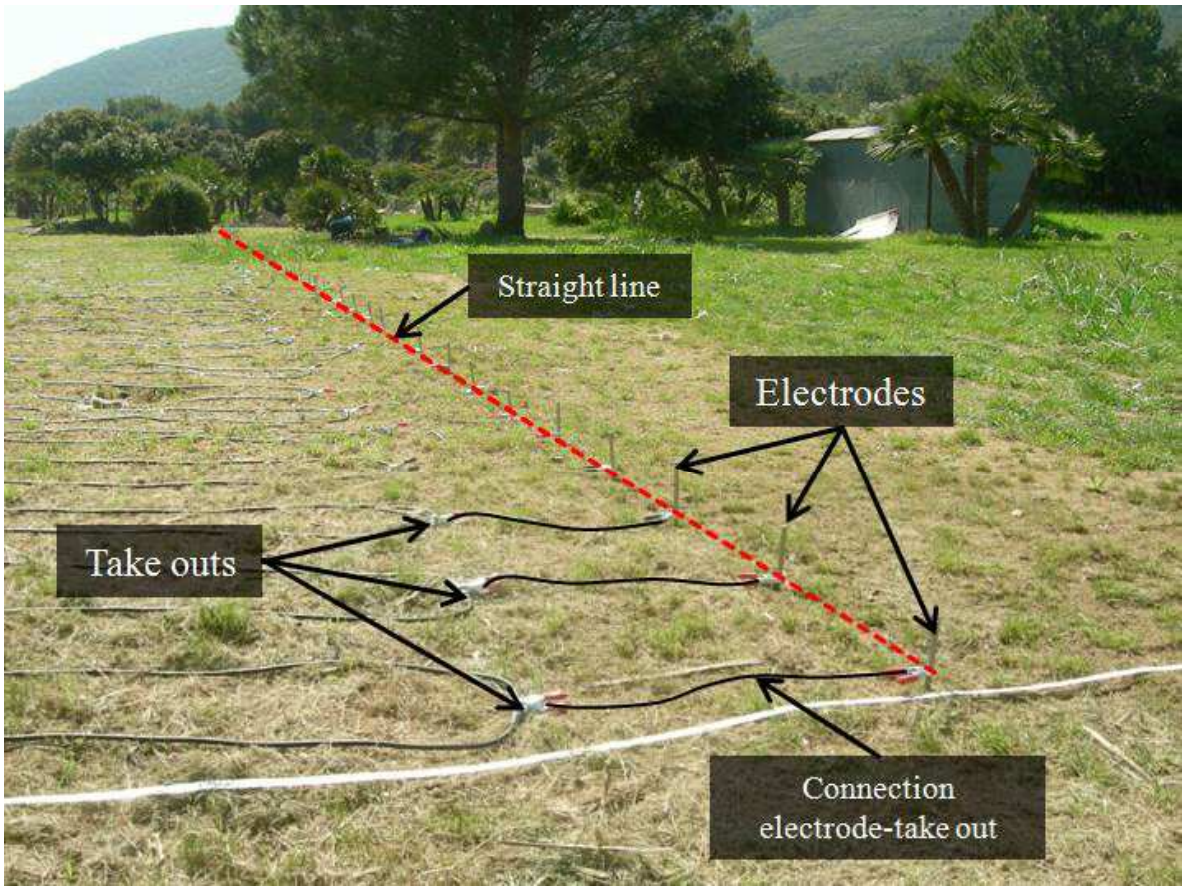

Fig. 1.10 - Acquisition line in the field. The 64 metal electrodes are connected to the takeout of the multicore cable through the wires of conjunction.

The cable is directly connected to a ES 10-64 switching module and to stainless steel electrodes hammered in the ground.

With this system, any electrodes may be switched to act as either current or potential electrodes and so within the constraints of the electrodes emplaced, any electrode arrangement can be employed (Barker et al., 2001).

The 12V external battery is required for measurements during ABEM Lund Imaging survey to ensure sustainable energy during data acquisition.

1.5 - Inversion programs

For a correct analysis of the resistivity values on a site, as previously mentioned, the first step is to select the correct electrode configuration to be used. This allows us to obtain the best results for targets that must be described.

Some commercial software have introduced the forward modeling programs, where the subsurface resistivity distribution is estimated. The purpose is to calculate the apparent resistivity values that would be measured by a survey over a specific structure and with a particular array. This method can reveal a useful tool, particularly during the planning phase of the investigation.

However, the most important part is the data inversion, because after the field survey, the resistance measurements are usually reduced to apparent resistivity values.

To plot the data from a 2D imaging survey, the pseudosection contouring method is normally used. The pseudosection gives a very approximate picture of the true subsurface resistivity distribution. However the pseudosection gives a distorted picture of the subsurface because the shapes of the contours depend on the type of array used as well as the true subsurface resistivity (Loke, 2010).

The data inversion corresponds to find a model that provides the correct interpretation of the apparent resistivity values in order to generate the most reasonable representation of the subsoil. A two-dimensional (2D) resistivity model can be therefore calculated by using several inversion programs and related equations, which are characterized by complexes mathematical techniques.

A correct 2D model discretization methods must be chosen with the purpose of divide in certain cells or region the measured.

For this thesis, the program RES2DINV ver. 3.4 (Loke, 2001), exploiting a method based on a powerful iterative computation, has been utilized. This software is designed to operate, as far as possible, in an automatic and robust manner with minimal input from the user, and it disposes of a series of default setting to provide an inversion of the apparent resistivity values.

For the same measured data set, there is a wide range of models that can give rise to the same calculated apparent resistivity values. To narrow down the range of possible models, normally some assumptions are made concerning the nature of the subsurface that can be incorporated into the inversion subroutine. In almost all surveys, something is known about the characteristic of the target in the subsurface, for example whether the subsurface bodies are expected to have gradational or sharp boundaries.

The default smoothness-constrained inversion formulation used by the RES2DINV program constrains the change in the model resistivity values to be smooth.

When the subsoil contains man-made structures, generally the resistivity values do not change in a gradual manner and the resistivity anomalies show the defined boundaries. In these cases it is preferable to apply the "select robust inversion" option.

This method is also known as an l_1-*norm* or robust or blocky inversion method, it tends to produce models that are piecewise constant (Ellis and Oldenburg, 1994).

For the inversion of electrical resistivity data in this thesis l_1-*norm* inversion method has been used.

In the RES2DINV inversion program is used a sophisticated algorithm to subdivide the subsurface in a model blocks (fig. 1.11), so that the arrangement of the blocks is loosely lied to the distribution of the data points in the pseudosection. Each block represents a data point of apparent resistivity. The depth of the bottom row of blocks is set to be approximately equal to the equivalent depth of investigation. The number of blocks normally does not exceed the number of data points.

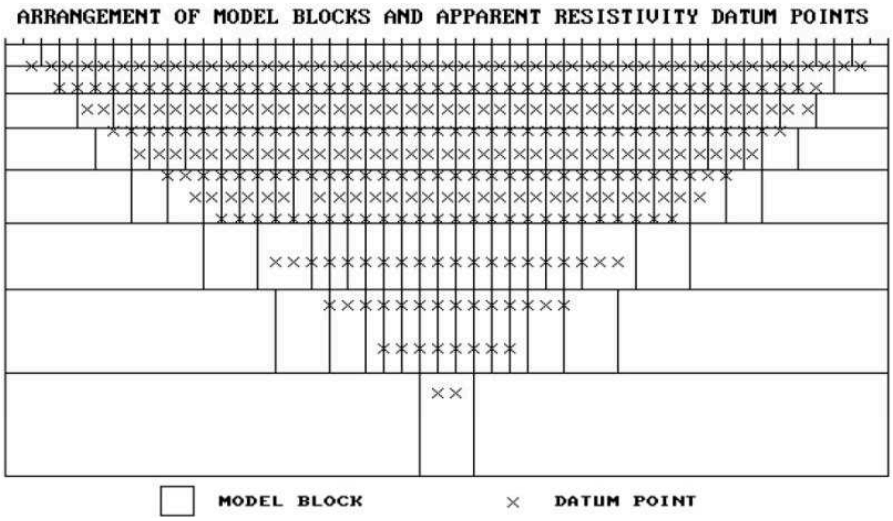

Fig. 1.11 - Subsurface model blocks used by the inversion program (Loke, 2010).

The arrangement of model block tries to reduce the difference between measured apparent resistivity values by adjusting the resistivity values of model blocks. The measure of this difference is given by the root mean square (RMS) error.

To get a good model, the data must be of equally good quality.

Bad data points are divided in two categories: i) systematic, usually caused by some sort of failure during the survey not referred to the true resistivity measurements, ii) random, which are linked with the resistivity anomalies due to telluric currents or low signal-to-noise ratio.
The systematic noise shows up as spots with unusually low or high values and can be easily removed manually for the data set. When the noise is of a more random nature, the noisy data points are not so obvious, so it might not be practical to remove them manually. In this case, a preliminary inversion of the data set is first carried with all the data point.
3-D inversion of field data set can be carried out in a similar way using the smoothness-constrained least-squares method used for the 2D inversion.
The subsurface is divided into several layers and each layer is further subdivided into a number of rectangular cells (fig. 1.12).

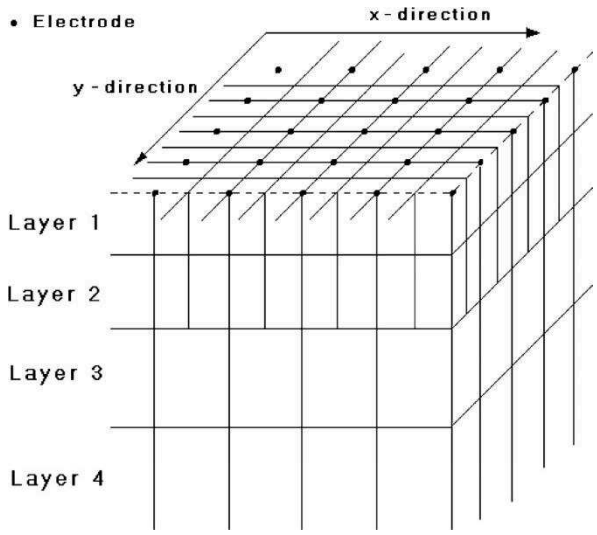

Fig. 1.12 - The model used in 3D inversion where the model cells are divided in horizontal direction (Loke, 2010).

A 3-D resistivity inversion program, RES3DINV ver.2.14 (Loke, 2004), has been used in this thesis to interpret the data from 3D surveys. This program attempts to determine the resistivity of the cells in the inversion model that will most closely reproduce the measured apparent resistivity values from the field survey.

References

BARKER, R.D., 1981. *The offset system of electrical resistivity sounding and its use with a multicore cable*. Geophysical Prospecting, 29, 1, 128-143

BARKER, R.D., VENKATESWARA, R.T., AND THANGARAJAN M., 2001. *Delineation of contaminant zone through electrical resistivity imagine technique.* Current science, 81, 3, 277-283

DAHLIN, T., 1996. *2D resistivity surveying for environmental and engineering applications.* First Break, 14, 7, 275-283.

DE LA VEGA, M., OSELLA A., LASCANO E., AND CARCIONE J.M. 2005. *Ground-penetrating Radar and Geoelectrical Simulations of Data from the Floridablanca Archaeological Site*. Archaeological Prospection, 12. 19-30.

GRIFFITHS, D.H., TURNBULL, J., AND OLAYINKA, A.I., 1990. *Two-dimensional resistivity mapping with a computer-controlled array*. First Break, 8, 4, 121-129.

GRIFFITHS, D.H., AND TURNBULL, J., 1985. *A multi-electrode array for resistivity surveying.* First Break, 3, 7, 16-20.

EDWIN, R.S., AND CORUH, C., 1988. *Basic Exploration Geophysics*. Virginia Polymeric Institute and State University, 445-478.

ELLIS, R.G. AND OLDENBURG, D.W., 1994, *Applied geophysical inversion*. Geophysical Journal International, 116, 5-11.

LOKE, M.H. 2001. *RES2DINV ver. 3.4: Rapid2-D Resistivity & IP inversion using the least-squares method.* www.terraplus.com

LOKE, M.H., 2004. *RES3DINV ver. 2.14: Rapid 3D Resistivity & IP inversion using the least squares methods.* www.geoelectrical.com.

LOKE, M.H., 2010. *Tutorial: 2-D and 3-D electrical imaging suveys.* Unpublished report: www.geoelectrical.com.

LOKE, M.H., AND BARKER, R.D., 1996. *Rapid least-squares inversion of apparent resistivity pseudosections by a quasi-Newton method.* Geophysical Prospecting, 44, 1, 131–152.

MUCHAIDZE, I., 2008. *Imaging in Karst terrain using electrical resistivity tomography*. Thesis for degree in master of science in geological engineering. Missouri University of Science and Technology.

MUZTAZA, N.M., SAIDIN, M.M., SHYEH S.K. AND SAAD R., 2012. *Locating and Mapping Archaeological Structure Using 2D Resistivity Method in Jeniang, Kedah, Malaysia.* 2012 International Conference on Geological and Environmental SciencesIPCBEE vol.36 IACSIT Press, Singapore, 44-48.

OHM, G.S., 1827. *Die galvanische Kette: mathematisch bearbeitet* (*The Galvanic Circuit Investigated Mathematically*). Graph. Darst, Riemann, Berlin, 245.

Chap. 2 - The electromagnetic method: Ground Penetrating Radar

Ground penetrating radar (commonly called GPR) is a high resolution electromagnetic technique that is designed primarily to investigate the shallow subsurface of the Earth, building materials, roads and bridges.

It is a technique that has been employed in such fields as engineering, geology, environmental studies, and more recently, archaeology (Daniels, 2000).

Ground-penetrating radar equipment is not inexpensive; however the cost of this technology has decreased in recent years, prompting more and more archaeologists to take advantage of this growing technology. Although GPR use and data interpretation is becoming more efficient and user-friendly, it is by no means self-explanatory (Welch, 2006).

The first application of GPR in archaeology was initiated soon after the first commercial equipment became available in the 1970s. One of the earliest documented uses of GPR for archaeological prospection occurred in the mid-1970 when Bevan and Kenyon (1975) and Bevan (1977) used GPR to look for radar reflections from buried walls and variety of other historic structures; and Vickers and Dolphin (1975) used GPR to look for radar reflections from suspected buried walls associated with the native American Indian structures at Chaco Canyon. A wide variety of GPR cases for archeological research have been published in the 1980_s to today (Vaughn, 1986; Imai et al., 1987; DeVore, 1990).

2.1 - Basic of electromagnetic theory

About 150 years ago, James Clerk Maxwell developed a scientific theory to explain electromagnetic waves. He noticed that electrical fields and magnetic fields can couple together to form electromagnetic waves and that a changing magnetic field will induce a changing electric field and vice-versa.

Electromagnetic waves are two waves in one. An electrical wave creating an electrical field moves along one plane, and a magnetic wave creating a magnetic field that moves perpendicular to the electrical field, as shown below. The two fields feed off each other, creating a self-propagating wave (fig. 2.1).

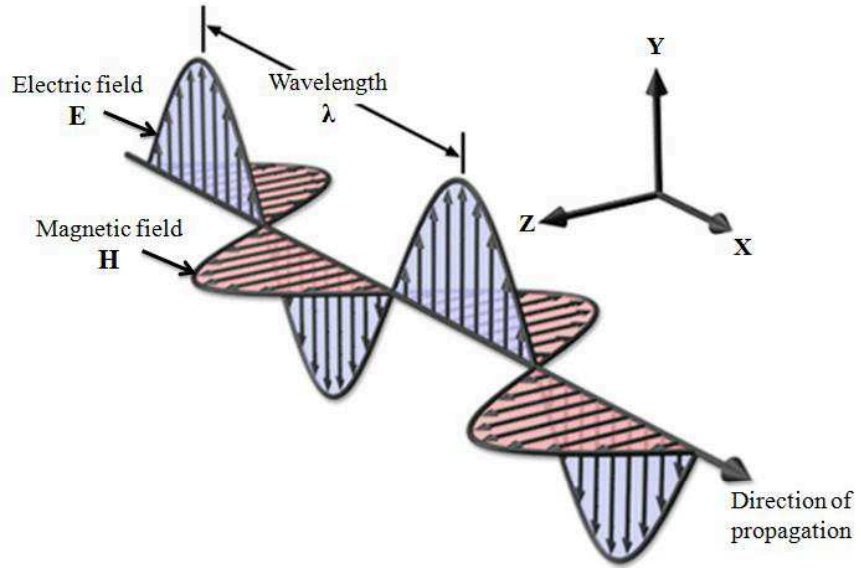

Fig. 2.1 - Electromagnetic wave; electric (E) and magnetic field (H) fluctuate normal to each other in the normal plane to the direction of propagation.

Consider now the circulation of both the electric field of the magnetic field (fig. 2.2), around a rectangle of width "dx" and height "l" in x-y and x-z planes respectively, omitting the intermediate steps can be obtained the characteristic equations of the two fields:

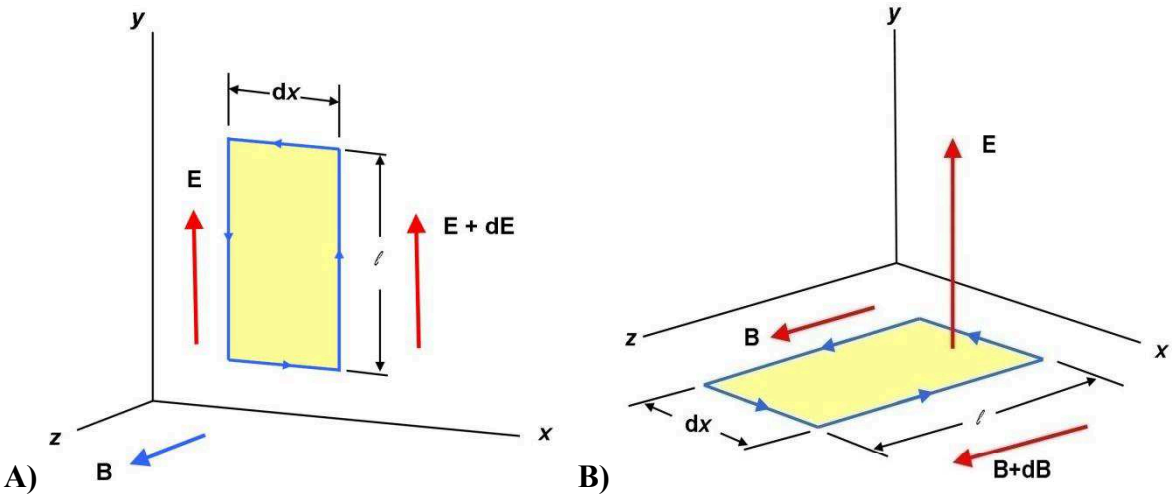

Fig. 2.2 - A) Circuitation of electric field E. B) Circuitation of magnetic field H.

$$\frac{\partial^2 E}{\partial x^2} - \varepsilon_0 \mu_0 \frac{\partial^2 E}{\partial t^2} = 0 \qquad (2.1)$$

Wave equation of the electric field for electromagnetic waves in vacuum.

$$\frac{\partial^2 B}{\partial x^2} - \varepsilon_0 \mu_0 \frac{\partial^2 B}{\partial t^2} = 0 \qquad (2.2)$$

Wave equation of the magnetic field for electromagnetic waves in vacuum.

In classical physics, light is described as a type of electromagnetic wave, and the speed *c* with which electromagnetic waves propagate through the vacuum is related to the electric constant (ε_0) and the magnetic constant (μ_0) by the equation:

$$c = \frac{1}{\sqrt{\varepsilon_0 \mu_0}} \qquad (2.3)$$

ε_0 has a defined value given approximately by: $8.854 \cdot 10^{-12}$ C^2/Nm^2.

μ_0 has a defined value given approximately by: $4\pi \cdot 10^{-7}$ Tm/A

In the practical case, if an electromagnetic wave produced by the GPR penetrates into the ground, the electric (ε) and magnetic (μ) constant are given respectively by the following relations:

$$\varepsilon = \varepsilon_0 \varepsilon_r \text{ and } \mu = \mu_0 \mu_r \qquad (2.4)$$

where ε_r and μ_r are the relative constants.

The magnetic permeability (***μ***) describes how intrinsic atomic and molecular magnetic moments respond to a magnetic field; it is a parameter that in normal conditions (not magnetic soils) is considered unitary and can be neglected.

The electric permittivity (***ε***) is associated to the displacement currents, developed with bound charges, which are constrained to limited distance of movement.

The dielectric constant or relative permittivity (ε_r) is the ratio of dielectric permittivity of material to that of free space; it is often more convenient to deal with this dimensionless term.

Consequently, the speed of propagation of electromagnetic waves in a medium is given by:

$$v = \frac{c}{\sqrt{\varepsilon_r \mu_r}} \tag{2.5}$$

Considering the magnetic permeability (μ_r) equal to one, the propagation speed of the electromagnetic wave in a real medium will be influenced only by the relative electric constant of the medium itself:

$$v = \frac{c}{\sqrt{\varepsilon_r}} \tag{2.6}$$

The simplest solutions of wave equations, both for the electric and magnetic fields are given by equations:

$$E(x,t) = E_{MAX} \cos(kx - \omega t) = E_{MAX}\, e^{i(kx-\omega t)} \tag{2.7}$$

$$B(x,t) = B_{MAX} \cos(kx - \omega t) = B_{MAX}\, e^{i(kx-\omega t)} \tag{2.8}$$

for which the amplitudes E and B vary with spacing (***x***) and time(***t***); ***ω*** is equal to ***2πf***.

An electromagnetic wave that crosses a medium, after a time ***t*** is attenuated, the 2.7 equation is:

$$E(x,t) = E_{MAX} e^{-\alpha x} \tag{2.9}$$

where ***α*** is the attenuation constant given by:

$$\alpha = \omega \sqrt{\left(\frac{\mu\varepsilon}{2}\right)\left[\left(\sqrt{1 + \frac{\sigma^2}{\omega^2 \varepsilon^2}}\right) - 1\right]} \tag{2.10}$$

where ***σ*** is the electric conductivity of the medium.

The propagation speed of electromagnetic wave in a medium is given by:

$$v = \frac{c}{\sqrt{\varepsilon_r \mu_r}\sqrt{1 + \frac{1}{2}\left(\frac{\sigma}{\varepsilon\omega}\right)^2}} \tag{2.11}$$

Electromagnetic waves travel at a specific velocity that is determined primarily by the permittivity of the material. The relationship between the velocity of the wave and material properties is the fundamental basis for using GPR to investigate the subsurface.

To state this fundamental physical principle in a different way: the velocity is different between materials with different electrical properties, and a signal passed through two materials with different electrical properties over the same distance will arrive at different times.

The interval of time that it takes for the wave to travel from the transmit antenna to the receive antenna is simply called the travel time or time of flight and is given by following relationship:

$$t = \frac{2d}{v} \tag{2.12}$$

where ***t*** is the travel time of electromagnetic wave in the ground; ***d*** is the distance by the antennas in the surface and the buried target into the ground, and ***v*** is the velocity of propagation of electromagnetic waves in the subsurface. The distance is double as considered the distance traveled by the emitted and the received wave

2.1.1 - Skin depth and electromagnetic properties of materials.

The reciprocal of the attenuation constant (eq. 2.10) is known as the skin depth and is equal to the distance over which the signal falls to **1/*e*** of its original value (fig. 2.3 A-B).

Since ***e***, the base of natural logarithms, is approximately equal to 2.718, signal strength decreases by almost two-thirds over a single skin depth.

The rather daunting attenuation equation simplifies considerably under certain limiting conditions. Under most survey conditions, the ground conductivity, σ, is much greater than $\omega\varepsilon$ and α is then approximately equal to:

$$\sqrt{\mu\sigma\omega} \tag{2.13}$$

If, as is usually the case, the variations in magnetic permeability are small, the skin depth (**1/α**) , in meters, is approximately equal to 500 divided by the square roots of the frequency and the conductivity (fig. 2.3 A).

Skin depth in meters $\approx 500\sqrt{\frac{1}{\sigma f}} = 500\sqrt{\frac{\lambda}{\sigma v}} = 500\sqrt{\frac{\rho}{f}} = 500\sqrt{\frac{\rho\lambda}{v}}$

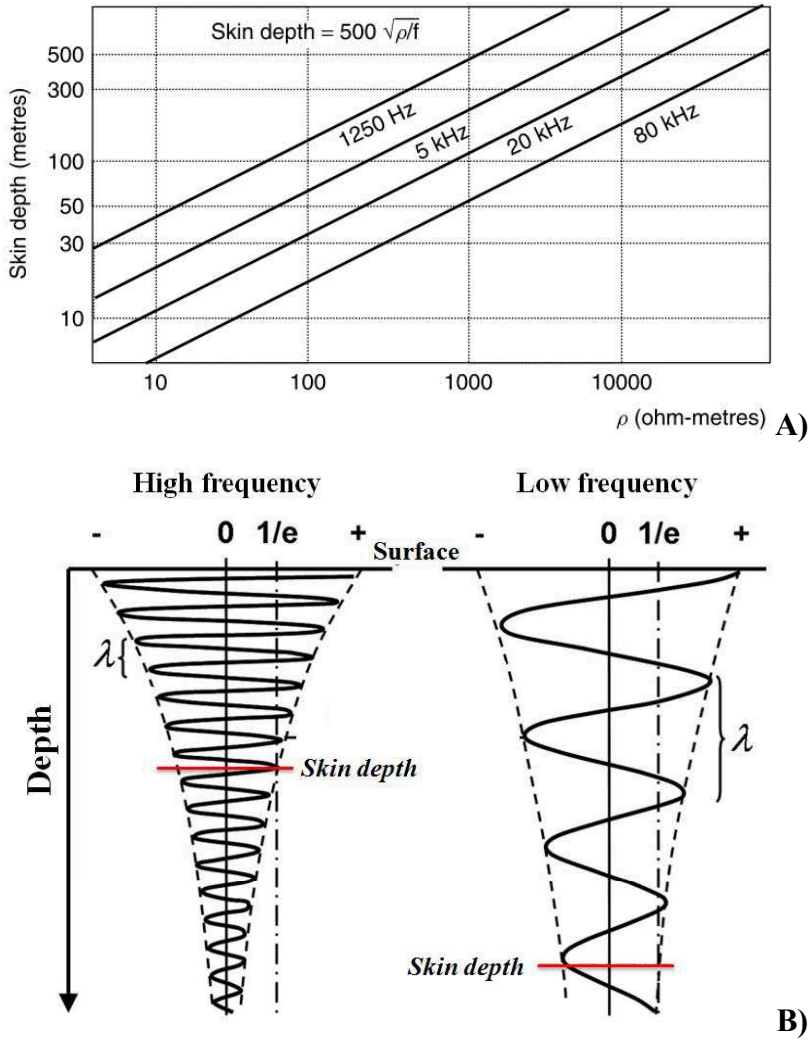

Fig. 2.3 - A) Variation in skin depth with frequency and resistivity. B) Ratio between the penetration depth of a wave and its frequency.

The maximum effective depth of penetration of GPR waves is a function of two main factors: i) the frequency of the waves that are propagated into the ground and, ii) the physical characteristics of the material through which they pass.

The physical properties that affect the radar waves, as they travel through a medium, are electrical conductivity and the magnetic permeability. Soils, sediments or rocks that are dielectric will permit the passage of a great deal of electromagnetic energy without dissipating it.

The more electrically conductive material, the less dielectric it is, and energy will attenuate at a much shallower depth. In a highly conductive medium the electrical component of the propagating electromagnetic wave is being conducted away in the ground, and when this happens the wave is entirely dissipated.

Highly electrically conductive media include those that contain salt water and some that have certain types of electrically conductive clay, especially if that clay is wet. If a soil or sediment contains soluble salts or there are electrolytes in the ground water will create a medium with a high electrical conductivity.

Magnetic permeability also affects radar penetration in a medium. It is a measure of the ability of a medium to become magnetized when an electromagnetic field is imposed upon it. Most soils and sediments are only slightly magnetic and therefore usually have a low magnetic permeability. The higher the magnetic permeability, the more electromagnetic energy will be attenuated during its transmission, and when this occurs the magnetic portion of the EM wave is destroyed, just as with increased electrical conductivity the electrical component is lost.

Media that contain magnetite, iron oxide cement or iron-rich soils can all have a high magnetic permeability and therefore transmit radar energy poorly.

Figure 2.4 lists typical values of radar parameters for some common materials. Velocities are generally well below the 0,30 $m \cdot ns^{-1}$ (300.000 $km \cdot s^{-1}$) velocity of light in free space.

Electrical conductivities at radar frequencies differ, and often increase with frequency at roughly log-linear rates.

Material	ε	σ mS/m	V m/ns	α dB/m
Air	1	0	0.30	0
Ice	3–4	0.01	0.16	0.01
Fresh water	80	0.05	0.033	0.1
Salt water	80	3000	0.01	1000
Dry sand	3–5	0.01	0.15	0.01
Wet sand	20–30	0.01–1	0.06	0.03–0.3
Shales and clays	5–20	1–1000	0.08	1–100
Silts	5–30	1–100	0.07	1–100
Limestone	4–8	0.5–2.0	0.12	0.4–1
Granite	4–6	0.01–1	0.13	0.01–1
(Dry) salt	5–6	0.01–1	0.13	0.01–1

Fig. 2.4 - Typical values of radar parameters for some common materials.

When an electromagnetic wave affects a separation surface between two media with different electromagnetic characteristics, it is partially reflected and partly refracted (fig. 2.5).

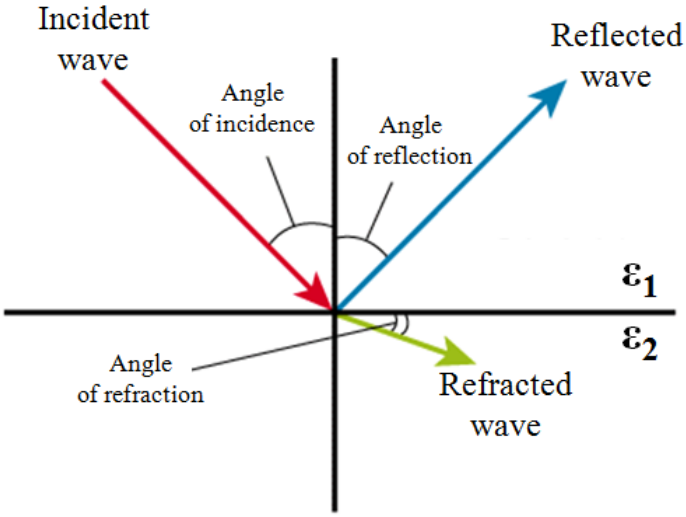

Fig. 2.5 - Refracted and reflected waves by the incident wave.

The percentage of incident radar energy reflected from an interface is governed by the size of the target and by the reflection coefficient (***R***). The proportion of energy reflected is determined by the contrast in waves velocity, and by the contrast in the relative dielectric constants of adjacent media.

The greater the contrast, the greater will be the amount of wave energy reflected. In all cases the magnitude of ***R*** lies in the range ±1. The proportion of energy transmitted is equal to **1-R**.

The equation 2.14 apply for normal incidence on a planar surface assuming no other signal losses, and refer to the amplitude of a signal.

$$R = \frac{v_2 - v_1}{v_1 + v_2} = \frac{\sqrt{\varepsilon_2} - \sqrt{\varepsilon_1}}{\sqrt{\varepsilon_1} - \sqrt{\varepsilon_2}} \qquad (2.14)$$

where ε_1 and ε_2 are the dielectric constants of the two layer crossed by the electromagnetic waves. Therefore, the greater the contrast between ε_1 and ε_2 and more marked will be the visible reflection from the instrument.

2.2 - Ground Penetrating Radar System

A GPR system is conceptually very simple because it is composed by four parts: a control unit, a transmitting antenna, receiving antenna and processing system, represented by a laptop.

The electromagnetic wave is radiated from a transmitting antenna, travels through the material at a velocity which is determined primarily by the permittivity of the material.

The wave spreads out and travels downward until it hits a buried object; then part of the waves energy is "reflected" back to the surface, while part of its energy continues to travel downward. The wave that is reflected back to the surface is captured by a receiving antenna, and recorded on a digital storage device for later interpretation.

In a GPR system if the transmitting and receiving antennas are separate, then the system is called a bistatic antennas arrangement. If the same antenna is used for transmitting and receiving the signal, then the antenna is called monostatic system (Daniels, 2000).

Antennas can be considered to be transducers that convert electric currents on the metallic antenna elements to transmit electromagnetic waves that propagate into a material. Antennas acting as a receiver of the electromagnetic radiation by capturing part of the electromagnetic wave. The received data is recorded, in real time, through the laptop. The diagram of the used GPR monostatic system and the method of application is showed below (fig. 2.6)

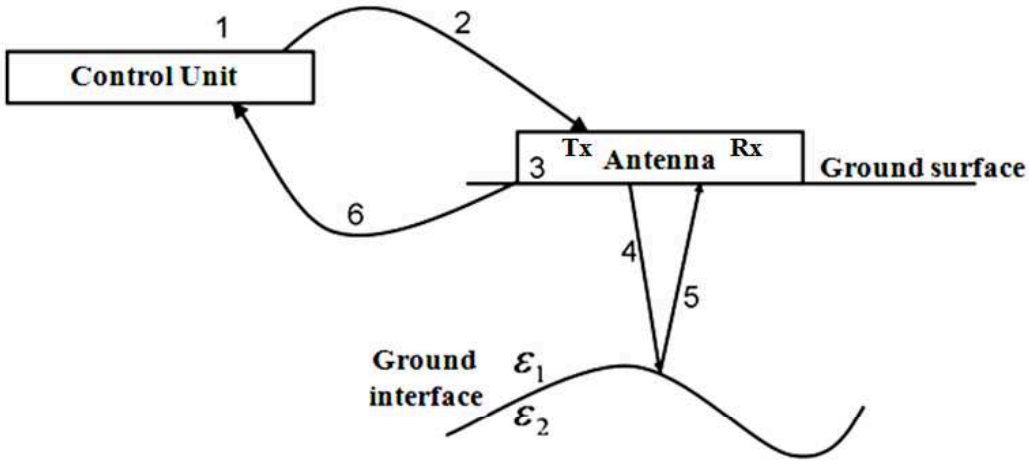

Fig. 2.6 - Scheme of a monostatic Ground Penetrating system.

Where:

1) the control unit generates a trigger pulse;

2) the pulse goes through the cable to the transmitter;

3) in the transmitter each trigger pulse is transformed into a bipolar pulse and increased in amplitude (the electrical signal becomes electromagnetic wave);

4) the pulse is then transferred into the subsurface through the antenna. The size of the antenna and the electrical properties of the subsurface determine the frequency of the input energy;

5) in subsurface, the reflection occurs in correspondence of contrast of dielectric properties;

6) the received antenna intercepts the signal back and sends it to the control unit, where it is processed and displayed.

For all electromagnetic survey carried out in this Ph.D. thesis has been used the GPR model "RIS_MF-HiMod" (fig.2.7). This device is composed of a control unit (DAD Control Unit Fast Wave) working simultaneously with two transmitters (Tx) 200 and 600 MHz and two receivers (Rx).

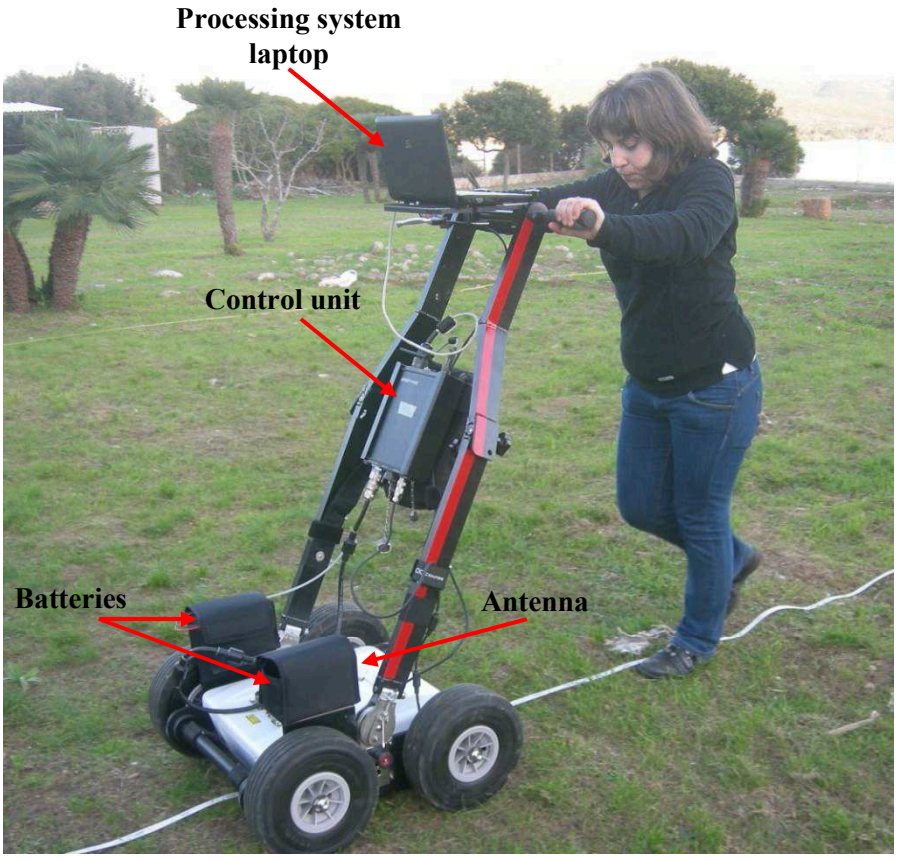

Fig. 2.7 - GPR IDS model "RIS_MF-HiMod".

2.3 - Processing GPR data

The objective of GPR data presentation is to provide a display of the processed data that is closely approximates an image of the subsurface, with the anomalies that are associated with the objects of interest located in their proper spatial positions. Data display is central to data interpretation. In fact, producing a good display is an integral part of interpretation.

There are three types of displays of surface data, these are: a one-dimensional trace (A-scan), a two dimensional cross section (B-scan), and a three dimensional display (C-scan).

Following are briefly described each of these types:

1) A-scan (or one dimensional data presentation) is obtained by a stationary measurement, emission and collection of a signal after placing the antenna above the position of interest. The collected signal is presented as signal strength vs. time delay.

2) B-scan (or two dimensional data presentation) is obtained as the horizontal collection from the ensemble of A-scans. The horizontal axis of the two dimension image is surface position, and the vertical axis is the round-trip marvel time of the electromagnetic wave.

3) C-scan (or three dimensional data presentation) is obtained from the ensemble of B-scans, measured by repeated line scans along the plane. Three dimensional displays are fundamentally block views of GPR traces that are recorded at different positions on the surface. Obtaining good three-dimensional images are very useful for interpreting specific targets. Targets of interest are generally easier to identify and isolate on three dimensional data sets than on conventional two dimensional profile lines (Abujarad, 2007).

These resulting radar images show streaks of black and white bands in various forms and shapes (real vision); some commercial softwares guarantee the data visualization in other formats, with colored zones of same reflection amplitude (modular vision). The general procedure for processing data is to store the data in the appropriate dimensional format and then apply appropriate algorithms.

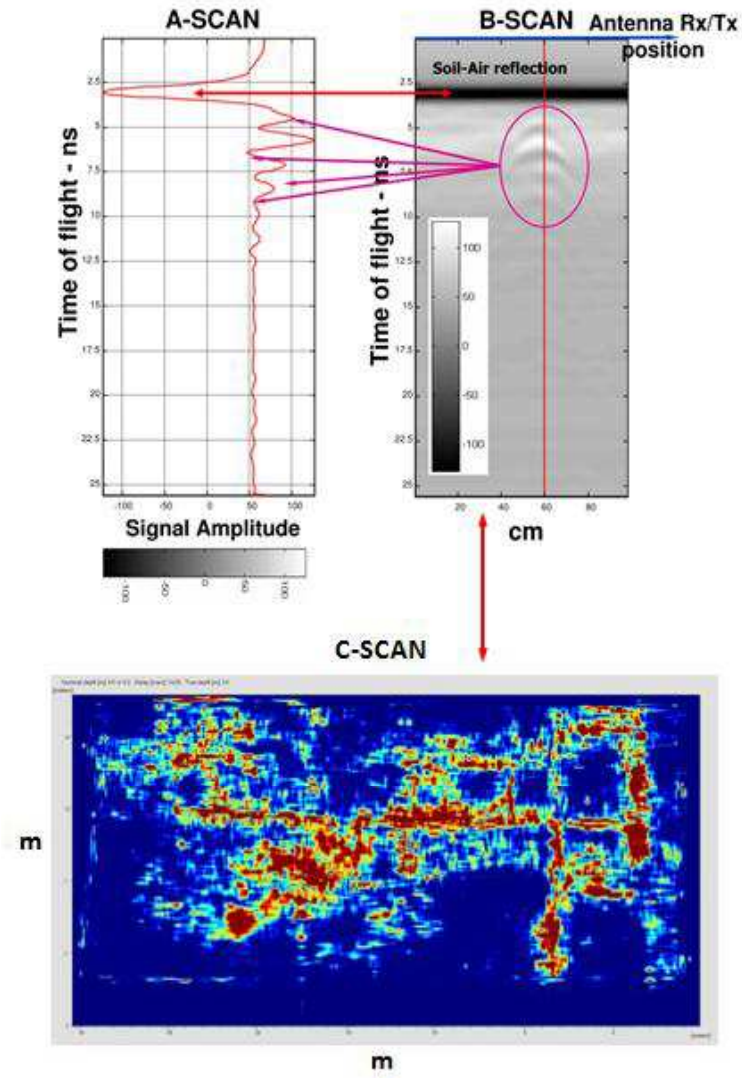

Fig. 2.8 - Scan display of a various scan types that can be obtained through a GPR survey.

The figure 2.9 represents the coordinate system for the scans description.

The A-scan is defined as: $f(x) = A(x_i, y_j, z_k)$ over the ranges k=1 to N, j=constant, i=constant.

The B-scan is defined as: $f(x,z) = A(x_i, y_j, z_k)$ over the ranges k=1 to N, i=1 to P, j=constant.

The C-scan is defined as: $f(x,y,z) = A(x_i, y_j, z_k)$ over the ranges k=1 to N, j=1 to P, with A=data sample; is noticeable that time and depth of the z-axis can be considered to be interrelated by the velocity of propagation inside the material where the wave is circulating (Daniels, 2004).

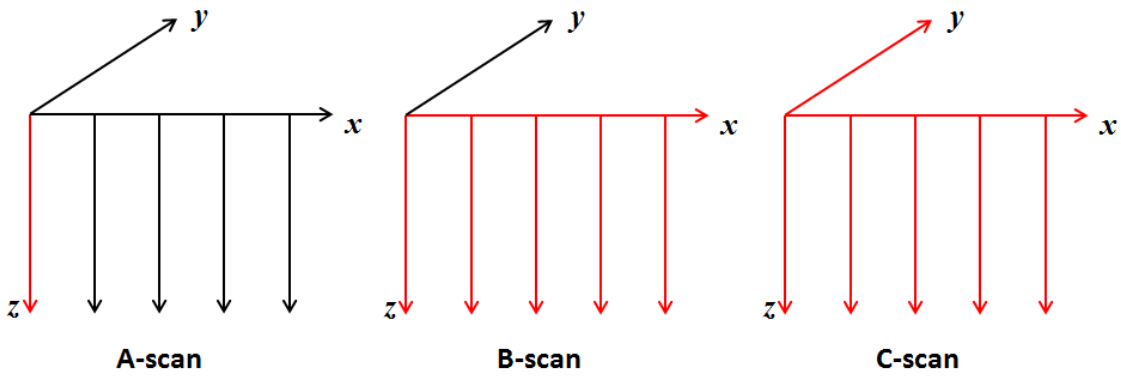

Fig. 2.9 - Coordinate system for the different types of GPR scans. The red lines show the coordinates along which the data relating to each scan are acquired.

The selection of suitable signals processing method is very important, considering the objective represented by the optimization the wavelet output. Processing software hence enables the application of different filters and gain functions to visualize the resulting reflection values as best is possible.

For Daniels (2004), the signals processing are primarily of reducing clutter; fundamentally, the signal to clutter ratio of the radar data is the key to target detection.

Most system noise in GPR systems can be reduced by averaging. GPR is heavily contaminated by clutter, and reduction of this is a key objective. Most important, the general objective of signal processing as applied to surface-penetrating radar is either to present an image that can readily be interpreted by the operator or to classify the target return with respect to a known test procedure or template.

In many cases, it is possible to use the results from a GPR survey with very modest processing. In these cases, the only processes that need to be made are to convert the data to a usable digital format, to make gain adjustments to the data, and to determine the depth to each eventual reflector (such as the water table) in the subsurface (this involves converting time to depth). For GPR data processing, in this thesis, has been used the software GRED v. 02.01.008 (IDS Ingegneria dei Sistemi). The main processes of elaboration used are show below:

i. *Converting the data to a usable digital format:* in most recently manufactured GPR units, the data is automatically recorded in digital format. IDS Company provides its own data format and relative elaboration software.

ii. *Move start time:* is a function of the control system, cable lengths, and antenna positioning. It is necessary, in order to perform an accurate GPR survey in the ground,

to calculate the two-way travel time from the precise moment when the EM wave pass between the air to ground interface.

iii. *Vertical filtering:* every single radar track contains a set of peaks that have a certain period. The aim of the filtering in the time domain (vertical filtering) is to remove any spurious frequencies, i.e. not connected to the targets present in the subsurface.

iv. *Horizontal filtering:* the set of traces related with a particular structure defines a horizontal frequency. The purpose of horizontal filtering (spatial domain) is to remove low frequencies (parallel bands) that are not connected to any structure, but which are generated in the area between the antenna and the surface.

v. *Migration:* the Migration process essentially constructs the target reflector surface from the record surface. Migration technique aims to relocate reflections to their true spatial position based on the velocity spectrum, to produce a real structure map of subsurface features. In some cases for a correct migration, many attempts, changing velocity are needed, finally as higher the velocity accuracy, as higher the real reproduction of the detected target (Mori, 2009).

vi. *Background removal*: noise that occurs as it the geometry of the system, clutter, artifacts and static reflections can be reduced with a background removal. The background filter subtracts reflections, which are constant over the entire radargram (Heilig et al., 2008). The software computes the average of all the scans accumulated and it removes them, to eliminate the antenna ringing and horizontal banding across the image; generally the first interface air-ground is involved in the process and cancelled, so that reflection and hyperbolas previously hidden by horizontal traces can hence be readily visible. The background removal also removes other horizontal features such as flat lying geology and the surface of the Earth, so time zero had to be located first.

2.4 - GPR signal types

The effect of subsurface materials on the propagating EM wave varies depending on the size, orientation, and chemical and physical properties of subsurface archaeological features and geological deposits. The result is a wide range of signal patterns, all of which fall under one of two basic categories: planar reflections, produced at transition between deposits and/or features; point source reflections, produced by discrete point targets (Dojak, 2012).

In addition, signals can be distinguished by variations in amplitude, as dictated by changes in subsurface materials and their effects on the amplitude of the EM wave:

- *Planar Reflections:* are reflections that appear as horizontal or sub-horizontal lines in reflection profiles and are generated from any lineal boundary between materials, such as buried stratigraphic and soil horizons, the water table, and horizontal archaeological features, such as house floors. These require only one distinct reflection to be resolved in reflection profiles. Planar reflections can be used to approximate the shape, depth, size, and orientation of subsurface boundaries and discontinuities.
- *Point Source Reflections:* are reflections which often appear as hyperbolas in reflection profiles. They are commonly generated from distinct, spatially-restricted, non-planar features ('point targets'), such as rocks, metal objects, walls, tunnels, voids, and pipes crossed at right angles. For these three-dimensional objects to be resolved, reflections must be received from at least two of the object's surfaces.
- *Hyperbolas:* are a form of point source reflection, and are due to the fact that GPR energy is emitted in a cone, which radiates outwards with depth. The hyperbolic image produced from point source reflectors is due to the fact that GPR energy is emitted in a cone, which radiates outwards with depth. As such, energy is reflected from objects that are not directly below the antenna; the reflection, however, is recorded as being directly below the antenna, and at a greater depth due to the oblique transmission of the wave. Only the apex of the hyperbola denotes the actual location of the point source.
- *Amplitude Changes:* are due to the variations in subsurface material properties. High amplitude reflections are generated at boundaries between materials of highly contrasting physical and chemical properties, and thus RDP values. In contrast, low amplitude values reflect materials of similar properties or uniform matrixes. Metal objects produce very distinct reflections, which are characterized by multiple stacked high-amplitude reflectors, referred to as multiples

References

ABUJARAD, F., 2007. Ground *Penetrating Radar signal processing for landmine detection.* PhD thesis, Otto Von Guericke Universität, Magdeburg, 124.

BEVAN, B.W., 1977. *Ground-penetrating radar at Valley Forge.* Geophysical Survey System, North Salem, New Hampshire.

BEVAN, B. AND KENYON, J., 1975. *Ground-penetrating radar for historical archaeology.* MASCA Newsletter, 11, 2, 2–7.

DANIELS, D., 2004. *Ground Penetrating Radar.* The Institution of Electrical Engineers, London, 752.

DANIELS, J.J., 2000. *Ground Penetrating Radar Fundamentals.* Prepared as an appendix to a report to the U.S.EPA, Region V. Unpublished Report. Department of Geological Sciences, The Ohio State University, 21.

DEVORE, S.L., 1990. *Ground-penetrating radar as a survey tool in archaeological investigations: An example from Fort Laramie national historic site.* The Wyoming Archaeologist, 33, 23–28.

DOJAK, L., 2012. *Ground Penetrating Radar Theory, Data Collection, Processing, and Interpretation: A guide for Archaeologist,* Available online at UBC's digital information repository (circle – https://circle.ubc.ca/handle/2429/41983), 89.

GRED v. 02.01.008, 2008. *Manuale Utente*, IDS Ingegneria dei Sistemi, Italia.

HEILIG, A., SCHNEEBELI, M., AND FELLIN, W., 2008. *Feasibility study of a system for airborne detection of avalanche victims with ground penetrating radar and a possible automatic location algorithm.* Cold Regions Science and Technology, 51, 178–190.

IMAI, T., SAKAYAMA, T., AND KANEMORI, T., 1987. *Use of ground-probing radar and resistivity surveys for archaeological investigations.* Geophysics, 52, 127–150.

MORI, G., 2009. *The use of Ground Penetrating Radar and alternative geophysical techniques for assessing embankments and dykes safety.* PhD thesis. Department Of Earth and Geoenvironmental Science - Alma Mater Studiorum Università di Bologna, 206.

VAUGHN, C.J., 1986. *Ground-penetrating radar surveys used in archaeological investigations.* Geophysics, 51, 595–604.

VICKERS, R. AND DOLPHIN, L.T., 1975. *A communication about an archaeological radar experiment at Chaco Canyon*. Museum Applied Science Center for Archaeology, Univ. of Pennsylvania, Philadelphia, Newsletter, 11, 1, 1-3.

WELCH, D.R., 2006. *The use of Ground-Penetrating Radar for Archaeology: determining site formation processes and subsurface features on Tutuila Island, American Samoa.* A senior scholar thesis. Texas A&M University, 39.

Chap. 3 - Integrated geophysical methods on a coastal archaeological site: the Sant'Imbenia Roman villa (Northern Sardinia)

3.1 - Site location and geological setting

The Sant'Imbenia Roman villa is located in the Nurra district in the northwestern Sardinia. The archaeological site lies upon the most protected side of the Porto Conte bay (fig. 3.1), an inlet bordered by the Capo Caccia promontory to the west and the Punta Giglio promontory to the east.

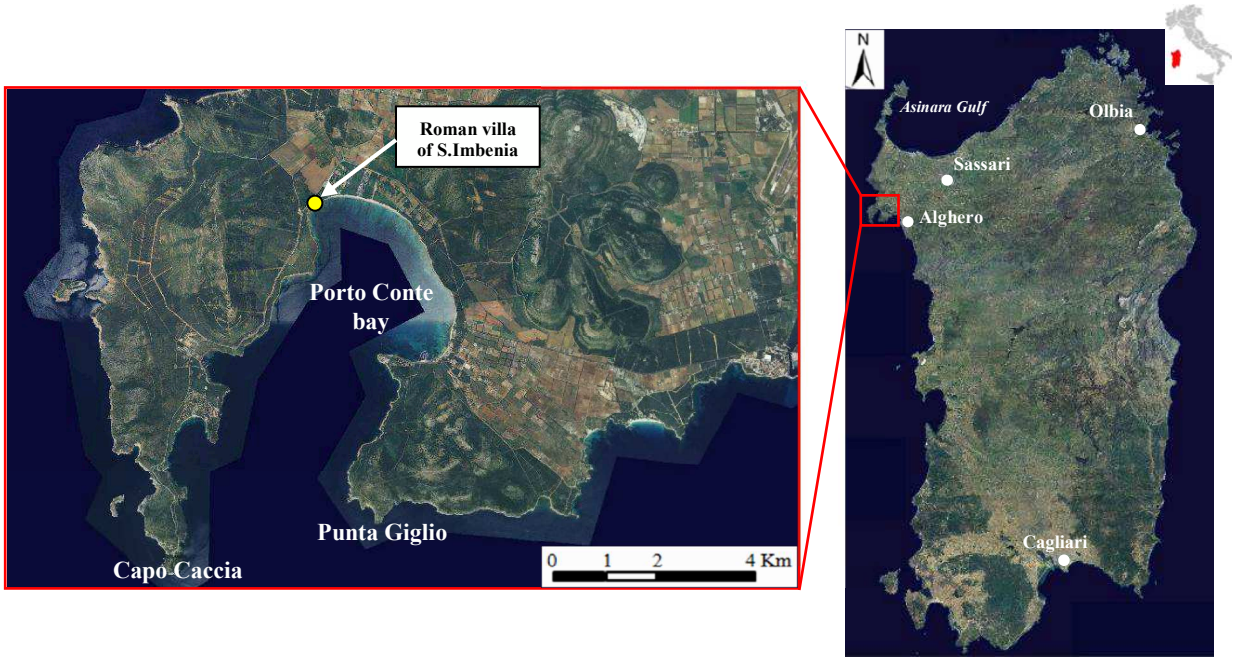

Fig. 3.1 - Location map of Sant'Imbenia Roman villa.

The Nurra district encompasses a structural high, which developed during the Tertiary age and where older rock sequences of the Varisican metamorphic basement are well exposed near the coast in the westernmost sector.

The study area lies in a sector where the Mesozoic succession outcrops widely (fig. 3.2).

The first marine transgressive deposits (facies Muschelkalk - Middle Triassic) (fig. 3.2 - **20**) consist of dolostones, limestones and evaporites, covering the terrigenous continental deposits (facies Buntsandstein - fig. 3.2 - **21**)

In the western portion of Sant'Imbenia archaeological site, in addition to Muschelkalk facies deposits, there are outcrops of evaporitic rocks, mainly gypsum, dolostones, dolomitic limestone and marls. These deposits in Keuper facies (Upper Triassic) (fig. 3.2 - **20**) are a marker for shallow waters environment and hot-dry conditions.

A carbonate sequence that encompasses the entire Jurassic system lies on the Triassic evaporites (facies Keuper). Its base consists of alternations of marls and limestones with thin dark pyrite-rich shale levels (fig. 3.2 - **18b**) (Monte Doglia, Monte Timidone).

Most of the sequence is made of dolostones and limestones; green marls with typical Purbeckian facies (Pecorini, 1969) also occur towards the top of this system grading into the Cretaceous limestone.

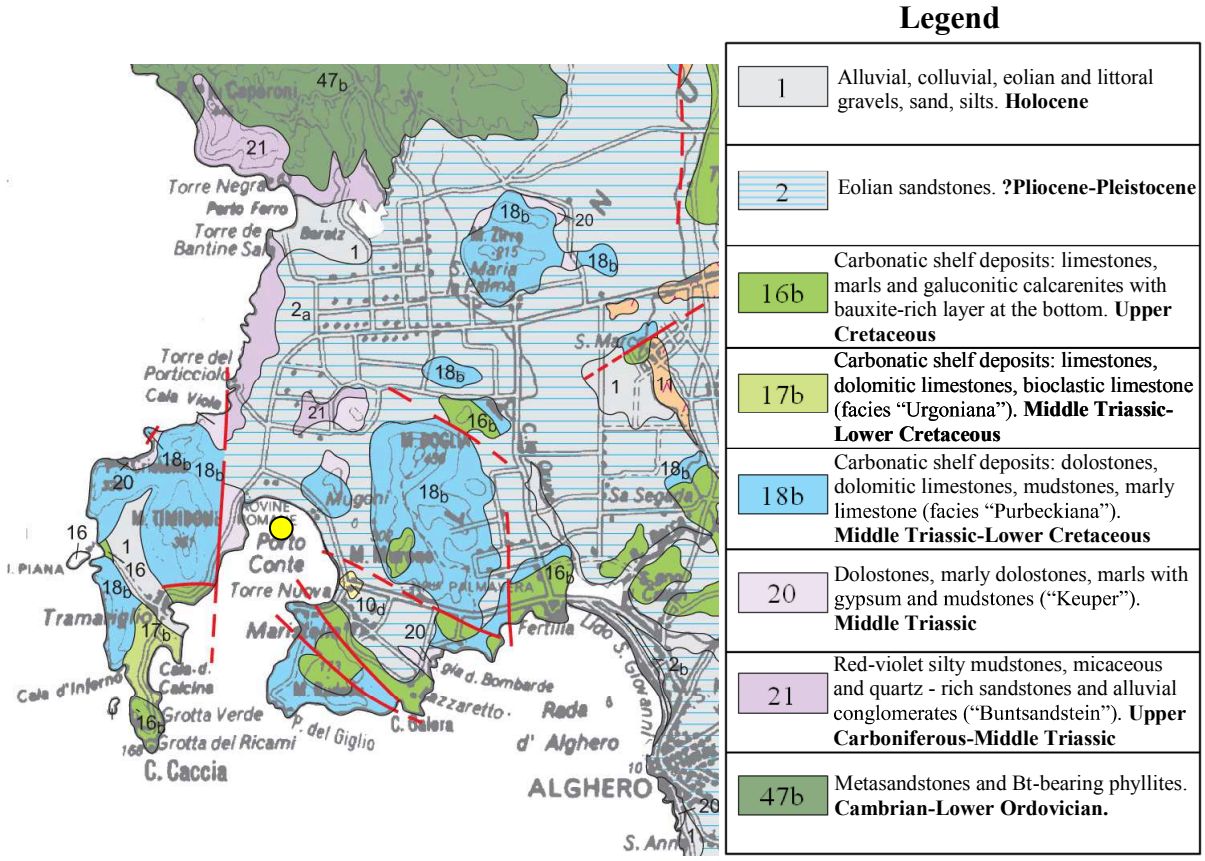

Fig. 3.2 - Geological map of the area around the archaeological site (Carmignani et al., 2001).

The Cretaceous succession lies on "Purbeckian" marls; it consists of two sequences separated by an angular unconformity, which is marked by bauxite deposits and represents a hiatus corresponding to the mid-Cretaceous (Mameli et al., 2007). The lower sequence is represented by limestone with typical Urgonian facies (fig. 3.2 - **16b**).

This limestone consists of a strongly karstified biosparite that, where not completely eroded, reaches 180 m in thickness. The upper Cretaceous sequence also consists of limestones with an important intercalation of glauconite-bearing, more or less arenitic marls (Ghiglieri et al., 2009).

The quaternary deposits (fig. 3.2 - **2a**), near the archaeological evidence, occur as alluvial deposits with pebbles of quartz and limestone, reddish sand and clay.

These deposits arise from the dismantling of surrounding lithologies and cover most of the Paleozoic, Mesozoic and Cenozoic successions.
These alluvial deposits represents the dominant foundation soil of the villa, even if Muschelkalk dolostones occur in southernmost part of the settlement.

3.2 - Archaeological features of the Roman villa (Manconi, 1999)

The uninterrupted political and economic stability that occurred during the Roman period (in Sardinia, 238 B.C. to 476 A.D.) encouraged the development of a settlement that is attested archaeologically by the remains of the large monumental complex of Sant'Imbenia Roman villa, that was constructed upon a spur of elevated land in close proximity to the sea (fig. 3.3).

Fig. 3.3 - The remains of monumental complex of Sant'Imbenia.

In Roman period, the term villa refers to a complex edifice that is often isolated in the countryside which generally consists of two principal areas: i) *pars urbana* or residential area and ii) *pars rustica* or working area.

The first area was the luxurious residential section, the well furnished home of the *dominus*, while the second portion was subdivided into numerous sections utilized for agricultural processes, the raising of livestock and all other commercial activities.

The products deriving from this villa and other rural settlements in the region were transported to ports and land-based centers where the commodities were distributed to many ports located throughout the broad territory controlled by Rome.

The fact that a Roman settlement existed in the area of Sant'Imbenia has been known for a long time. In fact, some of remains of the villa have always been visible, especially along the coast; however the extent of the complex must still be determined.

The structural components of the villa are spread over an area of less than one hectare. Due to the continuous advancement of the sea, part of the eastern portion of the estate has been destroyed. The damaging actions of the sea and the wind represent the most serious problems in terms of the site's conservation.

The villa was modified and enlarged several times over the course of time and was still in use by Late Antique period and early Middle Ages.

The villa's extended landscape was dotted with small settlements and farm, inhabited by freedmen and slaves who were responsible for conducting agricultural work and the gathering of natural resources. The adjacent water mirror, the sea, was almost always calm and must have serves as a natural fishery.

The villa's heyday seems to have occurred between the 1st an 2nd centuries A.D., evidence suggests that portions of the complex were destroyed by fire at once.

Over the course of several centuries, in particular between the 3rd and the7th/8th centuries A.D. The original plan was modified and the spaces that had been once used for a particular function later served different functions, the floor layers were raised considerably higher than those of the first edifice, and old apertures (doors and windows) were often sealed.

Even a spectacular *Opus sectile* and polychrome mosaic floors were covered by a plain surface composed of packed earth, clay and cement, often a top rubble from collapsed roofs.

Some of the flooring that followed the original scheme appear to have been constructed making use of re-utilized bricks or with a layer of lime that revealed trace of hearths.

The original walls, pillars and columns were elaborately painted and decorated with molded "stucco". The most common motifs centered upon sacred and mythological themes, while images of animals and plants abounded too.

Several kinds of construction techniques have been identified at the villa. The three most ancient of these are known as: i) *opus caementicium*, ii) *opus quadratum* and iii) a technique that made use of sandstone blocks.

Fig. 3.4 - Archaeological structures built with sandstone and limestone blocks.

- *Opus caementicium* was broadly employed in vaults and the cores of walls; it is identified by small blocks of local limestone and sandstone that were bonded with a mortar consisting of lime, sand, and cocciopesto (crushed terracotta).
- *Opus quadratum* was made using squared blocks of local limestone and sandstone.
- The third and most common technique saw the use of small blocks of local sandstone with regular shapes, but different sizes, that were set into cement cores in horizontal rows, forming regular planes.

Furthermore have been recognized the *Opus latericium* (also known as *opus testaceum*) and the *Opus vittatum* which consisted of alternating rows of sandstone blocks and bricks that were set into *opus caementicium* cores.

During the early Medieval period the *Opus africanum* construction technique was utilized, while later in the Middle Ages limestone blocks were used with or without mortar.

The earliest known archaeological work has been conducted within the villa between 1959 and 1960. This campaign led to an understanding of the architecture of the villa complex and the most of the excavation work reached the paved levels, for the most part mosaic.

Further research took place between 1979 and 1980, in order to consolidate and conserve what had been exposed twenty years earlier (fig. 3.5).

Fig. 3.5 - The archaeological structures consolidated in 1979-1980.

More recent works, begun in 1994, intended to document the site in a more complete manner and install facilities in order to make the entire archaeological site accessible to the public. A fence was installed around the whole site (fig. 3.6A) and a number of severely damage portions of the villa that are in contact with the sea, have been restored (fig. 3.6B).

A

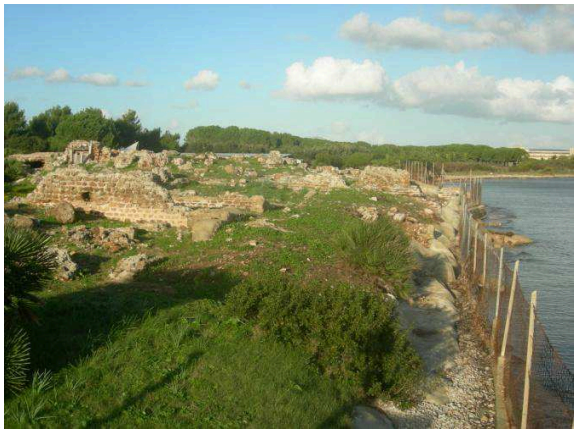

B

Fig. 3.6 - A) Fence installed around the site. B) Stabilization of the structures directly in contact with the sea.

The archaeological campaigns have brought to light 49 different spaces, which are located along 133-meter long stretch of the coast (fig. 3.7), where are recognizable: the residential portion (*pars urbana*), the small bath complex (*pars calida*) and the working area (*pars rustica or frumentaria*).

Despite their complete or partial submersion in the sea, many individual rooms have been identified as residential spaces, while the function of other rooms has not been determined - perhaps they served as baths or utilitarian space.

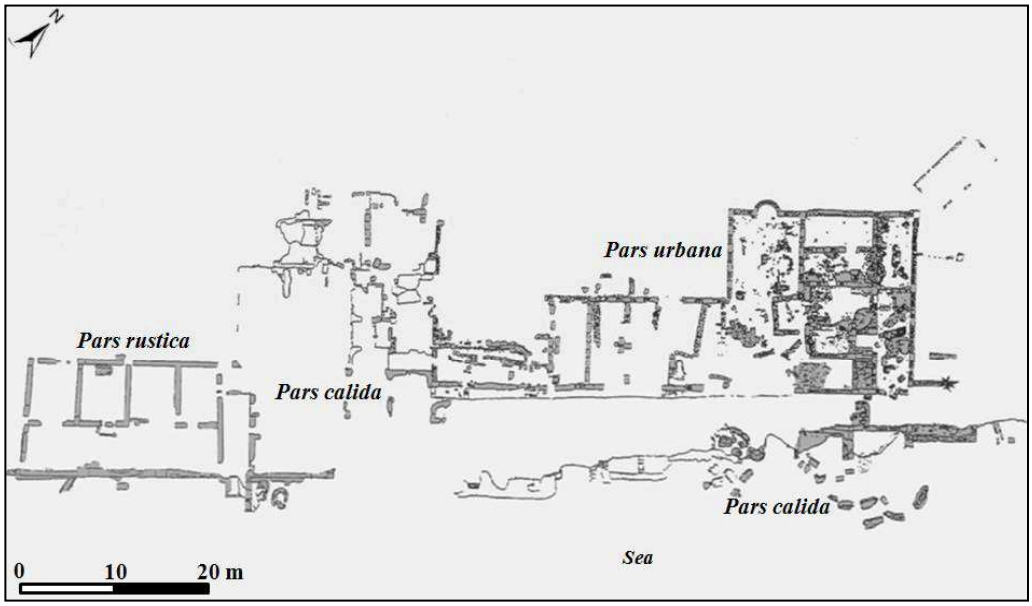

Fig. 3.7 - Excavation map showing archaeological relics.

3.3 - Objective of geophysical surveys

In order to delineate the areas for further archeological excavations, a multi-method geophysical survey was carried out in north-east portion of Sant'Imbenia Roman villa, with the collaboration of Superintendence of Archaeological Heritage for Sassari and Nuoro provinces, the University of Sassari and the Center for GeoTechnologies of Siena University.
The aims of this project are:

- Identify the buried structures whit electromagnetic (GPR) and electric (ERT) surveys in an archaeological site close to the shore.
- Compare the models obtaining by both methods in order to assess their effectiveness in defining the targets of interest.
- Provide to archaeologist an useful tool for further targeted surveys.

The methods have been chosen according to the requirements archaeological area to be investigated, hypothesizing the type, size and depth of the buried targets to detect.

3.4 - GPR surveys

An unexplored area of approx. 700 m^2 adjacent to the excavations was investigated with electromagnetic method (fig. 3.8A).

These surveys were conducted in reflection mode using a monostatic GPR (Ground Penetrating Radar) IDS model "RIS_MF_HiMod", composed of a control unit (DAD control unit Fast Wave) working simultaneously with two transmitters (Tx) 200 and 600 MHz and two receivers (Rx) (par. 2.2).

The complete coverage of the area was performed by regular grid 34x22 metres, with 68 transverse (T) and 44 longitudinal (L) lines, (fig. 3.8B) running acquisition every 50 cm. The extremes of the investigated area were spatially located using a GPS "Leica TM Viva".

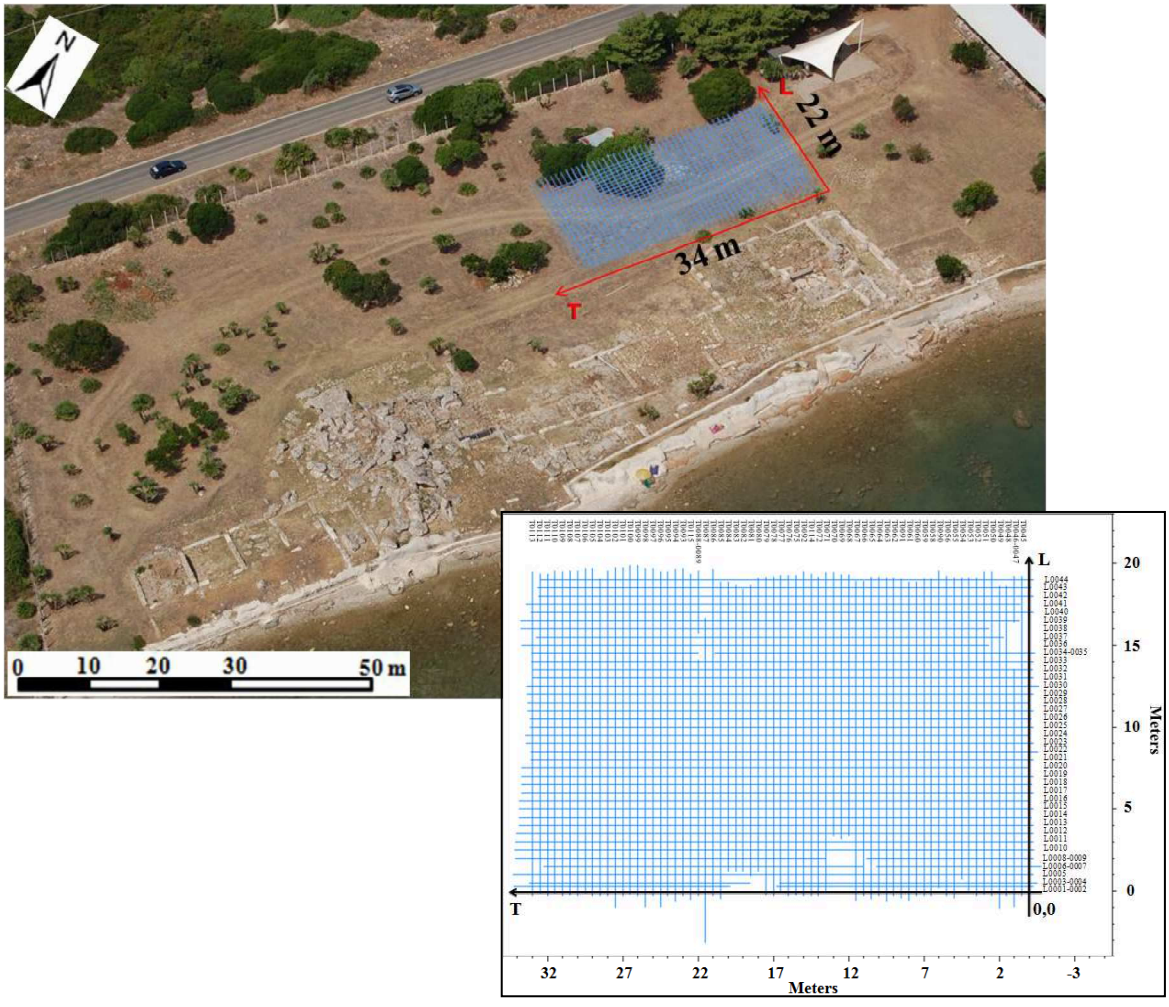

Fig. 3.8 - A) Location of GPR investigations in the field. B) Detail of GPR survey grid.

3.4.1 - Data processing and interpretation: B-scan

The GPR data were processed by the software 2D GRED Basic v. 02.01.008 (IDS Ingegneria dei Sistemi) using several options described in paragraph 2.3 as: "Move start time"; "Background removal", "Vertical band pass filter", "Gain adjustments" (smoothed gain) (GRED, 2008).

The graphical result for each acquisition line is a 2D radar cross-section (B-scan) or radargram, where the longitudinal axis (*x-axis*) corresponds to the length of the profile, while the vertical axis (*y-axis*) corresponds to the depth of investigation proportional to propagation speed of the electromagnetic waves through the medium.

In figures 3.10 and 3.11, are shown six representative B-scans, three transverse and three longitudinal (fig.3.9) of the investigated area.

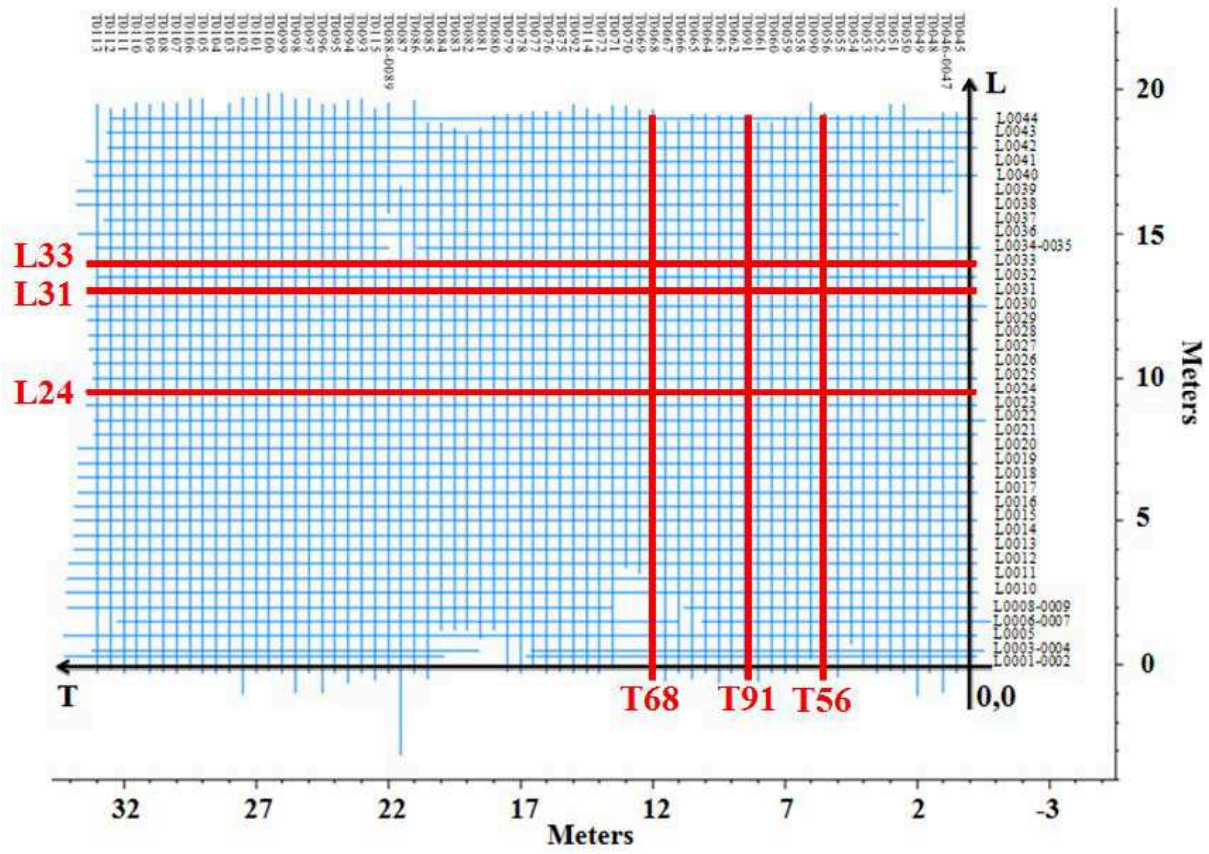

Fig. 3.9 - GPR survey grid. The red lines show the following B-scan (fig. 3.10 - 3.11).

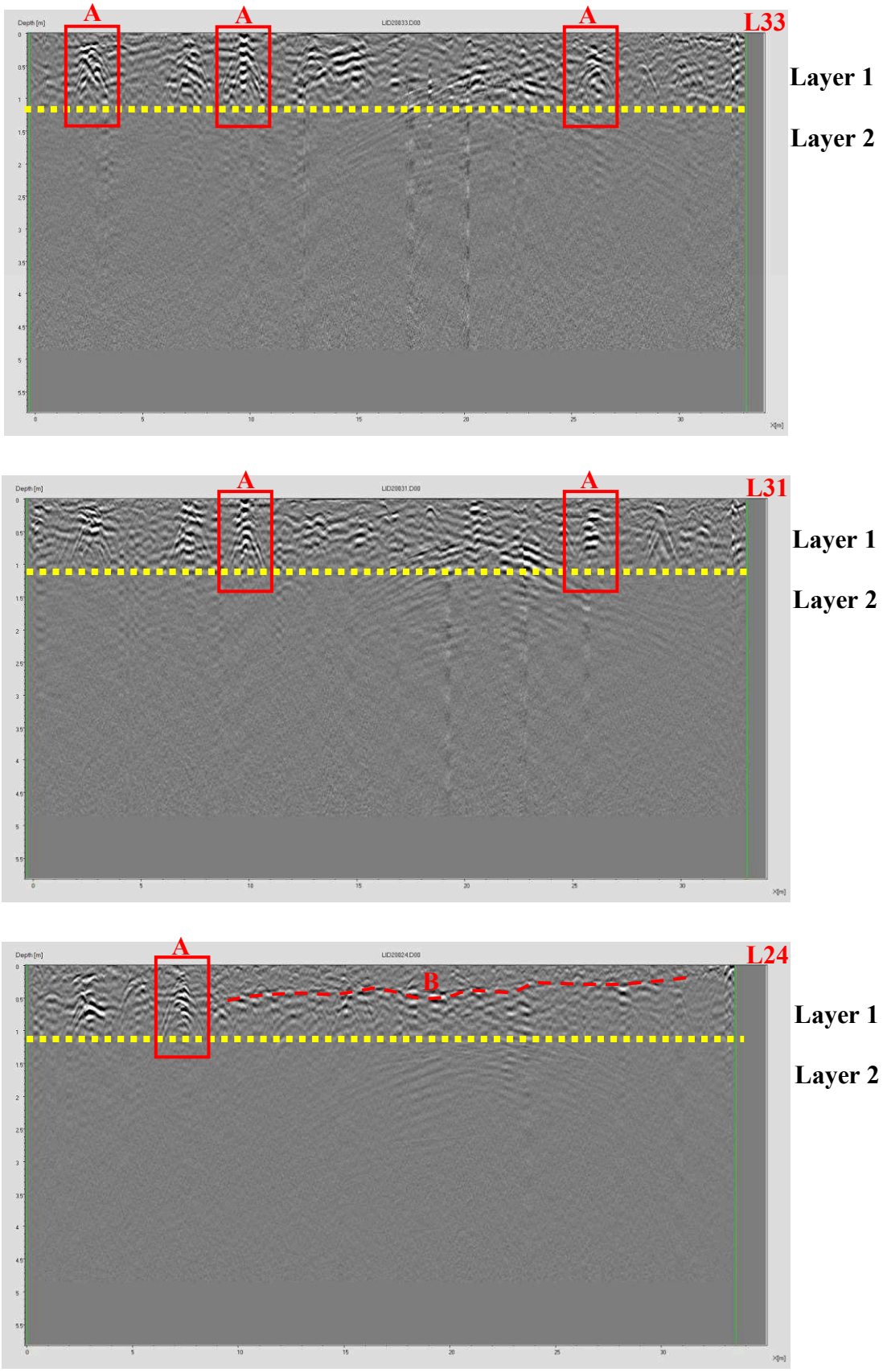

Fig. 3.10 - Longitudinal GPR B-scans carried out using a 200 MHz transmitter, which reveals the different anomalies. Anomalies A are vertical targets, while anomalies B indicate the continuous targets.

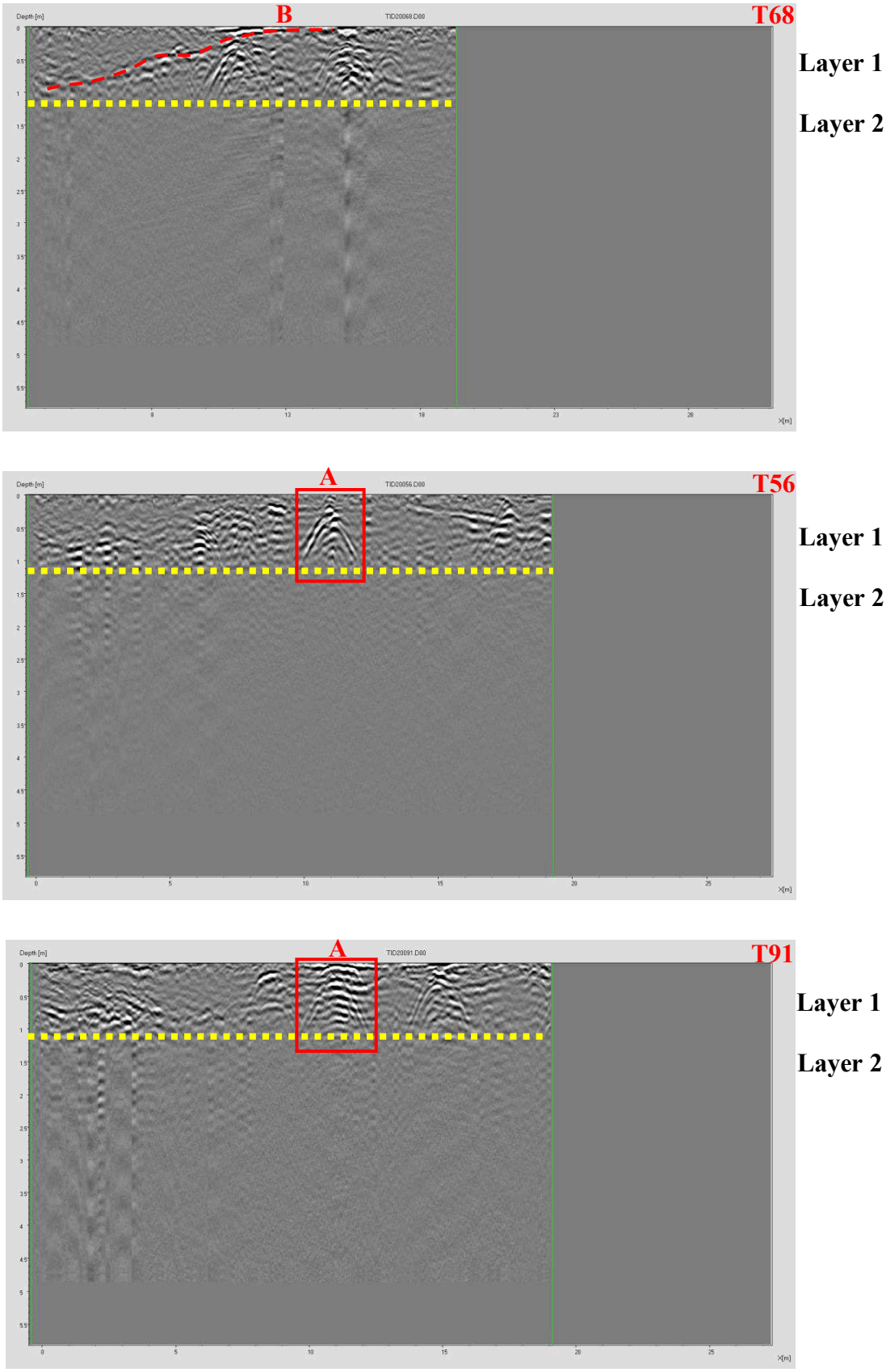

Fig. 3.11 - Transverse GPR B-scans carried out using a 200 MHz transmitter, which reveals the different anomalies. Anomalies A are vertical targets, while anomalies B indicate the continuous targets.

In all B-scans are detected two distinct levels. The first level shows anomalies indicating the presence of man-made buried structures and ranging from the surface to 1 meter deep.
In the second level (beneath 1m depth) the strong attenuation of electromagnetic waves is probably due to high moisture conditions that do not allow recognizing any targets, and the signal-to-noise ratio results to low to give any information.
In the first level, two types of anomalies can be distinguished:

- Single anomalies: are marked by typical hyperbolic shape (target A fig. 3.10 - 3.11) which suggests the presence in the site of well-defined single buried walls, with regular shape and disposed transversely to the data acquisition line.
  The presence of buried walls causes a strong anomaly in electromagnetic waves propagation, owing to the difference in the conductivity values between the man-made structures and the ground surrounding.
  In the hyperbolic signals, the radius of curvature at the peak and the length of the asymptotes give the size of the object causing it.

- Continuous anomalies: are identified by an elongated shape (target B in fig. 3.10 - 3.11) and can be ascribed to different types of buried structures: i) close together walls arranged in a chaotic form (collapsed structures or stone-filled chambers); ii) discontinuity surfaces (transition between two surfaces with different conductivity) as the limit of two level described above iii) may represent situations where survey lines are aligned parallel to linear structures of buried relicts.

The similarities between the detected anomalies and the repetitive appearance in successive profiles allowed us to assume here the presence of several buried walls in longitudinal and transverse directions.
Figure 3.12 shows, as a example, the L33 radargrams acquired with the two different frequencies (200 and 600 MHz), in order to revealed the presence of comparable signals but with different resolution.
Lower frequency antenna (200MHz) with long wavelength provides the deepest penetration (1 meter) but shows a minor resolution at shallower depth.
Conversely higher frequency antenna (600 MHz) with short wavelengths have shallower penetration depths (0,80 meters), and therefore offer better resolution in definition of detected signals.

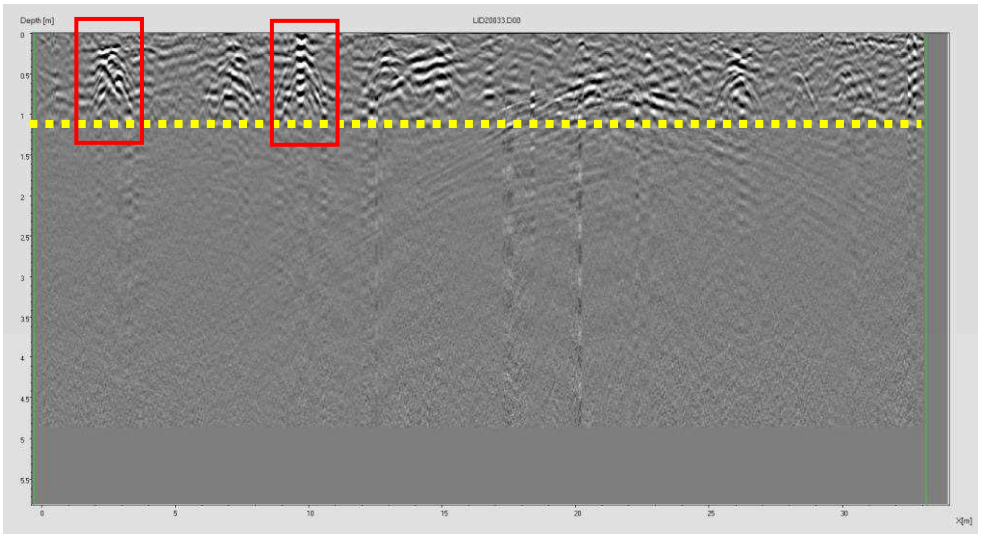

200 MHz

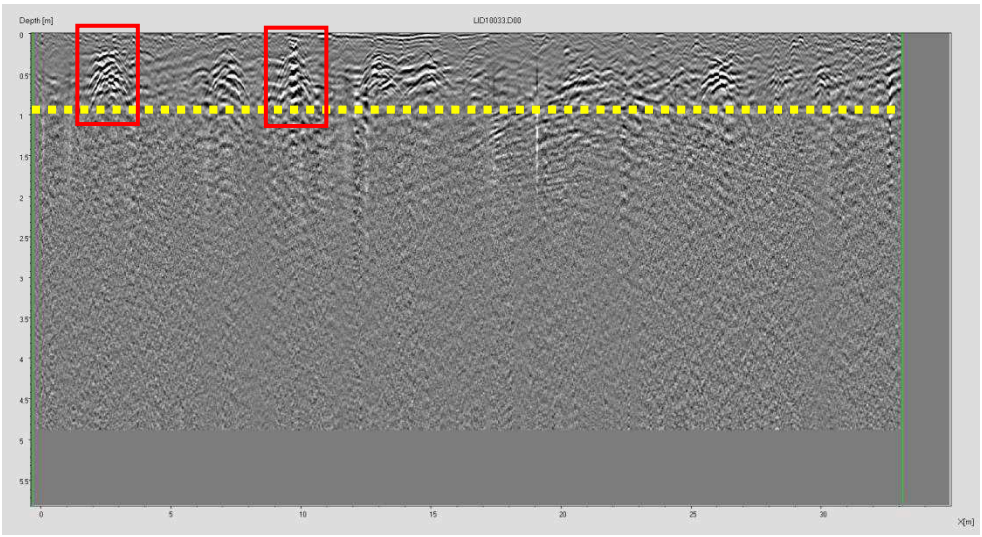

600 MHz

Fig. 3.12 - GPR profiles carried out with 200MHz and 600MHz transmitters.

3.4.2 - Data processing and interpretation: C-scan

By interpolation of the longitudinal and transversal B-scans, through the software GRED IDS, has been possible to create the radar time slices at different depths or C-scans (par. 2.3).
The three dimensional view of GPR traces is very useful for show the aerial distribution of the traces of buried archaeological relics in the investigated site.
Targets of interest are generally easier to identify and to isolate on three dimensional data set than on conventional two dimensional profile lines.
The C-scan presented following shown the presence of buried targets (orange-red in colours), clearly visible in the shallow layers (fig. 3.13 -3.14).

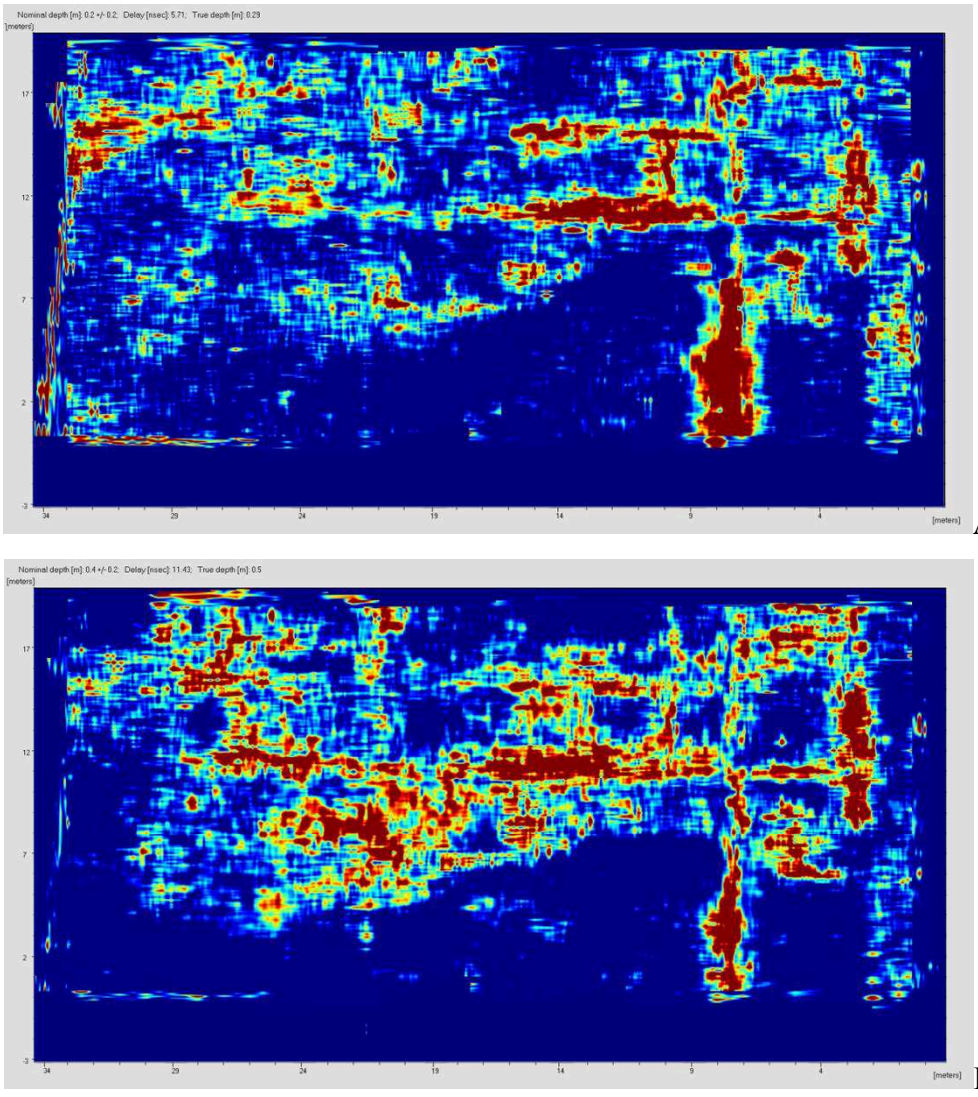

Fig. 3.13 - Radar time slice or C-scan at different depth. A) Depth 0,29 meter. B) Depth 0,5 meter.

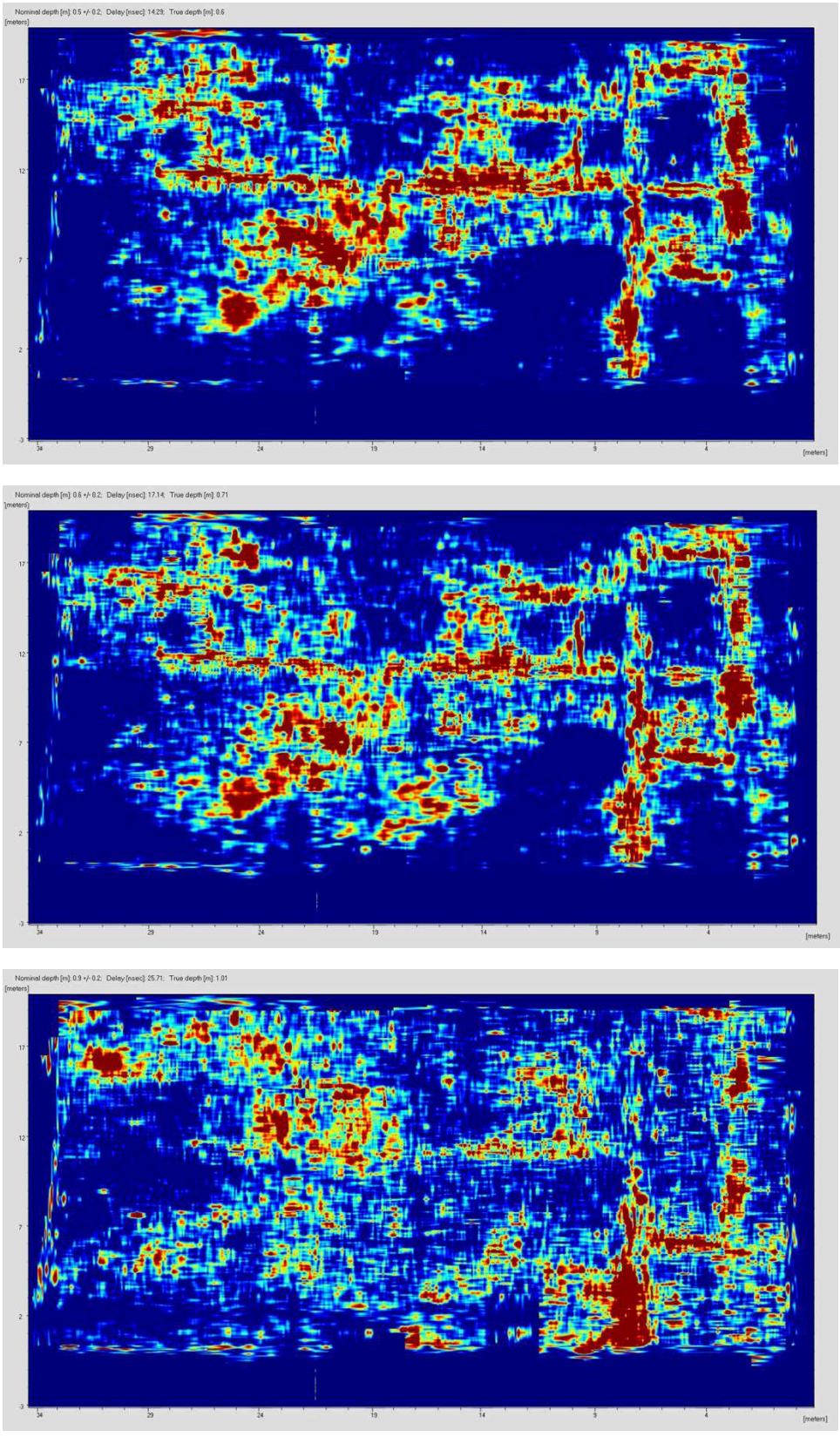

Fig. 3.14 - Radar time slice or C-scan at different depth. A) Depth 0,6 meter. B) Depth 0,71 meter. C) Depth 1,01 meter.

In the C-scan at 0,6 m in deep (fig. 3.15), anomaly trend with regular distribution are well evidenced. These anomalies exhibiting a band-like shape of criss-cross lines, suggesting oriented buried obstacles that probably represent the walls arranged both transversely and longitudinally to enclose of the rooms. Instead, when the anomalies show chaotic reflections might be supposed the presence of collapsed walls or stone-filled chambers.

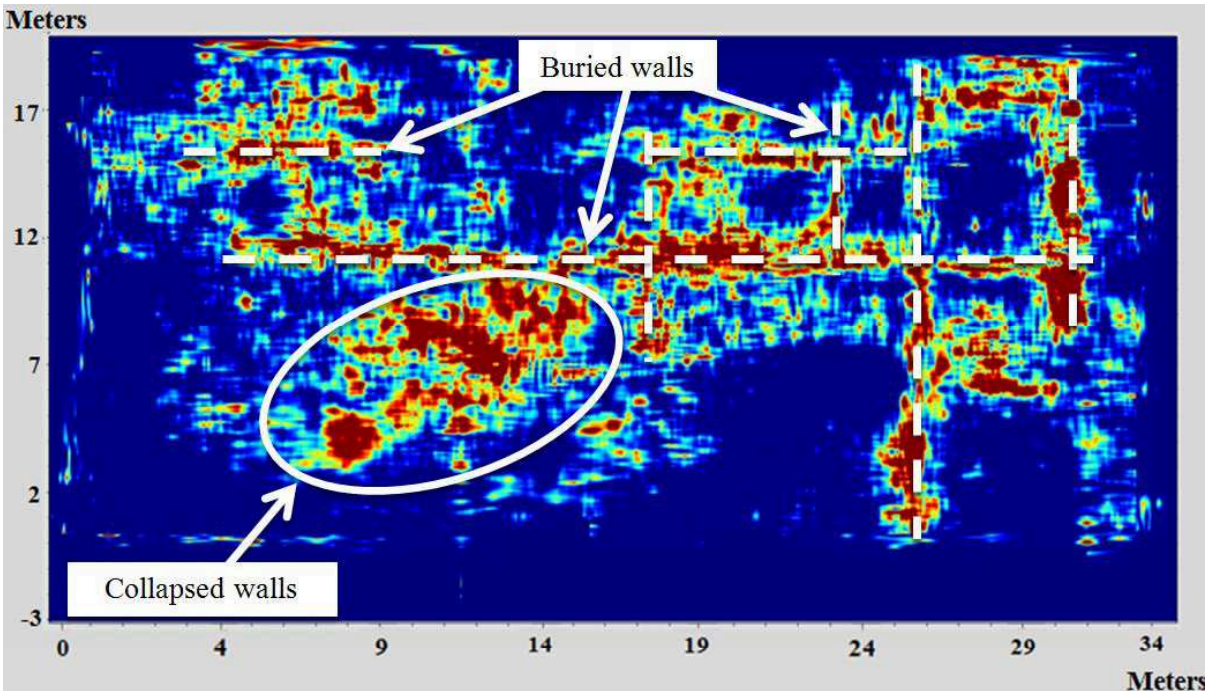

Fig. 3.15 - Radar time slice or C-scan at 0,6 meter in depth which is evident the alignment of buried structures.

3.5 - Electrical resistivity survey

The geoelectrical surveys were conducted by a multi-electrode system, consisting of Abem Terrameter SAS1000 control unit combined with ES 10-64 electrode selector (par.1.4).
Eight 2D electrical profiles (SW-NE oriented) were performed where GPR data have showed possible interesting targets (fig.3.16). For each 2D electrical lines, 64 metal electrodes were deployed in a straight line with constant spacing of 50 cm and a unit length of 31,5 m.
The measurements were carried out using Dipole-Dipole array ($n = 2$), sensitive to horizontal changes in resistivity and thus suitable for detecting vertical structures like walls and cavities.

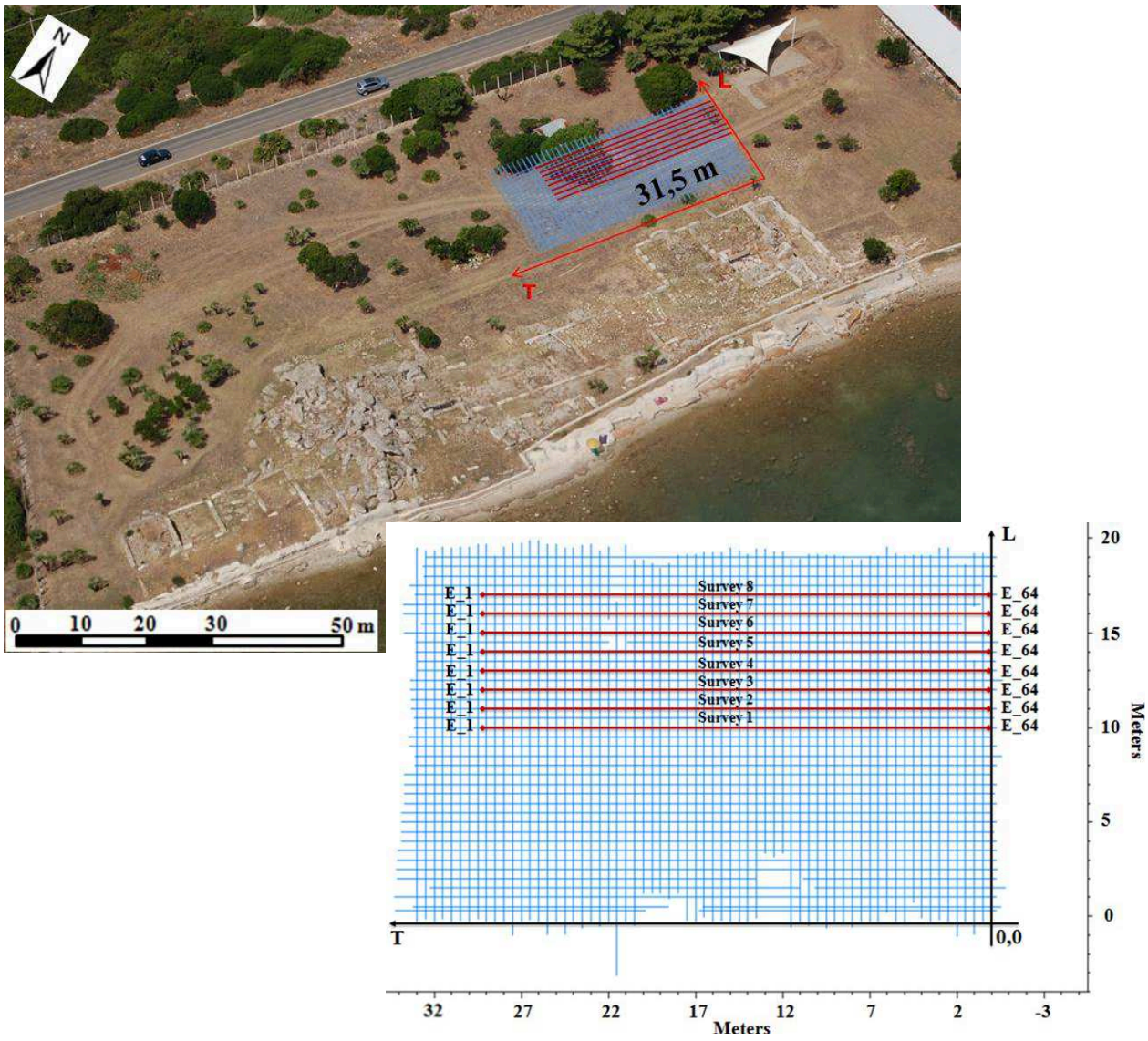

Fig. 3.16 - Location of geoelectrical survey lines respect to the GPR survey grid.

3.5.1 - Data processing and interpretation: 2D-electrical sections

The apparent resistivity values for each electrical line were downloaded from the Terrameter SAS 1000 control unit to the PC, and then were converted in a format that is acceptable by the RES2DINV inversion software (Loke, 2001).
Before performing the inversion process all acquired resistivity data have been examined and the "bad data points" have been removed in some cases manually and pre-inversion, in other cases automatically and post-inversion.
The *l1-norm* implementation (robust-constrained) of the regularized least-squares optimization methods and the finer model with the cell width of half the minimum electrode spacing were applied. The identical colours scale was chosen to represent all resistivity models (fig. 3.17 - appendix A). Good convergence between the observed and model resistivity data was achieved after five iterations as indicated by RMS error lower than 3.0% for all the profiles.
The archaeological structures with high resistivity values (greater than 60-70 Ω·m, red-purple in colour) can be clearly distinguished from the surrounding soil which has the much lower resistivity values (less than 60 Ω·m, green-blue in colour).
The anthropised shallow level (layer 1), has a thickness of approx. 1-1,2 meters and it shows resistivity anomalies both as continuous trend and as a spot with regular shape. All anomalies have high resistivity values and are ascribed to wall structures.
The conductive deeper level (layer 2) does not show the presence of man-made structures and extends approx. from 1-1,2 meters down to the maximum investigation depth.
A schematic interpretation of the main detected signals in layer 1 is reported in fig.3.18.

- **Signal T**: it has a regular shape and a width ranging between 0,5 and 2 metres. This signal, with resistivity values greater than 90 Ω·m, is presents in the shallow layer of all tomographies, to a maximum depth of 0,8m. Particularly, T1 and T2 signals, at the stations at 29m and at 24m (*x-axis*) respectively, recur in all tomographies and represent two continuous walls transverse respect to the acquisition lines
- **Signal L**: it has an elongated shape in x-direction and variable length between 6 and 20 meters. This signal, with resistivity values greater than 80 Ω·m reaches the maximum depth of 0,8 m.
- **Signal C**: it is detect in 1, 2 and 5 tomographies. The regular geometry and resistivity values (50-70 Ω·m) suggest the presence of a cistern filled by collapsed materials.

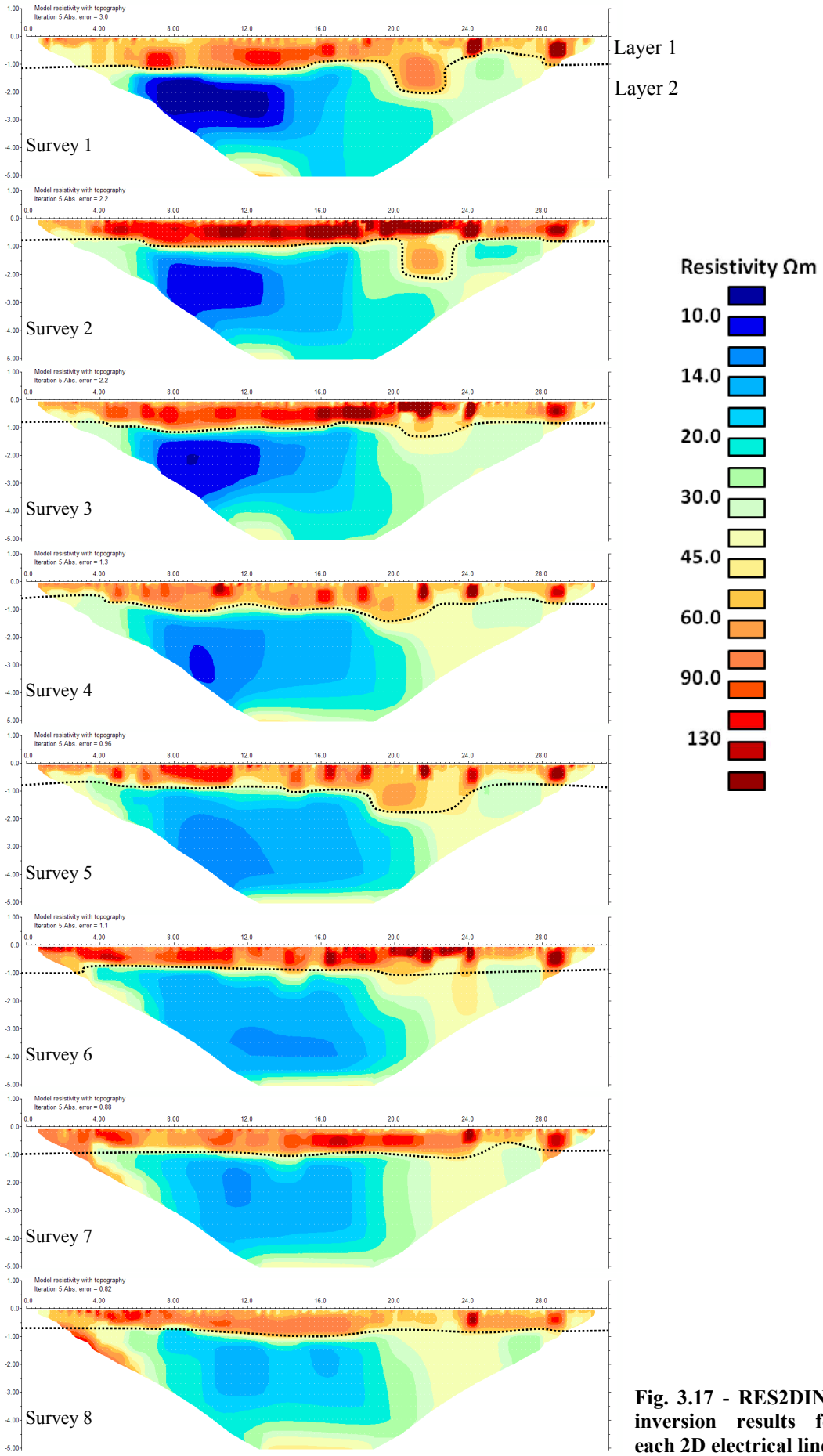

Fig. 3.17 - RES2DINV inversion results for each 2D electrical line.

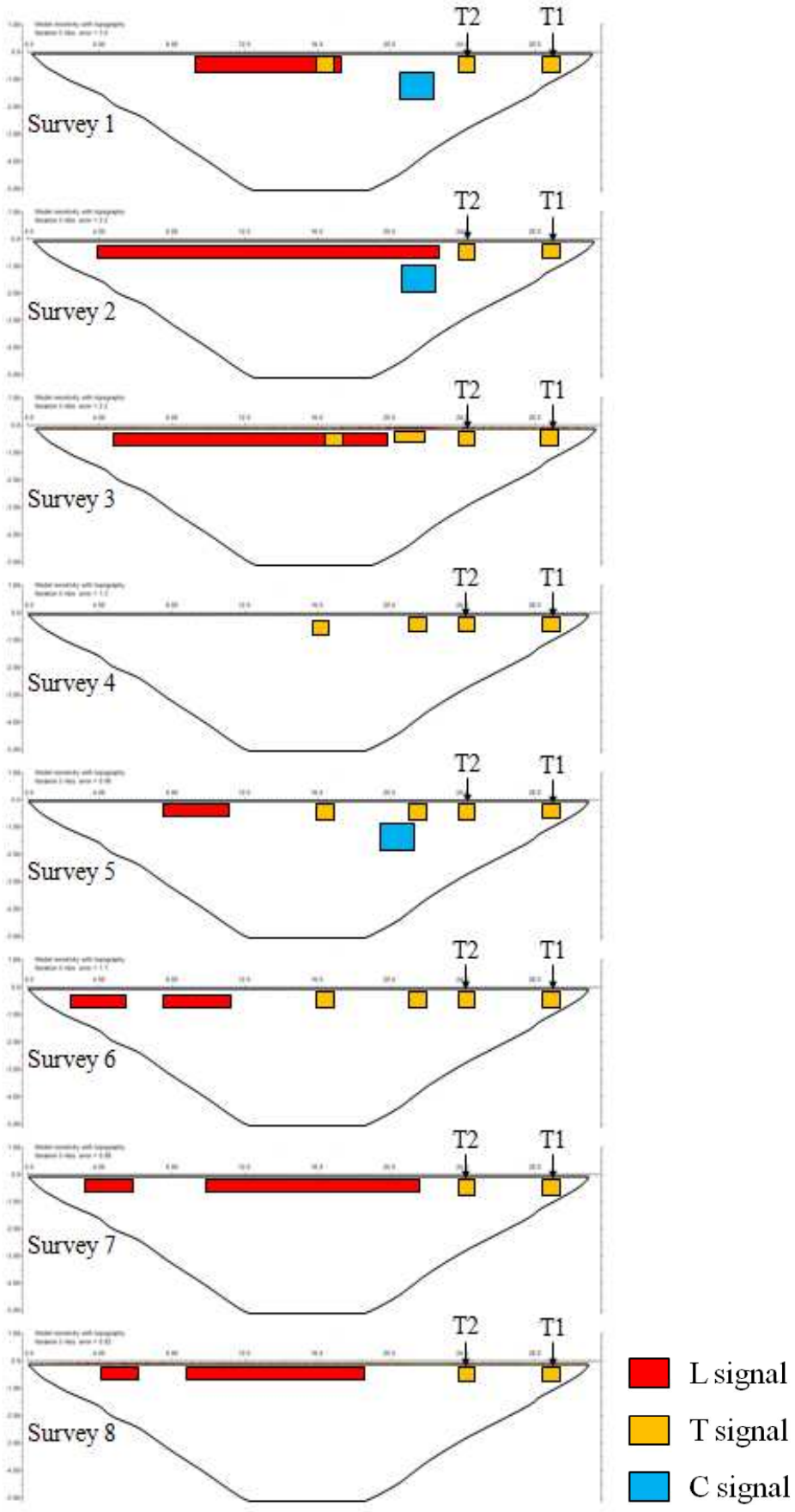

Fig. 3.18 - Schematic interpretation of the main detected signals in layer 1 for each 2D electrical lines.

In layer 2 is detected a anomaly conductive lens, with resistivity values less than 10 Ω·m, which tends to shrink proceeding from 1 to 8 surveys (from the sea to inland) (fig.3.17).

The surveys 1 and 2, performed in December, have been repeated in April (fig. 3.19), confirming the presence of conductive lens.

In April, this lens shows resistivity values higher (greater than 15 Ω·m) than the previous.

This data evidence that the seasonality and the proximity to the sea play a key role on the degree of soil saturation and the electrical response of the medium.

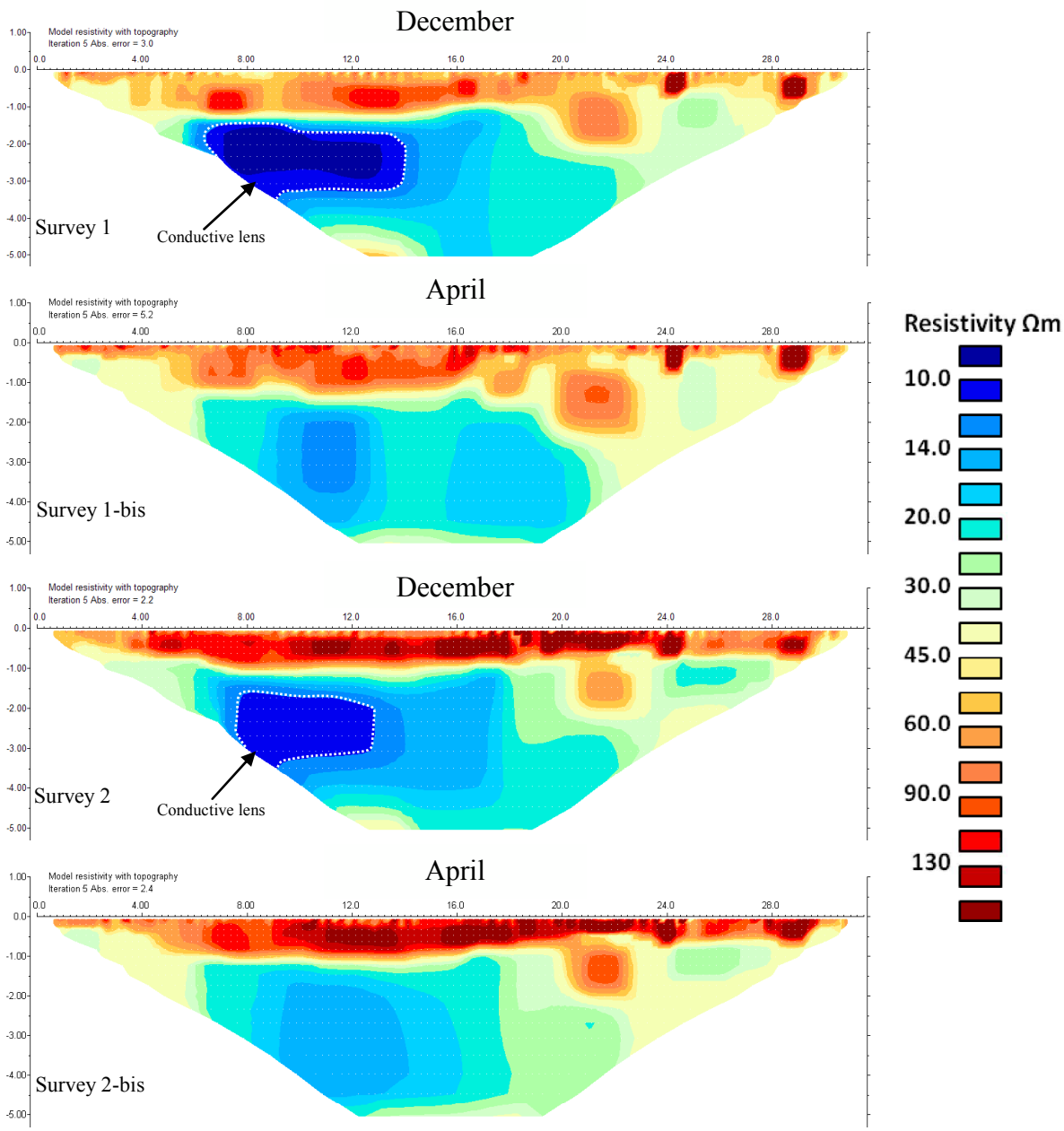

Fig. 3.19 - Comparison of electrical resistivity tomographies carried out at different times.

3.5.2 - Data processing and interpretation: 3D-horizontal depth slices

To produce a single 3D data set, all 2D survey data files were rearranged using option entitled "collate data into Res3dinv format" in the file menu of RES2DINV software.
Data integration gave rise a grid size of 64 x 8 electrodes in the x-and y-direction respectively, and it provided 8860 data points.
The collated 3D data set were inverted using RE23DINV computer code (Loke and Barker, 1996), which automatically produces the subsurface horizontal depth slices.
The 3D data set were inverted using *l1-norm* implementation of the regularized least-squares optimization method, and the forward problem was solved using the finite element method (Silvester and Ferrari, 1990).
To reduce the inversion time, the Incomplete Gauss-Newton method with a convergent limit of 0,012 was used and the Jacobian matrix was recalculated for all iterations.
We used a model blocks where the top three layers are divided by half in the horizontal directions.
Good convergence between the observed and model resistivity data was achieved after six iterations as indicated by an RMS error misfit of 2.56%.
The final 3D resistivity model consist of 16 layers in the vertical directions, resulting in a total of 7056 model cells.
In figure 3.20 8 resistivity horizontal depth slices between 0 and 2,40 meters from ground level are shown.
This model, also called 2,5D, provide an overview of the complete spatial structures in the subsurface and facilitate the reconstruction of the environments.

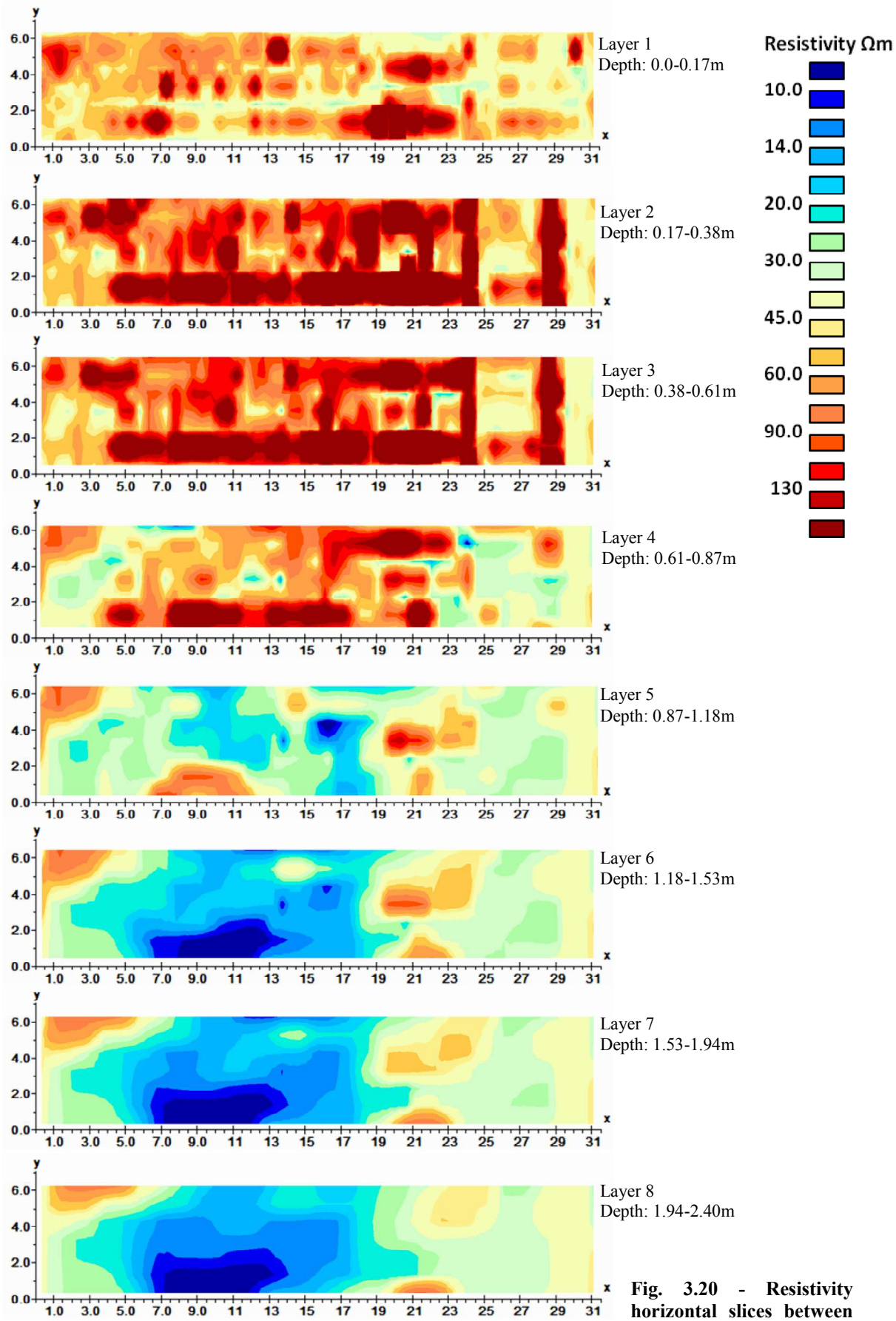

Fig. 3.20 - Resistivity horizontal slices between 0 and 2,40 meters from ground level.

Particularly, in the resistivity horizontal depth slice to a depth between 0,38 and 0,61m (fig. 3.21) are clearly discernible alignments of walls arranged transversely and longitudinally to the acquisition data lines.

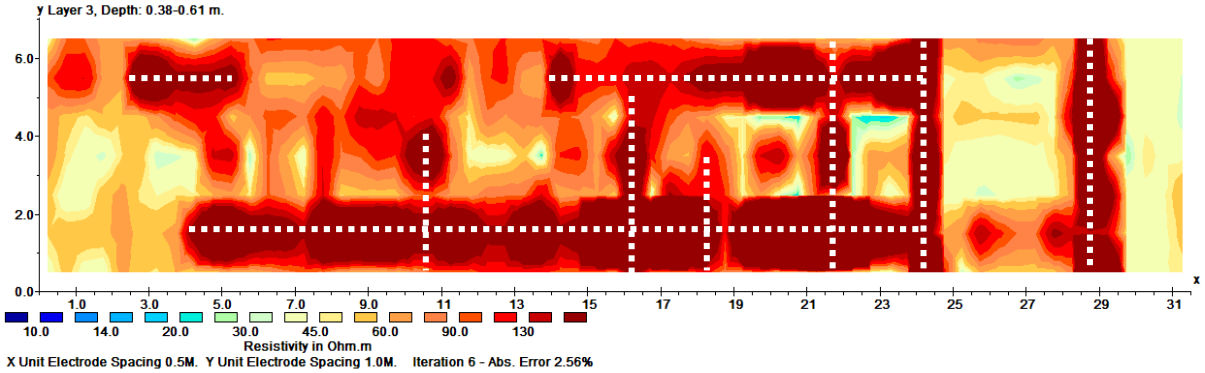

Fig. 3.21 - Resistivity horizontal slice to a depth between 0,38 and 0,61m.

Another electrical data processing was performed using the RockWorks software ver.2009.3.23. for 3D representation (fig. 3.22).

In this case, the resistivity values of the man-made buried structures were isolated, in order to obtain a more clearly definition of the wall structures and of the environments enclosed from these.

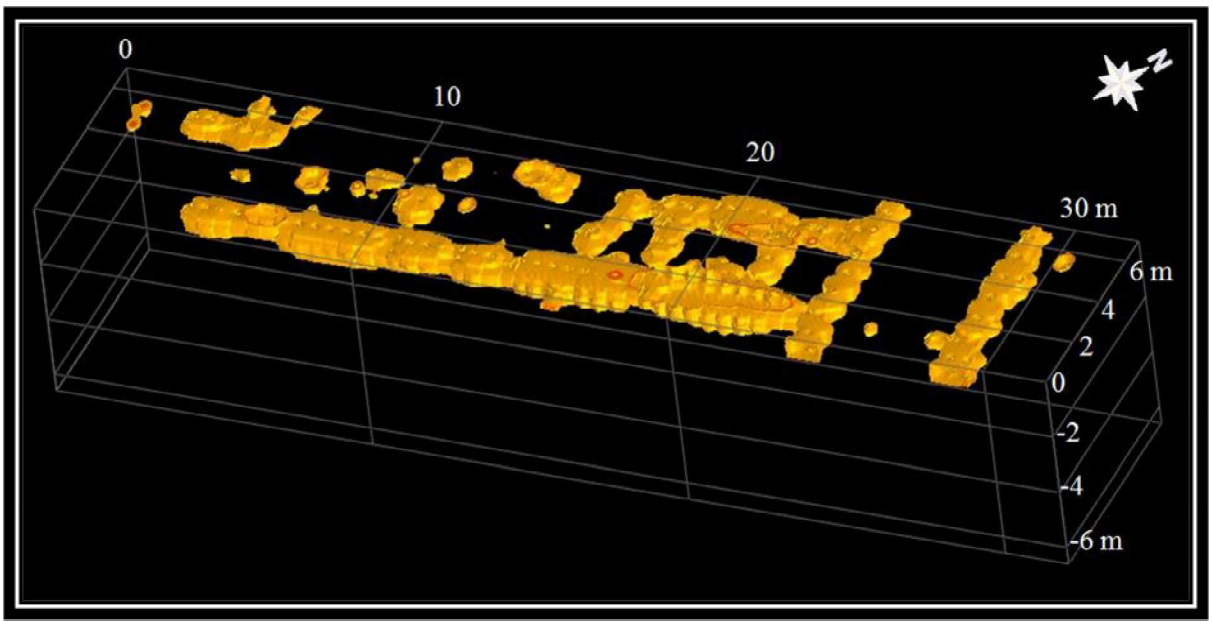

Fig. 3.22 - RockWorks visualization whit resistivity anomalies (ρ = 130Ω·m) related to buried structures.

3.6 - Integration and comparison between the two methodologies.

The comparison among the models shows a good correlation between the different signals, reducing the uncertain typical of indirect methods (fig.3.23).

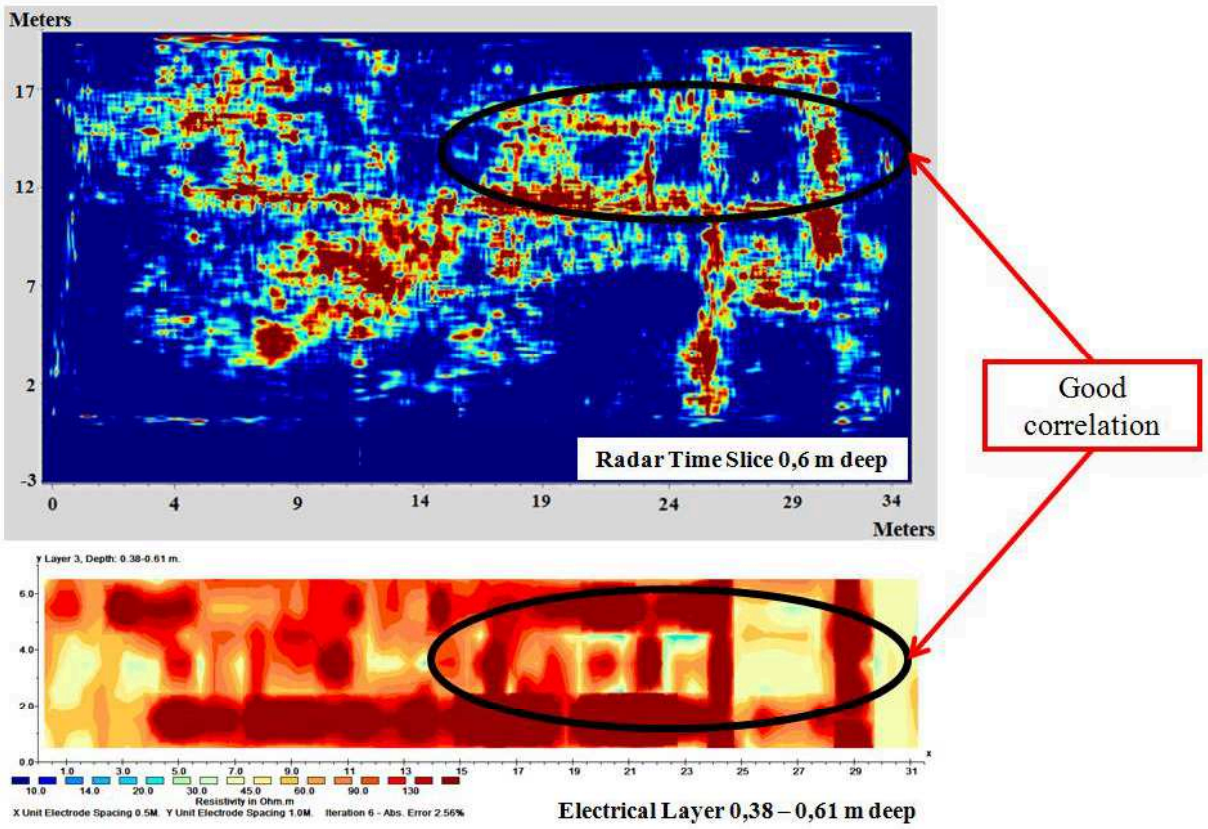

Fig. 3.23 - Visual comparison between the different methodologies used for buried structures reconstruction.

By comparison between the two applied methods we can say that:

- The radar acquisitions have proved as a expeditious investigation technique that gives accurate information about the spatial arrangement of the targets.
  In Sant'Imbenia archaeological site we scanned a surface area of approximately 700 m^2 in two days with this method. The radar scans have allowed us to investigate down to the maximum depth of 1 meter, in fact, only the electromagnetic features of the first level have allowed to detect the targets with high resolution.
  Beneath the first level, the conductive values have caused a strong attenuation of electromagnetic signal and a loss of information.

- The electrical resistivity acquisitions are relatively slower than radar acquisitions, in fact the eight electrical tomographies have required a working week to cover a surface of 256 m^2. In all tomographies has been reached the investigation depth of 5 meters, related to the length of the acquisition line.

  The high resistivity contrasts in the subsoil have allowed a clear identification of buried man-made structures respect to conductive zone at the deepest level.

3.7 - Discussion and conclusions

The application of geophysical methods in Sant'Imbenia archaeological site helped in defining the depth, vertical extension, location, thickness of buried walls.

The good performance of these techniques was facilitated by physical property contrasts generated by the buried targets, with respect to the surrounding medium.

The measured resistivity values allocated to buried walls (ρ > 60-70 Ω·m) are compatible with resistivity values of the rocks constituents the adjacent walls highlighted by the excavations (limestones and sandstones).

The comparison between the results evidenced a good correlation between the electrical and electromagnetic models on the same targets.

This study showed that the combined usage of electromagnetic imaging and resistivity tomography techniques in archaeological prospection studies yields more information upon which archaeologists can base further investigations of the site.

The models in figure 3.24 evidenced that the residential area (*pars urbana*) stretches inland.

In addition, the particular arrangement of the architectural remains suggest the presence of an inner courtyard that is typical of many Roman villas.

Trial trenches and soundings should be planned during future campaigns in order to verify the subsoil structures issued from the geophysical surveys.

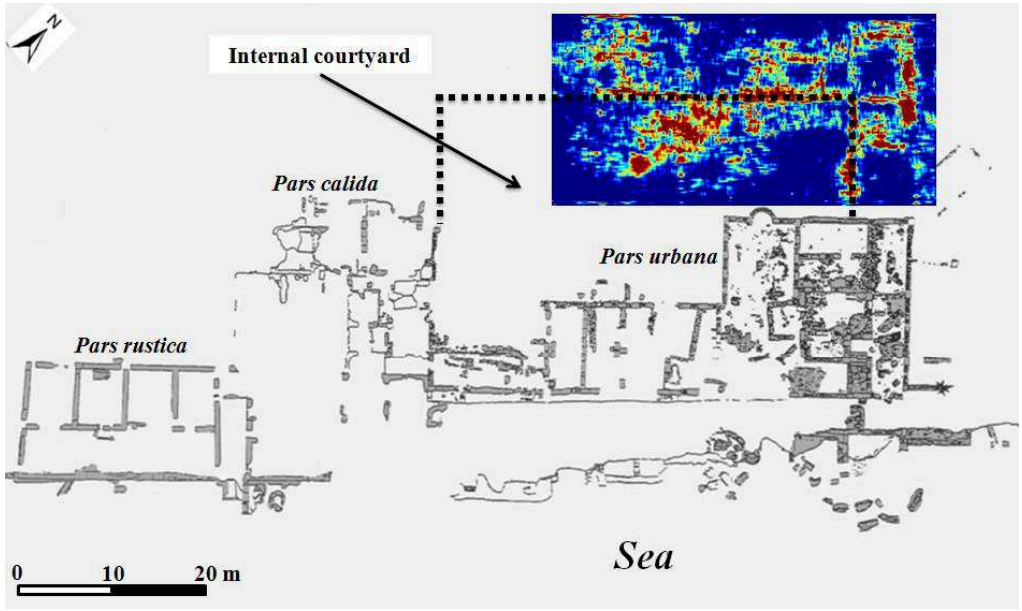

A)

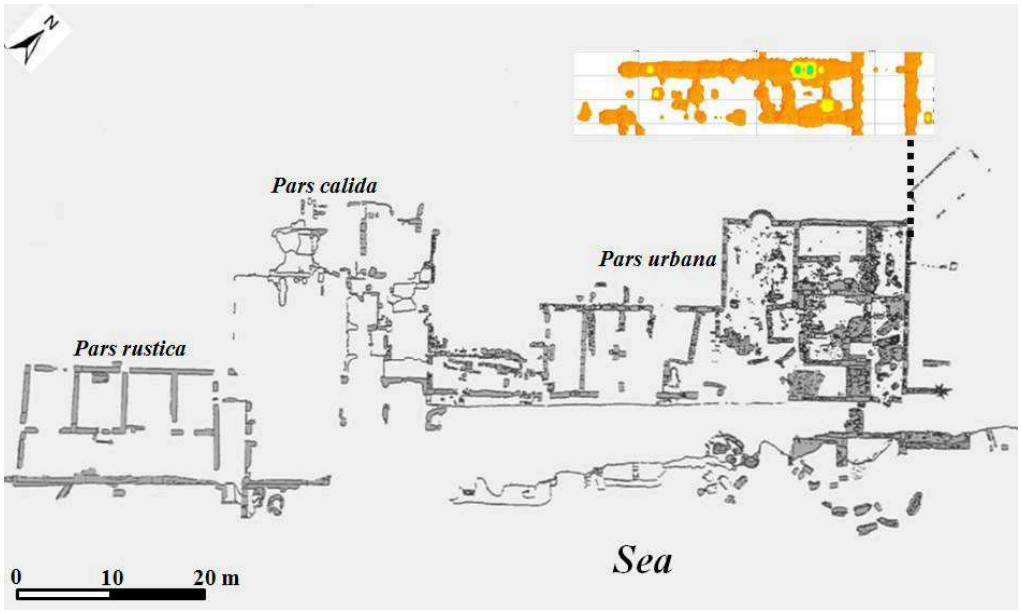

B)

Fig. 3.24 - Geophysical models plotted in plant of excavations. A) GPR model. B) Electrical resistivity model.

References

CARMIGNANI, L., OGGIANO, G., BARCA, S., CONTI, P., SALVADORI, I., ELTRUDIS, A., FUNEDDA, A., AND PASCI, S. 2001. *Geologia della Sardegna - Note illustrative della Carta Geologica scala 1:200000. Memorie Descrittive Carta Geologica d'Italia,* LX, 283.

GHIGLIERI, G., OGGIANO, G., FIDELIBUS, M. D., ALEMAYEHU, T., BARBIERI, G., AND VENIER, A. 2009. *Hydrogeology of the Nurra Region, Sardinia (Italy): basement-cover influences on groundwater occurrence and hydrogeochemistry.* Hydrogeology Journal, 17, 447-466.

GRED ver. 02.01.008, *Manuale Utente*, IDS Ingegneria dei Sistemi, Italia, 2008.

LOKE, M.H., 2001. *Res2Dinv software users manual, version 3.4.* Geotomo Software, Penang, Malaysia, 98.

LOKE, M.H., and BARKER, R.D., 1996. *Rapid least-squares inversion of apparent resistivity pseudosections by a quasi-Newton method.* Geophysical Prospecting, 44, 1, 131–152.

MAMELI, P., MONGELLI, G., OGGIANO, G. AND DINELLI, E., 2007. *Geological, geochemical and mineralogical features of some bauxite deposits from Nurra (Western Sardinia, Italy): insights on conditions of formation and parental affinity.* International Journal of Earth Science, 96, 887-902.

MANCONI, F., 1999. *The Roman Villa of Sant'Imbenia - Alghero.* Soprintendenza Archeologica per le province di Sassari e Nuoro. Betagamma editrice.

PECORINI, G., 1969. *Le Clavatoracee del "Purbeckiano" di Cala d' Inferno nella Nurra di Alghero (Sardegna nord-occidentale).* Bollettino della Società Sarda di Scienze Naturali, 5, 1-14.

SILVESTER, P.P., AND FERRARI, R.L., 1990. *Finite elements for electrical engineers (2nd. ed.).* Cambridge University Press, 516.

Chap. 4 - Ground Penetrating Radar and Geoelectrical Surveys to investigate the Santa Filitica Archaeological Complex (Northern Sardinia)

4.1 - Introduction

Based on the archaeological evidences, we decided to investigate, with Ground Penetrating Radar (GPR) and Electrical Resistivity Tomographies (ERTs), an unexplored area adjacent to the excavations at the monumental complex of Santa Filitica (Sorso, SS).
Of great interest was to test the performance of the two methodologies in this coastal and multilayered archeological site, consequently more complex than Sant'Imbenia site examined in chapter 3.

4.2 - Site location and archaeological features

The Santa Filitica archaeological complex is located on the Asinara Gulf shore in northern Sardinia, at the eastern edge of a wide fertile plain characterized by Miocene-aged carbonate and siliciclastic sediments and bounded by a mainly andesitic volcanic relief.
It lies along the road between the Roman colony of *Turris Lybissonis* (Porto Torres) and the Roman town of *Tibula* (between Castelsardo and Santa Teresa di Gallura) (fig.4.1).

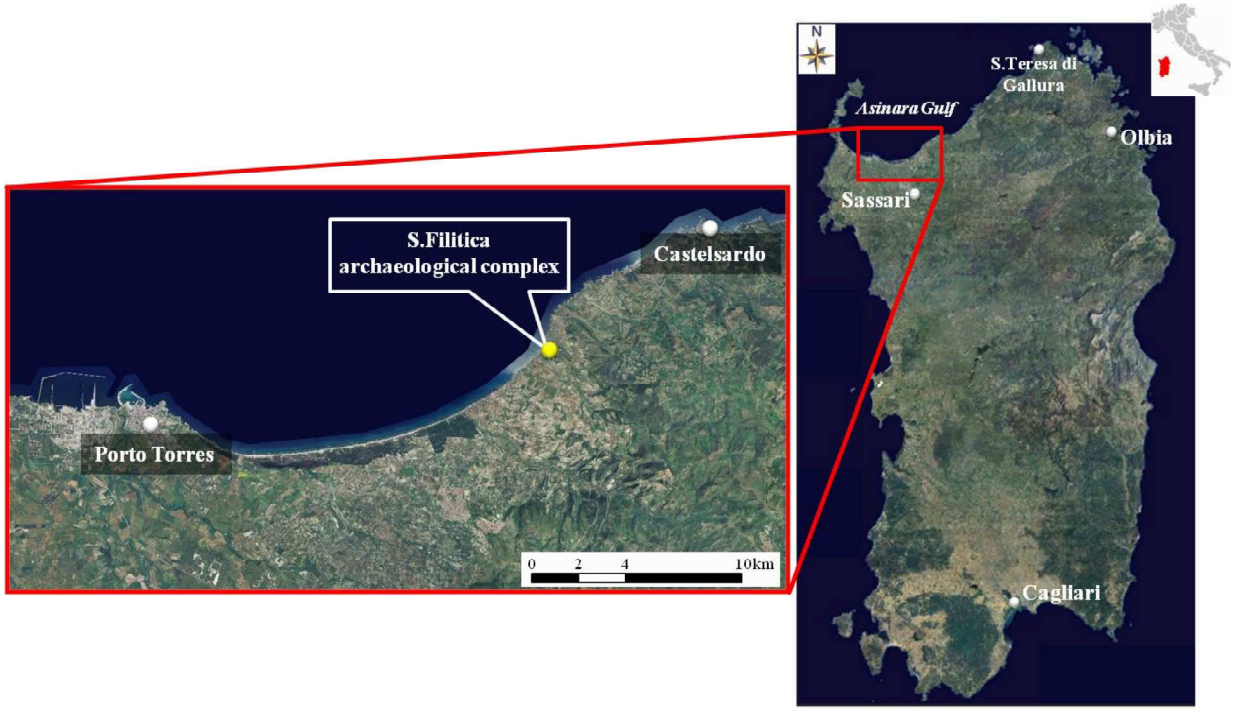

Fig. 4.1 - Location map of Santa Filitica archaeological complex.

In the site the archaeological remains are clearly visible from long time. In fact, the first archaeological investigations were undertaken in 1980, starting from an emergency excavation after the discovery and the theft of part of a mosaic floor revealed by leaching of the slope next to the beach.

Santa Filitica is a multilayered archaeological complex, consisting of the remains of an imperial Roman villa, a settlement to V-VI century A.D., and a village of Byzantine period, reflecting a long continuity of use of the site since at least III to the IX century A.D (Rovina, 2003).

The architectural complex extends, to the east and south, beyond the current limits of the excavation, whereas to the west the settlements ends against the shoreline.

The archaeological campaigns have highlighted 14 different spaces of the Roman villa (fig.4.2).

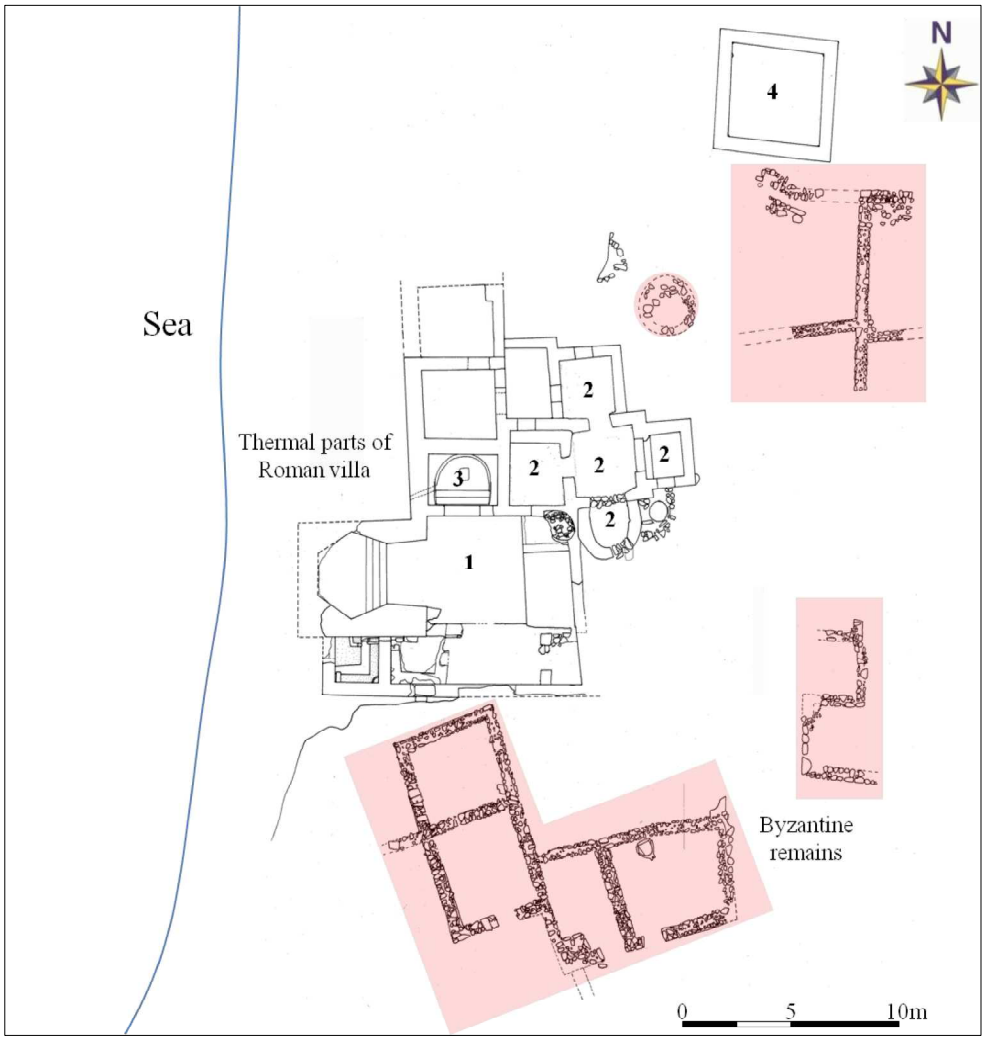

Fig. 4.2 - Excavation map showing archaeological relics, the reddish areas highlighted the Byzantine remains. In the Thermal part of the Roman villa can be distinguished: 1) *frigidarium*, 2) cruciform building, 3) heated tub, 4) cistern (Rovina et al., 1999).

These spaces form the north-western extremity of the residential part of the complex, and represent the thermal portion.

The thermae were arranged around a large rectangular room (*frigidarium* - ***1***) connected to the north with a heated tub (**3**) and a cruciform building (**2**). The cruciform building contains two large tubs and rooms with mosaic floors used to tepid baths and warm sauna.

An ideal reconstruction of thermal environments of Roman villa is reported in figure 4.3A.

The rooms were equipped with an efficient heating system, consisting of interspaces in the walls and hanging floors on pillars of bricks (*suspensurae*).

On the *suspensurae* the raised floor, consisting of large stone slabs covered by "cocciopesto" or mosaics was leaning.

The heated rooms were connected by spaces beneath the floor, in which the fires were lighted (*praefurnia*). The hot air that warmed the rooms was conveyed by openings in the empty spaces under the floors and in walls interspaces. The walls of thermal rooms remains were covered with cocciopesto and refined with plaster (fig. 4.3B).

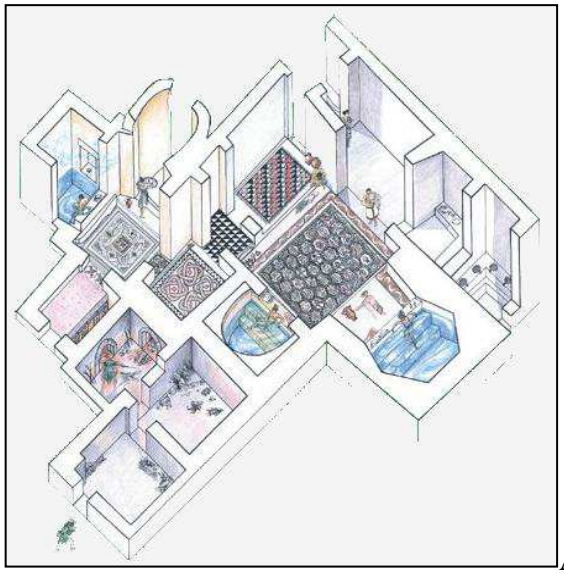

A)

B)

Fig. 4.3 - A) Ideal reconstruction of thermae. B) Relics of walls in the thermal portion of Roman villa.

The thermal baths were characterized by a complex hydraulic system that guaranteed supplying and circulation of water and its drain after use.

At the northern end of the complex there is a large cistern (fig. 4.2 - **4**) for gathering water, located in the highest point of the area to ensure proper slopes towards rooms of the villa.

The age and the causes of the manor abandonment are unknown.

The latest excavations have ascertained that in the early VI century, and perhaps already at the end of the V, the building spaces were reoccupied by a new community, with a different destination from the original.

In particular, conspicuous and prolonged metallurgic activity must have been developed in some thermal rooms (Rovina et al., 2008). In fact on the Roman mosaic-paved bottom of this thermae, excavations have exposed the remnants of a furnace consisting of a sole made up of stony slabs and tiles bound with clay, attached to a wall of Roman age.

Furthermore, several holes accommodating poles, which might have sustained a provisional cover or precarious walls as a shield for the bellows, have been discovered.

In this sector of the villa, evidence of the works is apparent in both the ground surface, where ash, slag, and burnt remnants are plentiful, and the accumulation layers, particularly those close to the furnace.

On the slags recovered in the site were carried out analyzes that have allowed to identify the probable supply areas of raw materials (Mameli et al., 2008).

The original plan was modified and the spaces that had been once used for a particular function later served different functions.

In the cruciform building the original plan was modified, some access points were closed, while others were open, by changing substantially the internal space of the rooms.

The disused cistern of Roman period was cleaned up by the collapse of the walls and converted into a burial place (fig. 4.4A), where four tombs were built with square blocks and mortar, and it were covered by large slabs of local sandstone (fig. 4.4B).

Following the cessation of metallurgic activity, cruciform building was still busy for residential use, as was witnessed by overlapping beaten floors with hearths and remains of food above the layers related to the furnace.

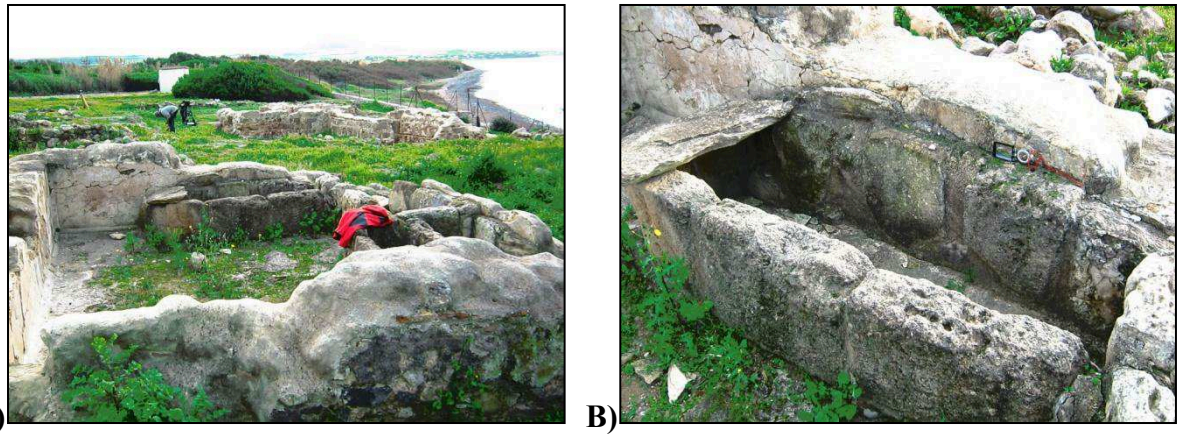

Fig. 4.4 - A) Roman cistern converted into a burial place with four tombs. B) Detail of tomb.

Between the VI century and the VII century, the whole complex of the villa was abandoned and almost completely submerged by alluvial fillings. They have raised the ground surface more than one meter and a half in the area close to the sea.

On this new surface another inhabited of Byzantine period has been constructed, the remains of which were only partially highlighted by the excavations (fig. 4.2).

The village was made up of terraced houses arranged around the cruciform thermal building which was roofless and filled by sediments and used as a burial place.

The houses consist of a single room with rectangular shape, built with dry stone walls and large blocks of reusing of the Roman villa (fig. 4.5 A-B). The beaten floors were made by clay or sand and the roofs were probably built with straw and branches.

A)  **B)** 

Fig. 4.5 - Byzantine remains with quadrangular shape and built with dry stone walls.

4.3 - Geological setting

The Santa Filitica archaeological complex lies in the north-eastern Turritano coastal plain (Federici et al., 1987).

This plain consist of a narrow flat-land, which lies in 20 km long strip parallel to the coast-line, and of a NW gently dipping surface, eastward and southward edged by weak relief, which never exceed 400m above sea level.

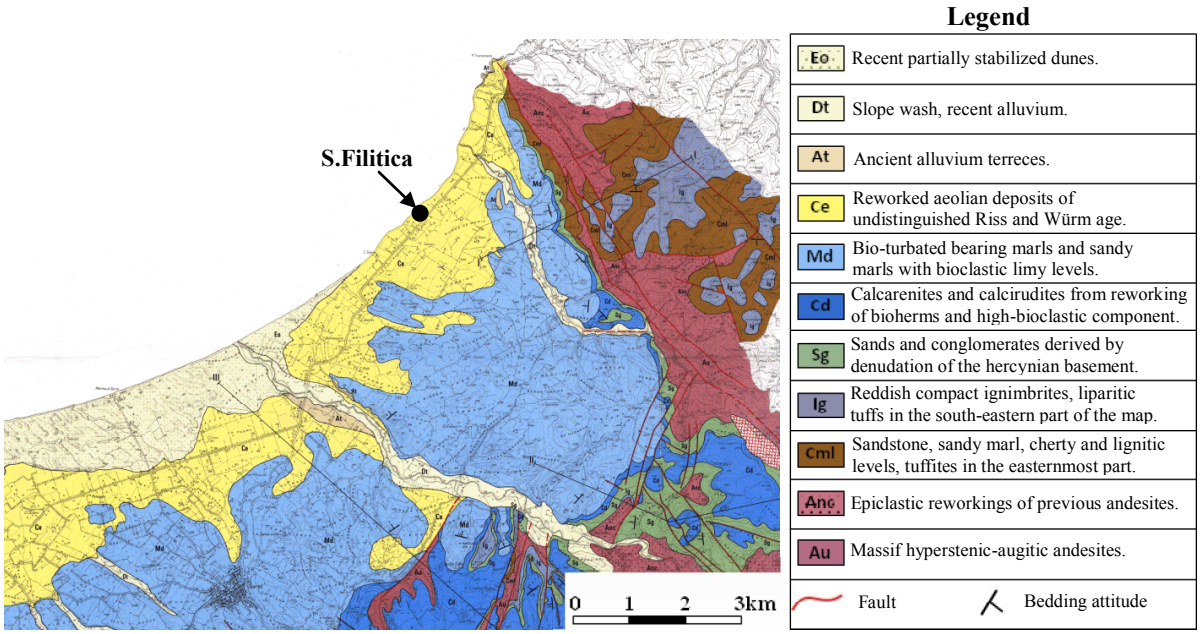

Fig. 4.6 - Geological map of the area around the archaeological site (from Oggiano, 1987 - mod.).

The oldest lithologies outcropping in the area are volcanites of the Oligo-Miocene calcalkaline cycle, these are hyperstenic-augitic andesites (**Au**) well exposed in the structural highs just to the east and south of the site (fig. 4.6).

Above the andesites rests a sedimentary arenaceous marly-tuffitic of Acquitanian age it consist of:

a) yellowish arenaceous marly as a sequence with siliciclasts of muscovite, rich in quartz and plagioclase;

b) dark-gray micaceous marls rich in carbonaceous remains and layers of black chert;

c) quartz-feldspathic tuffites and sandstones (with Gasteropoda, Lamellibranchia, planktonic Foraminifera and Pectinids) (**Cml**).

This arenaceous marly-tuffitic sedimentary sequence is topped, with erosive contact, by red-purple ignimbritic flows with rhyodacitic composition (**Ig**).

The sedimentary deposits associated with Upper Burdigalian transgression overlaps the ignimbritic flow and consist of:

- Coarse sands and conglomerates (**Sg**), the sands have a quartz-feldspar composition, while the conglomerates are made of granitic or high-grade metamorphic pebbles. The rocks derived from reworked of Hercynian basement of the Gallura district.
- Calcarenites and calciruditi (**Cd**) resulting from reworked of hermatipic body with silicoclastic and marine fossils-rich.
- Marly-arenaceous sediments consisting of yellowish gray marls, strongly bioturbated and intercalated with marly limestones with high bioclastic component (**Md**).

The part of the plain near the coast-line is occupied by Quaternary deposits overlying the Burdigalian transgressive sediments. The main aeolian deposits (**Ce**) have been recognized: the oldest belonging to Riss time, the second to the Würm time and finally a Holocenic not yet planated dunas field (parabolic, longitudinal, hock-shaped dunas types).

Embedded between the Rissian and Würmian aeolianites a Tyrrenian episode marked by a beach rock "panchina" less extended deposit is represented by lacustrine to brackish environment limestone lying behind the old Tyrrenian coastal barrier.

The settlement lies on reworked aeolian deposits which rest on the Miocene

The structuring of Turritano area is closely related to the Neogene Tectonics. A distensive movement generated a NNW trending asymmetrical graben, inward a more wide one of Oligocene age and with a NS trend.

This distensive event has generated the NW-SE trending normal fault delimiting the eastern edge of semigraben which form the Porto Torres basin (Funedda et al., 2000).

4.4 - GPR survey

The electromagnetic surveys were conducted in reflection mode using a monostatic GPR (Ground Penetrating Radar) IDS model "RIS_MF_HiMod", composed of a control unit (DAD Control Unit Fast Wave) working simultaneously with two transmitters (Tx) 200 and 600 MHz and two receivers (Rx) (par. 2.2).

The electromagnetic data were acquired by 84 transverse (T) and 150 longitudinal (L) lines with 0,5m spacing in order to build 4 different irregular grids (fig. 4.7). The grids, located in function of the obstacles on the ground, cover a total area of about 900 m^2. The extremes of the investigated areas were spatially located using a GPS "Leica^{TM} Viva".

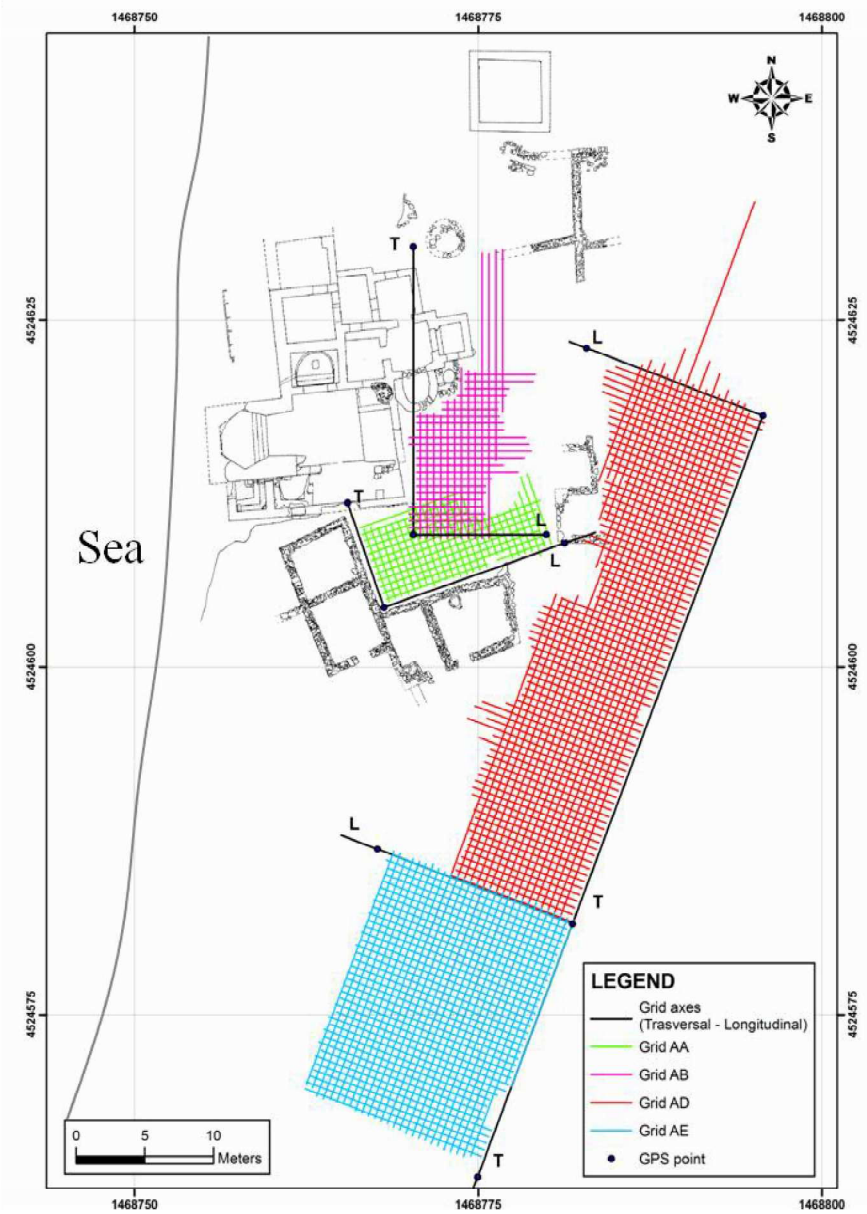

Fig. 4.7 - Site plan including GPR surveys location.

4.4.1 - Data processing and interpretation: B-scan

The GPR data files were exported to computer and analyzed in 2D GRED Basic v. 02.01.008 software.

The data were processed means of a conventional signal processing procedure consisting of the following steps: "Move start time"; "Background removal", "Vertical band pass filter", "Horizontal band pass filter" and "Gain adjustments" (smoothed gain) (GRED, 2008) described in paragraph 2.3.

By filtering of electromagnetic data acquired both 200 and 600 MHz antennas, 488 radargrams (B-scan) were obtained and from their analysis can distinguish two levels:

- the first shallow level extends from the surface down to a depth of approx. 1,5m and shows anomalies attributable at different man-made structures. In fact, can be recognize the individual targets with hyperbolic shape which identify transversal buried walls and elongated targets which identify continuous walls or close together walls arranged in a chaotic form as collapsed structures.
- the second deepest level shows a strong attenuation of EM waves, probably due to high moisture conditions that do not allow recognizing any targets, and the signal-to-noise ratio results to low to give any information.

Figure 4.8 shows some transverse and longitudinal representative B-scans of the the work area.

In radargrams **A** and **B** can be observed at x-intervals [3, 4] m, the semi-hyperbolas, with vertices located approximately at *x=3,20m* and *x=3,60m* respectively. These reflectors are marked with red rectangular areas and are produced by diffraction of the transversal walls where appreciable contrast occur.

Low intensity areas around the walls are due to relatively weak or no appreciable reflections. In general, interfaces with simpler geometries and more contrasting transitions between both media produce more intense reflections, whereas uneven and low contrasting interfaces usually produce more complex and weak reflections. Uneven boundaries or smooth transitions could be consequences of partial collapses or mixing of walls and surrounding materials.

It can be noted the presence of some continuous quasi-horizontal reflectors, as from (x, y)=(1.5, 0.5) to (x, y)=(12, 1) in **C**-radargram and ranges from 0.2m to 0.8m in deep in **D**-radargram (fig. 4.8).

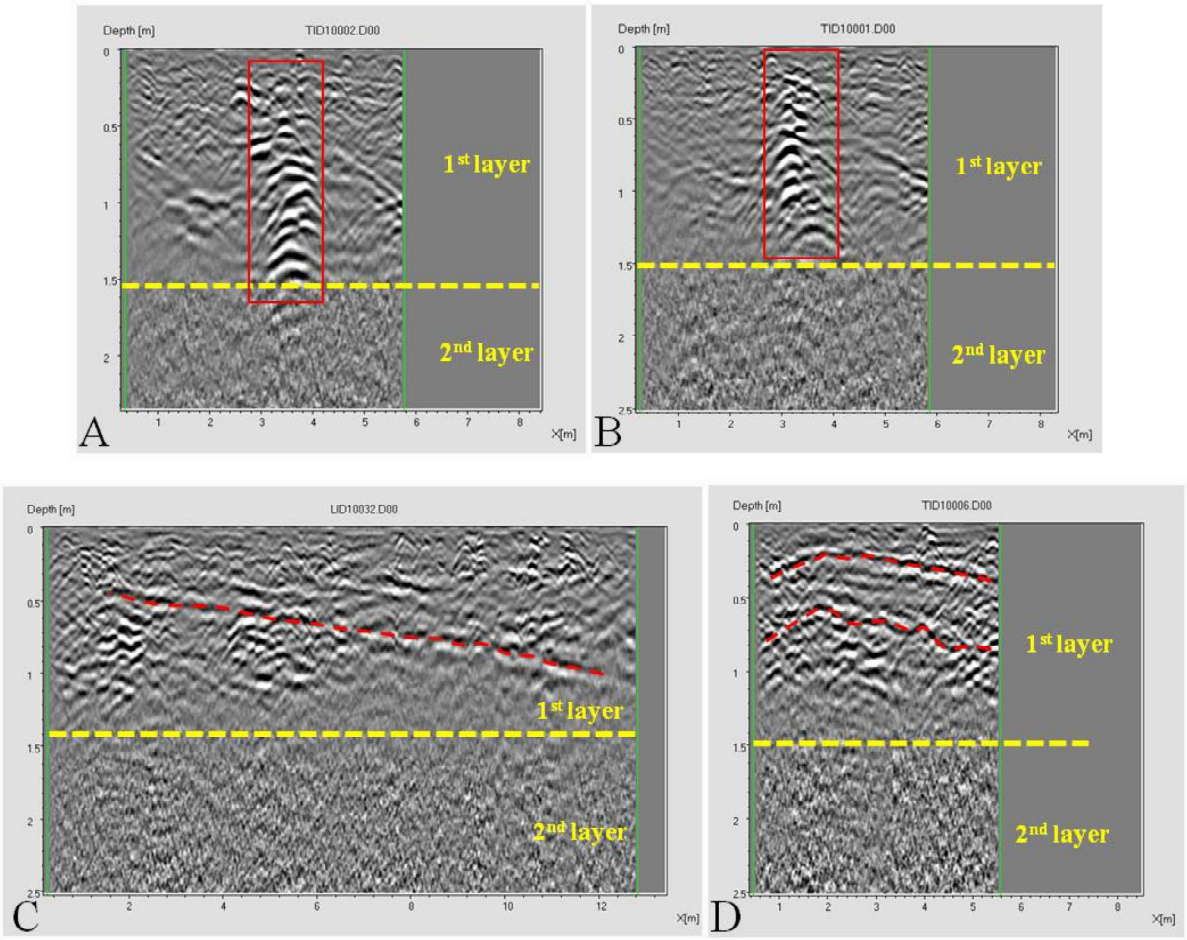

Fig. 4.8 - Radargrams which reveals different anomalies. A-B) vertical targets and C-D) longitudinal targets.

These continuous reflectors can be interpreted as buried walls parallel to the profile direction or as discontinuity surfaces. In these radargrams are present other signal patterns as small size hyperboles and poorly defined and weak reflections.

In fact, if a wall was deteriorated by erosion or by a partial collapse and if sediments of similar properties were deposited close to it, their signals could become weaker and the chaotic structures are view.

Overall, the individual anomalies (hyperbolic shape) have been detected mainly in the **AA** and **AB** grids (green and purple in colours-fig. 4.7), while a greater number of elongated anomalies have been found in the **AD** and **AE** grids (blue and red in colours-fig. 4.7).

4.4.2 - Data processing and interpretation: C-scan

The B-scans of each grid were interpolated by GRED-IDS software to obtain C-scans or radar time slices at different depths (par. 2.3).

In elaborated C-scans, frequently the signals appear blurred and distorted and don't give clear indication of the areal distribution of structures. The likely presence of the buried targets is highlighted by orange-yellow colour changes (fig.4.9).

In some cases the data interpolation has allowed to identify only the areas which is greater the density of buried structures, in others the multilayered site and the many collapses walls have caused a strong signal noise. This didn't allow the identification of structures with regular shape or the detection of preferential alignments related to any environments.

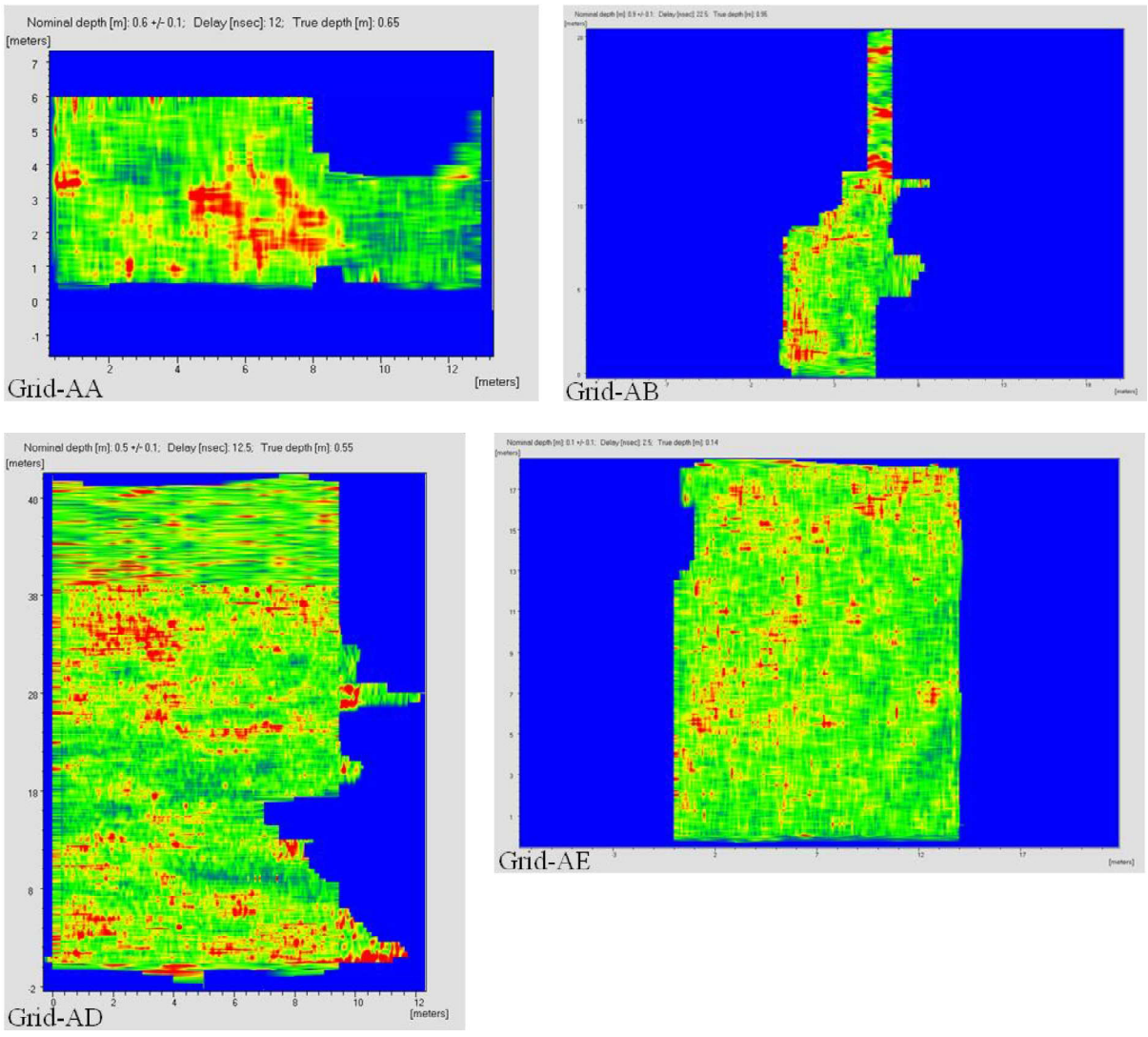

Fig. 4.9 - C-scans of different surveyed grid in the study area.

4.5 - ERT survey

The resistivity data acquisition system used in this survey was the SAS 1000 ABEM Lund Imaging System (Dahlin, 1996), combined with ES 10-64 electrode selector (par.1.4)
Electrical surveys have covered two rectangular areas at to the east (SFA) and the south (SFB) of the current limits of excavation (fig 4.10).
The SFA area (measuring 31,5 x 9m) was investigated by a set of 10 parallel 2D electrical lines, while SFB area (measuring 31,5 x 7m) was investigated by a set of 8 parallel 2D electrical lines. For both surveys an inter-line spacing of 1m was adopted.
For each 2D electrical line, 64 stainless steel electrodes were deployed in a straight line with constant spacing of 50 cm and a unit length of 31,5 m. The measurements were carried out using Dipole-Dipole array, sensitive to horizontal changes in resistivity and thus suitable for detecting vertical structures like walls and cavities.

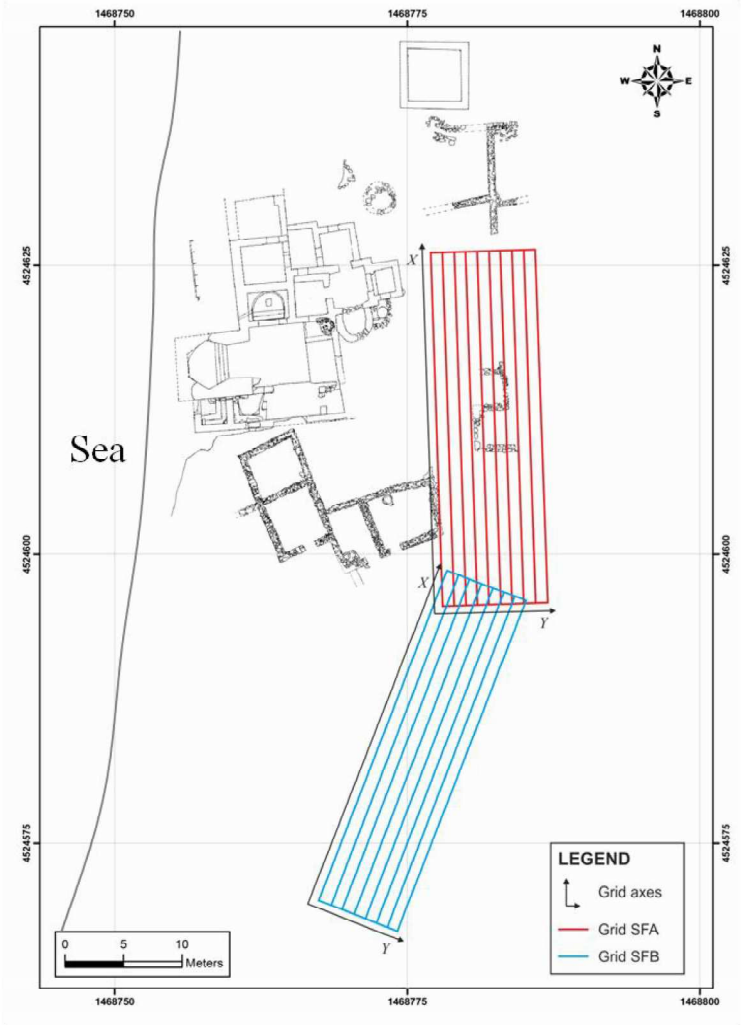

Fig. 4.10 - Site plan including electrical resistivity surveys position. Red lines indicate 2D ERT of SFA grid, while blue lines show 2D ERT of SFB grid.

4.5.1 - 2D electrical data processing and interpretation

The data from each 2D survey line was initially inverted independently by the RES2DINV software (Geotomo software) to give 2D cross-sections (Loke and Barker, 1996a).

The forward problem was solved using the finite-element method (Silvester and Ferrari, 1990), in which node positions were adjusted to allow topography to be taken into account in the inversion process.

Before performing the inversion process all resistivity data were examined and the "bad data points" were manually removed.

All 2D apparent resistivity data were inverted with the l_1-*norm* implementation (robust-constrained) of the regularized least-squares optimization method and a finer model with a cells width of half the minimum electrode spacing was used.

The identical colours scale was chosen to represent all resistivity models and the inversion results are shown in figures 4.11 (SFA lines) - 4.12 (SFB lines) and appendix B.

For lines of both areas, a good convergence between the observed and model resistivity data was achieved after 4-5 iterations as indicated by an RMS error lower than 4% for all the profiles.

In all lines can be discriminated a more superficial level characterized by anomalies ascribable to archaeological structures. These anomalies can be clearly distinguished from the surrounding soil by means of resistivity contrasts.

The archaeological targets have resistivity values higher than 75 Ω·m (fig. 4.11, red-purple in colours), while the resistivity of the surrounding soils is much lower than 75 Ω·m (green-blue in colours).

The level containing the resistive anomalies (layer 1) in SFA area is found from the ground surface to at approx. 2m in deep, while it reached greater depths (about 3m) in SFB area.

The conductive deeper level (layer 2) does not show man-made structures and it extends from the base of layer 1 to the maximum investigation depth.

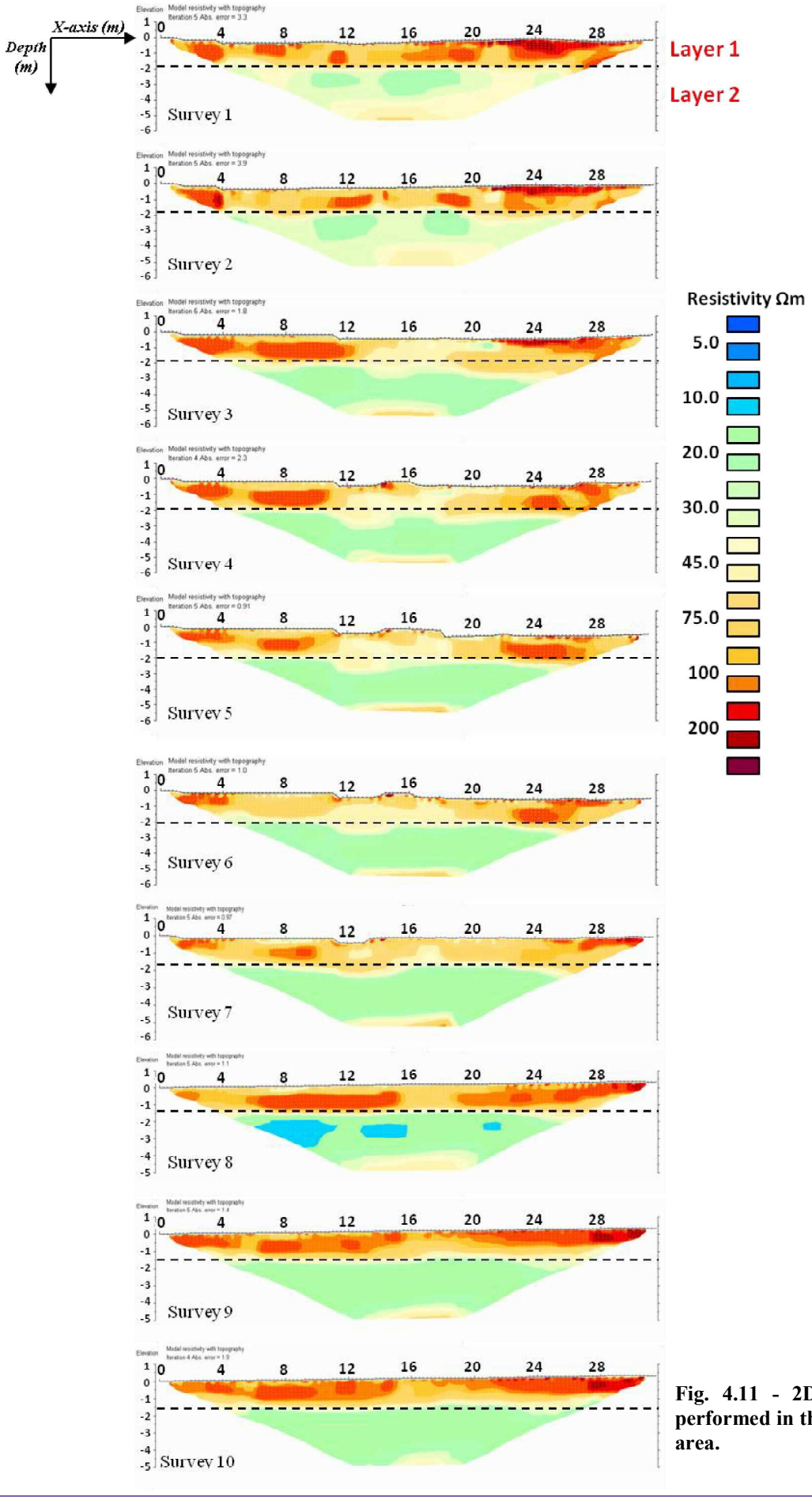

Fig. 4.11 - 2D ERT performed in the SFA area.

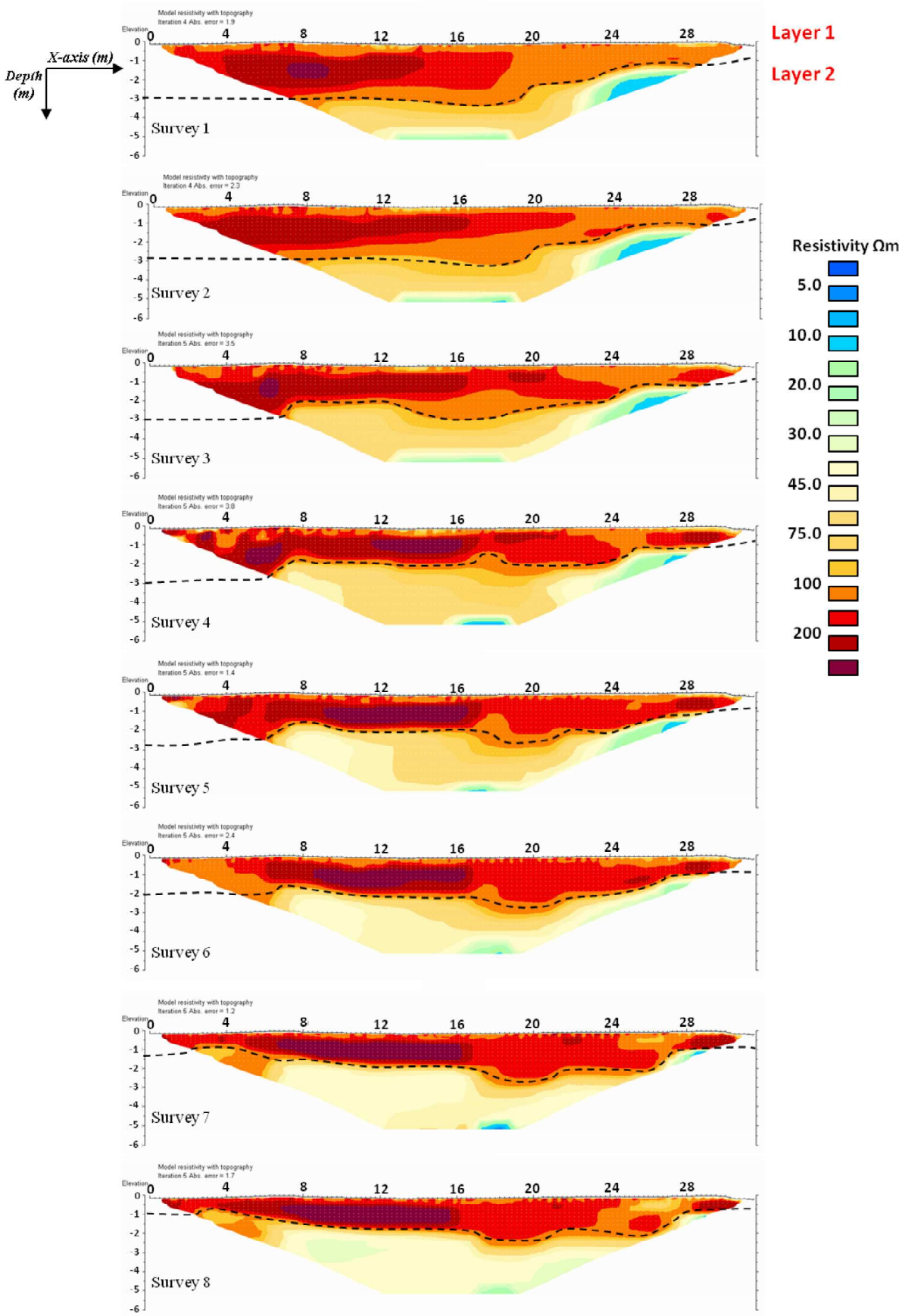

Fig. 4.12 - 2D ERT performed in the SFB area.

By a detailed analysis of layer 1 of the parallel 2D electrical tomographies (S-N oriented) in SFA area, both individual signals and continuous signals oriented along x-axis have been identified (fig. 4.11).

The individual signals, with regular shape, probably represent the walls arranged perpendicular to data acquisition lines. For example, the signals can be clearly distinguished in survey 1 at x-intervals [2 - 4]m; [6 - 8]m; [11 - 12]m and present a width that varied from 0,5 to 2,5 meters.

The continuous signals suggest the presence of wall structures parallel to the data acquisition lines, in some points interrupted by likely collapses or piecing of other walls.

These signals with more or less homogeneous resistivity are found mainly in 8-9-10 surveys.

In the SFA area the alignments of transverse and longitudinal structures are identifiable, but these are often interested by overlapping and collapsing of the walls to give chaotic shapes.

The base of the anthropized level (layer 1) in the 2D parallel ERT (SW-NE oriented) of the SFB area (fig. 4.12), appears irregular and deeper than that detected in 2D ERT of the SFA area.

This level shows compact structures with high resistivity values ($\rho > 75\Omega \cdot m$).

Particularly a resistive body with values greater than 200 $\Omega \cdot m$ and elongated geometrical shape in x-direction has been detected. It extends continuously from the start of profile to station 16m (*x-axis*) in all tomographies.

This anomaly is probably due to the denser structures (walls, plans flooring) with chaotic forms and characterized by collapsing.

4.5.2 - 3D electrical data processing and interpretation

The 2D data files were rearranged by RES2DINV software to produce a single 3D data set for each investigated areas (SFA-SFB).

Data integration gave rise of two grids with different size: 64 x 10 electrodes (*x, y directions*) with 11289 data points for SFA area, and 64 x 8 electrodes (*x, y directions*) with 9014 data points for SFB area.

The collated 3D data sets were inverted using RES3DINV computer code (Loke and Barker, 1996b), which automatically produces the subsurface horizontal depth slices.

The 3D data sets were inverted using *l1-norm* implementation of the regularized least-squares optimization method, and the forward problem was solved using the finite element method (Silvester and Ferrari, 1990).

To reduce the inversion time, the Incomplete Gauss-Newton method with a convergent limit of 0,012 was used and the Jacobian matrix was recalculated for all iterations.

Initial damping factor of 0,150 was used to invert the apparent resistivity data. After each iterating process, the inversion subroutine generally reduced the damping factor used; a minimum limit of 0,010 was set to stabilize the inversion process.

Good convergence between the observed and model resistivity data was achieved after four iterations for SFA area and after six iteration for SFB area as indicated by an RMS error of 3.90% and 2.26% respectively.

Each final 3D resistivity models consist of 16 layers in the vertical directions, resulting in a total of 9072 and 7056 model cells for SFA area and SFB area respectively (fig. 4.13-4.14).

In the area SFA the horizontal depth slices, have allowed the identification of some areas in which are recognizable expected alignments both longitudinally and perpendicularly to the data acquisition lines (for example layer 3 - Depth 0.38-0.61m)

For the area SFB the horizontal depth slices showed the compact and continuous structures with higher resistivity values.

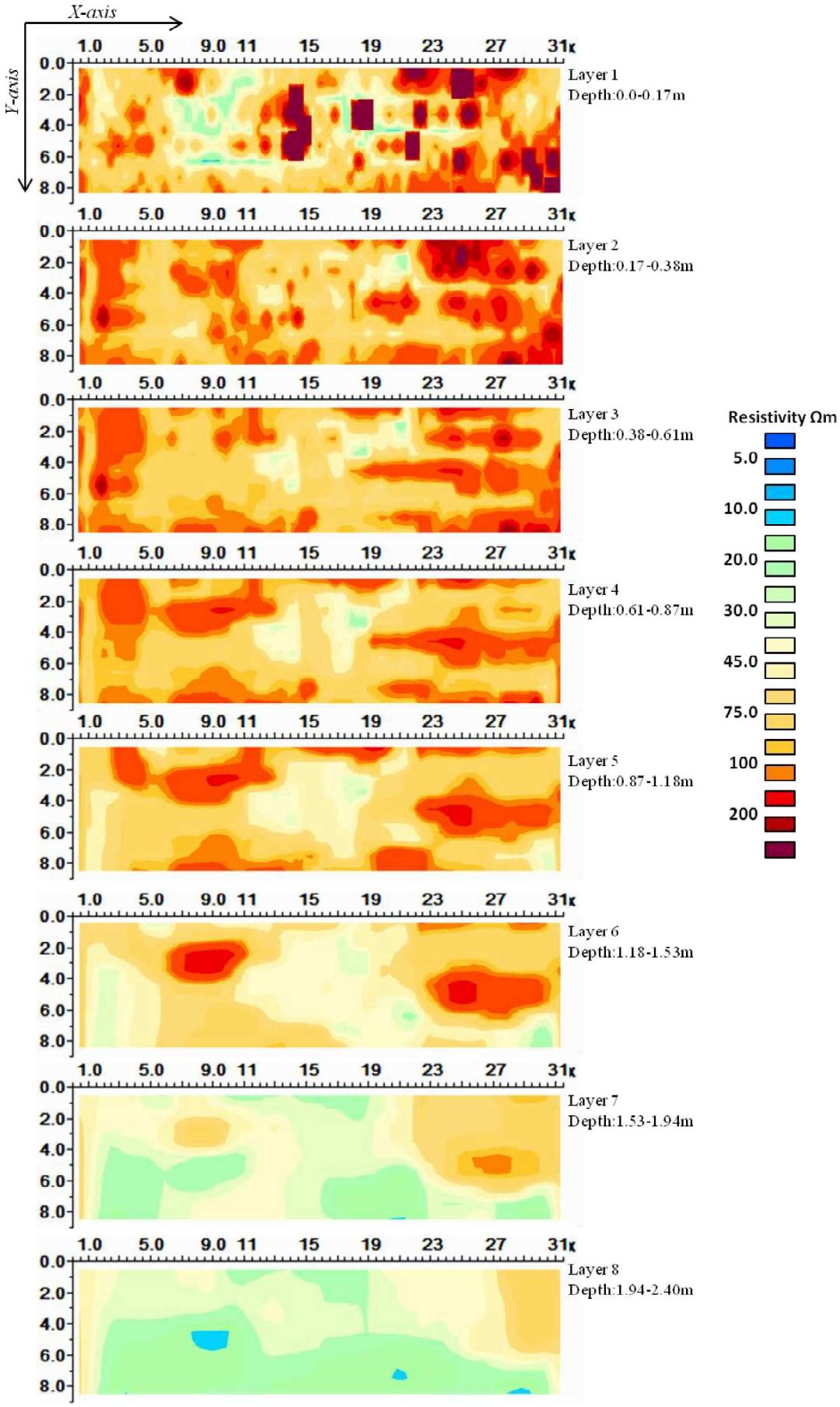

Fig. 4.13 -Horizontal depth slices after six iterations for SFA area. The RMS error is 3.90%.

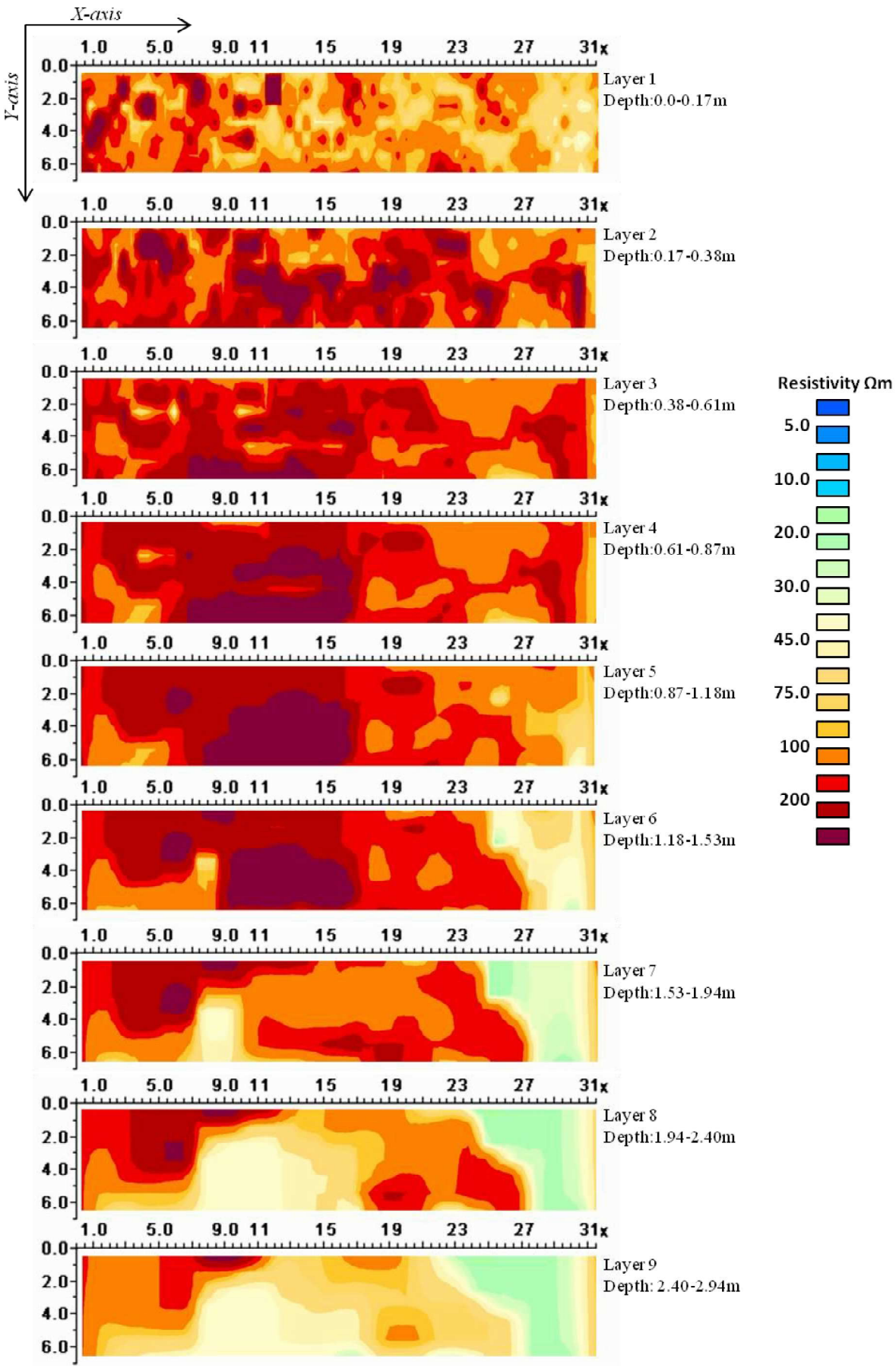

Fig. 4.14 -Horizontal depth slices after six iterations for SFB area. The RMS error is 2.26%.

The data output by RESS3DINV were also displayed in a virtual 3D space by means of Rockworks software, where have been gridded resulting in two models comprising 11424 voxels for SFA area and 10976 voxels for SFB area (fig. 4.15).

Interpolation was carried out using an inverse-distance method, by which a weighted average of the closest data point from each 90° sector around each node was calculated.

In the 3D models is clearly distinguishable the anthropized level (layer 1) from the underlying soil (layer 2) (fig. 4.15, models A-D).

With further processing were isolated the resistivity values of the archaeological buried structures and is recognizable a multilayered in the SFA area (model B).

In fact in the model C are distinguish in the shallow portions the remains of the Byzantine structures with resistivity values greater than 180 Ω·m.

Beneath Byzantine remains, the Roman structures appear more continuous to enclose the environments, in some cases with similar trend to those highlighted by the excavations.

For the area SFB in the Rockworks models we have isolated the resistivity values relating to anthropic structures and does not recognize alignments of walls (model E).

These processed models have confirmed the assumptions made for SFB area by 2D models and suggest the presence of structures with chaotic shape and rich in collapsed walls.

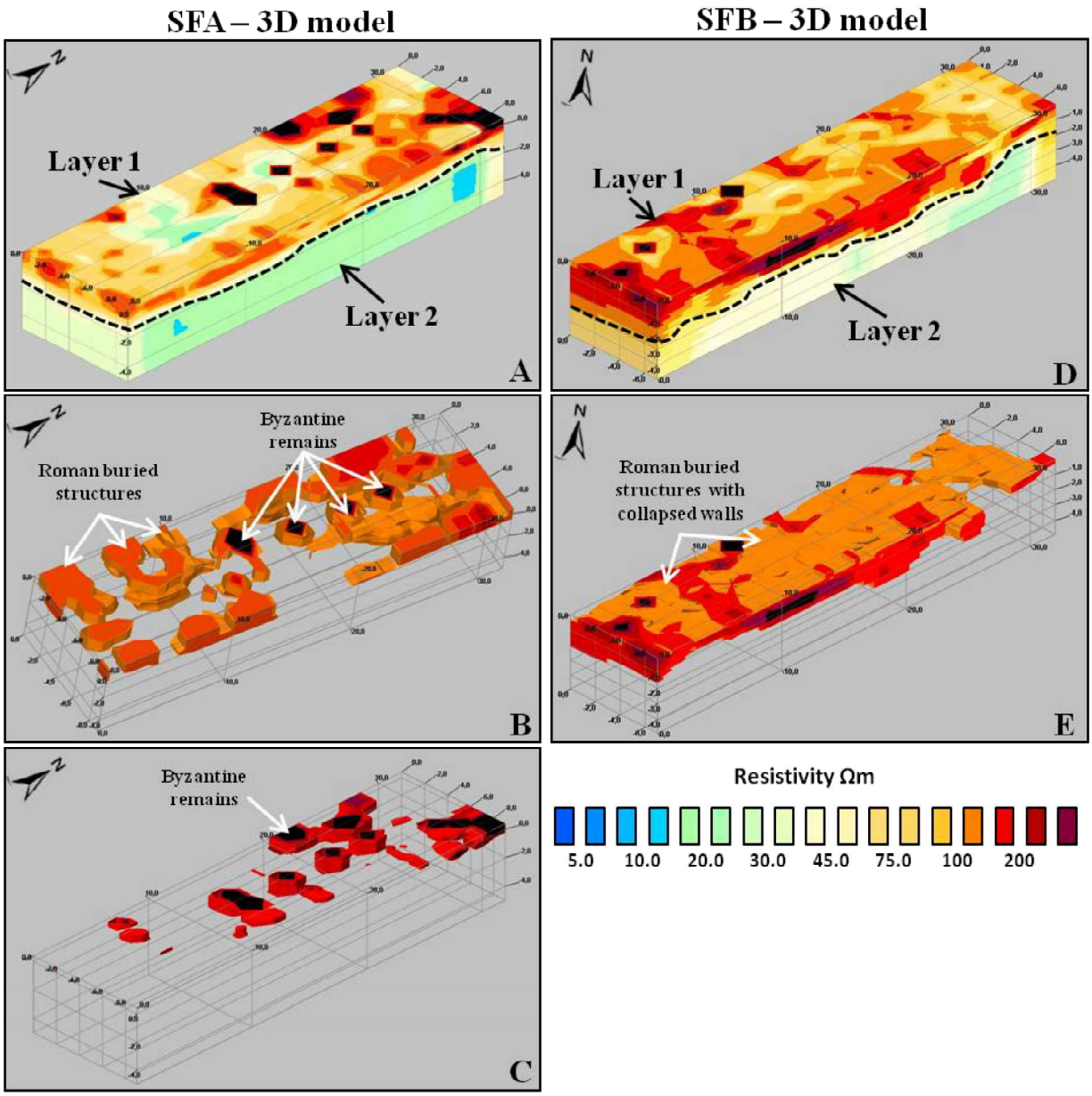

Fig. 4.15 - 3D resistivity models displayed in a 3D virtual space.

4.6 - Comparison between two different acquisition methods

Only in some cases, the 2D electrical tomographies and radargrams (B-scan), have shown a good fitting of the data, identifying precisely the same targets.

In these cases, the concordance between the two models has allowed a better definition for examined targets, reducing the intrinsic uncertainty of the indirect methods (fig. 4.16A).

Conversely, the 3D models have shown poor correlation between the identified anomalies.

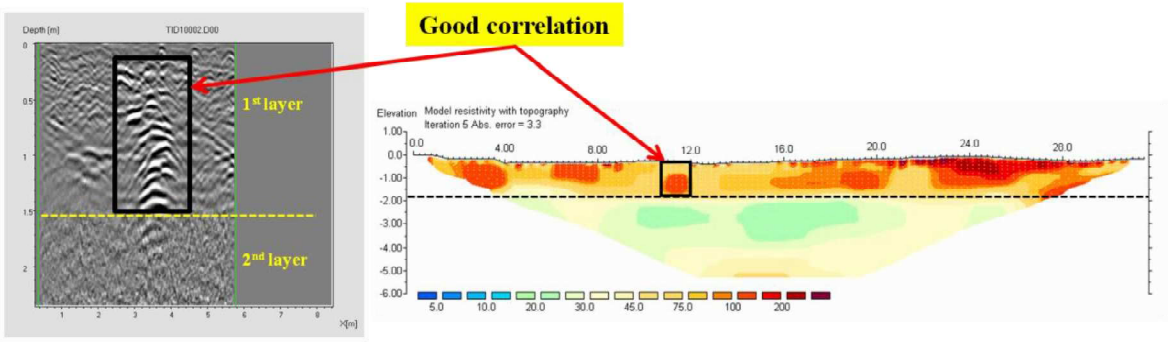

Fig. 4.16 - A) Example of good correlation between 2D electrical and electromagnetical sections. B) Example of poor correlation between electrical horizontal depth slices and C-scans.

Particularly, the C-scans have provided only information about the presence or absence of the structures in the investigated areas, while the electrical horizontal depth slices have successfully recognized some alignments of the structures (fig. 4.16B).

This is due at some characteristics of the site which negatively affected the electromagnetic method, as soil saturation and the multilayered of the archaeological structures.

Moreover, even the different investigation times and the depth reached distinguish the two geophysical methods.

With GPR method was scanned an area of about 900m^2 in three working days, while by electrical method were performed 18 tomographies, covered an area of 539.5m^2 in two weeks.

With GPR method, a good quality data were provided only for the layer 1 (1.5-2 meters in deep) due to the strong attenuation of the signal in the underlying layer, while with the ERT surveys was reached the depth of 5 meters, directly proportional to array length.

4.7 - Discussion and conclusions

The geophysical surveys, performed in the Santa Filitica archaeological complex, revealed anomalous patterns related to buried man-made structures throughout investigated area.
The layer containing the archaeological targets was distinguished with the 2D sections of both methods.
The Roman structures, later reworked in the Byzantine period, resulted in a thickening of buried structures in some areas of the site, causing a low electromagnetic contrast between targets and host alluvial sediments, thus producing a weak and confused signals in the C-scan.
Moreover, the seawater infiltrations into the deeper level have caused a high moistening, resulting in a strong attenuation of the radar waves.
Conversely, the electrical surveys have detected the alignments of structures only in the SFA area, whereas the many collapses in the SFB area yielded chaotic forms that do not allow a clear distinction of the buildings.
Only in some cases the complexity of the site allows a good fittings between the models obtained with both geophysical techniques.
Nevertheless, the integration of the two methods resulted in a comprehensive overview of the study area, otherwise not achievable with a single methodology.
Overall, the surveys provide a simple and useful tool for localize future excavations.
The plotting of the electrical horizontal depth slices on the excavation plant (for example at 0.38-0.61m in deep) allows to hypothesize the prolongation of the structures inland o the East and along to the South (fig. 4.17). In addition, some Byzantine structures were distinguished from the underlying Roman structures.

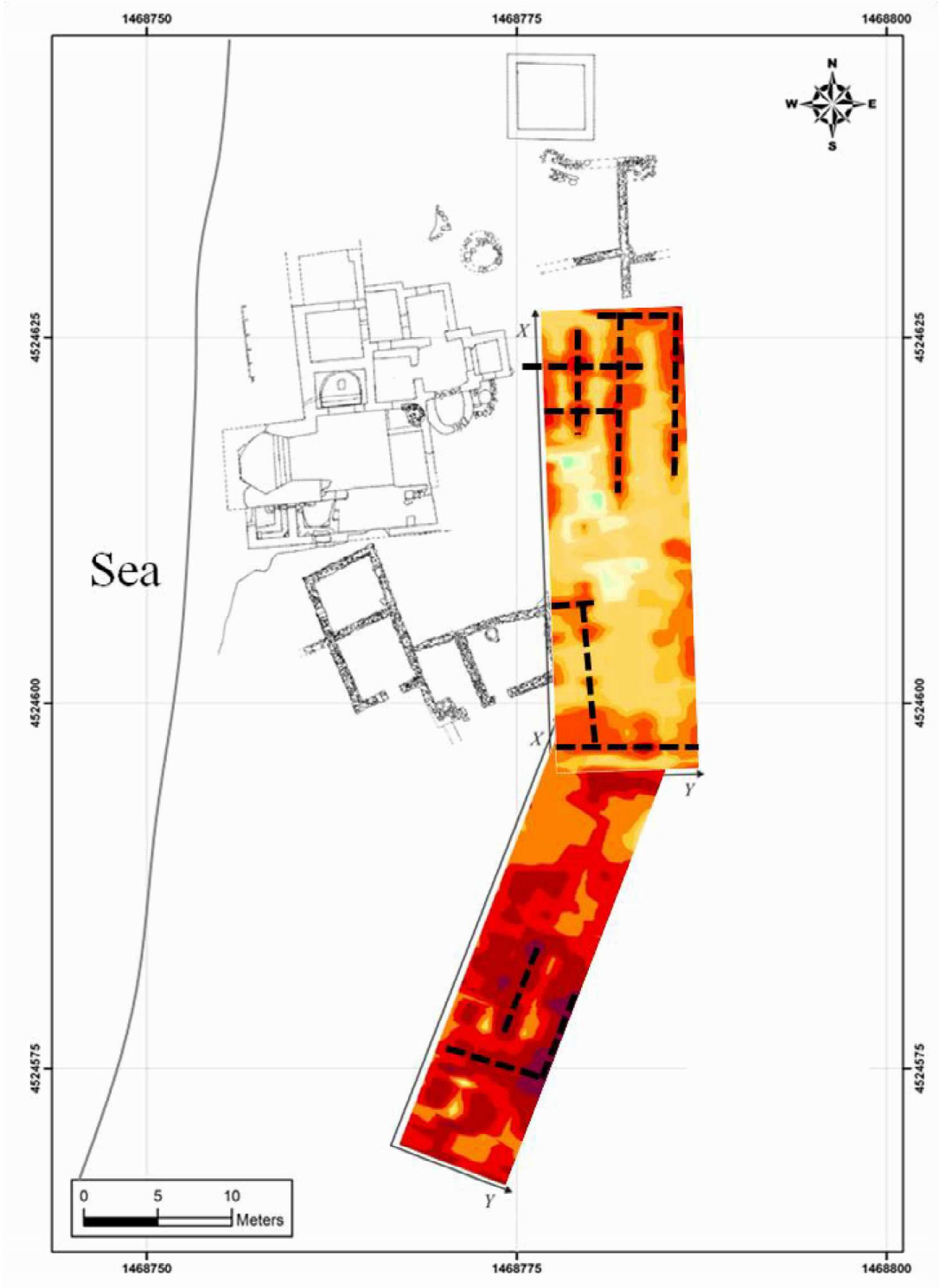

Fig. 4.17 - Electrical horizontal depth slices (depth 0.38-0.61m) for both SFA and SFB areas plotted in plant of excavation.

References

DAHLIN, T., 1996. *2D resistivity surveying for environmental and engineering applications.* First Break 14, 7, 275–283.

FEDERICI, P.R., GINESU, S., AND OGGIANO, G., 1987. *Genesi ed evoluzione della pianura costiera turritana (Sardegna Settentrionale).* Geografia Fisica e Dinamica Quaternaria, 10, 103-121.

FUNEDDA, A., OGGIANO, G., AND PASCI, S., 2000. *The Logudoro basin: a key area for the tertiary tectono-sedimentary evolution of North Sardinia*. Bollettino della Società Geologica Italiana, 119, 31-38.

GRED ver. 02.01.008, *Manuale Utente*, IDS Ingegneria dei Sistemi, Italia, 2008.

LOKE, M.H., AND BARKER, R.D., 1996a. *Rapid least-squares inversion of apparent resistivity pseudosections by a quasi-Newton method.* Geophysical Prospecting, 44, 1, 131–152.

LOKE, M.H., AND BARKER, R.D., 1996b. *Practical techniques for 3D resistivity surveys and data inversion techniques.* Geophysical Prospecting 44, 3, 499–524.

MAMELI, P., MONGELLI, G., OGGIANO, G., AND ROVINA, D., 2008. *Geochemical and textural approach to iron ore provenance of metallurgical slags: a case study from VI century settlement in North Sardinia.* Program and Abstracts 37th International Symposium on Archaeometry, Siena 12-16 Maggio 2008, 393.

OGGIANO, G., 1987. *The Turritano coastal plain, North Sardinia - Geological map.* Geografia Fisica e Dinamica Quaternaria, 10.

ROVINA, D., GARAU, E., MULLEN, G.J., DELUSSU, F., AND PANDOLFI, A., 1999. *L'insediamento altomedievale di Santa Filitica (Sorso-SS): interventi 1980-89 e campagna di scavo 1987.* Relazione Preliminare. Archeologia Medievale 26, 179-216.

ROVINA, D., 2003. *Santa Filitica a Sorso: dalla villa romana al villaggio bizantino.* Soprintendenza Archeologica per le province di Sassari e Nuoro. BetaGamma, 31.

ROVINA, D., GARAU, E., AND MAMELI, P., 2008. *Attività metallurgiche presso l'insediamento tardo antico di Santa Filitica a Sorso: dati preliminari archeologici ed archeometrici.* L'Africa Romana 17, 4, 2673-2696.

SILVESTER, P.P., AND FERRARI, R.L., 1990. *Finite elements for electrical engineers (2nd. ed.).* Cambridge University Press, 516.

Chap. 5 - Integrated geophysical methods: general considerations.

Unreliability or ambiguity of the interpretation often affect results of geophysical surveys.
The aim of this research was to compare and integrate Ground Penetrating Radar (GPR) and Electrical Resistivity Tomography (ERT) methods for detection of shallow targets in two case studies.
In this way was demonstrated as a more reliable and accurate interpretation of the data is obtained by integrating the results of these two geophysical methods, even if the ERT method has proved more performant. In detail the benefits and limitation observed for each technique are listed below:

GPR benefits:

- Non-destructive nature: in both cases the GPR investigations have not produced changes in the site features.
- Ability to maximize research efficiency: GPR surveys were conducted quickly (it has covered several hundred square meters or more in a single day) and at a relatively low cost. GPR has aided in identifying areas of high potential for future excavation, thereby maximizing data collection and minimizing time and costs.
- High-quality data: in particular in the Sant'Imbenia site, the GPR data were easily integrated with ERT data and archaeological excavation information to obtain the spatial reconstruction of the site.

GPR limitations:

- Poor definition of GPR signals below the man-made structures: the proximity of the two sites to the coast has caused a high saturation in the deepest ground levels causing a loss of definition in the GPR signals.
- Difficulty in recognizing targets in complex and multilayered archaeological contests: GPR has had difficulty in distinguishing the archeological structures when they are surrounded by a similar context. For this reason, when used on its own, GPR may be of little benefit to archaeological investigations in complex and multilayered site (S.Filitica archaeological complex).

ERT benefits:

- The method has shown a high investigation depth directly related to the array length. This allowed us to clearly define, in both cases, the depth of shallow buried man-made structures from the underlying conductive soil.
- The method has proved suitable in recognizing buried man-made relics, structural alignments and define spaces even in complex and multilayered archaeological site.

ERT limitation:

- Compared to the GPR, the ERT method is more time consuming to cover the same investigated areas.

Ringraziamenti

Un sentito ringraziamento va alla mia tutor di tesi, la Dott.ssa Paola Mameli che in questi tre anni mi ha saputo guidare offrendomi la sua professionalità e il suo sostegno.
Ringrazio il Prof. Giacomo Oggiano per i suoi preziosi consigli, il Dott. Guido Cerri, il Prof. Vincenzo Pascucci, il Dott. Leonardo Casini, il Dott. Stefano Cuccuru, il Dott. Antonio Brundu, il Dott. Antonio Puccini e tutte le persone che nel mio lavoro quotidiano all'interno del dipartimento mi hanno sostenuto.
Un ringraziamento particolare va alla Dott.ssa Daniela Rovina della Soprintendenza per i Beni Archeologici delle province di Sassari e Nuoro per i consigli e le numerose informazioni.
Inoltre ringrazio il Prof. Luigi Carmignani e i ragazzi del laboratorio di Geofisica e Geofisica Applicata e del laboratorio di Geotecnologie per l'Archeologia del Centro di GeoTecnologie di San Giovanni Valdarno dell'Università degli Studi di Siena.
Grazie a Simona, Rosa, Luigi e Bea per il sostegno e la sopportazione, soprattutto in questi ultimi mesi.

APPENDIX A

Sant'Imbenia 2D ERT

Survey 1

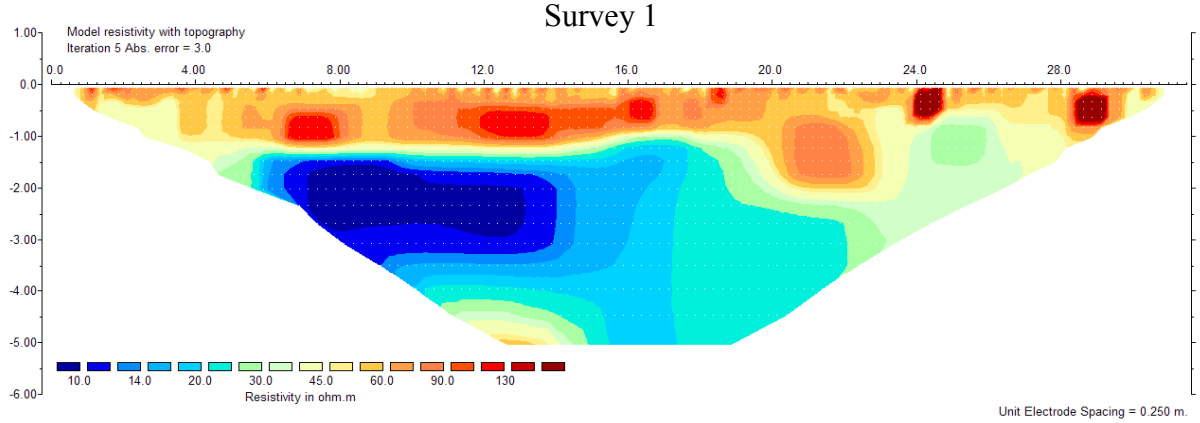

Horizontal scale is 9.52 pixels per unit spacing
Vertical exaggeration in model section display = 1.50
First electrode is located at 0.0 m.
Last electrode is located at 31.5 m.

Survey 2

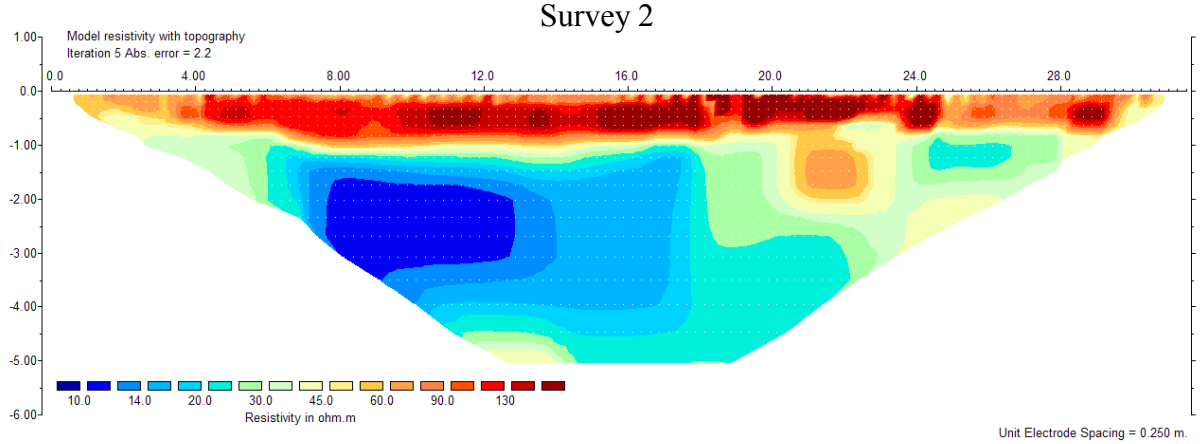

Horizontal scale is 9.52 pixels per unit spacing
Vertical exaggeration in model section display = 1.50
First electrode is located at 0.0 m.
Last electrode is located at 31.5 m.

Survey 3

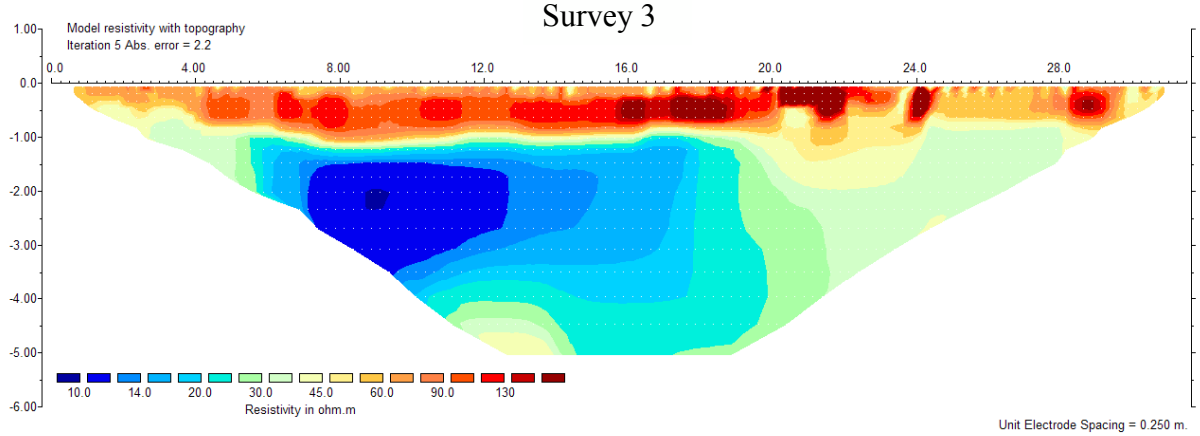

Horizontal scale is 9.52 pixels per unit spacing
Vertical exaggeration in model section display = 1.50
First electrode is located at 0.0 m.
Last electrode is located at 31.5 m.

Survey 4

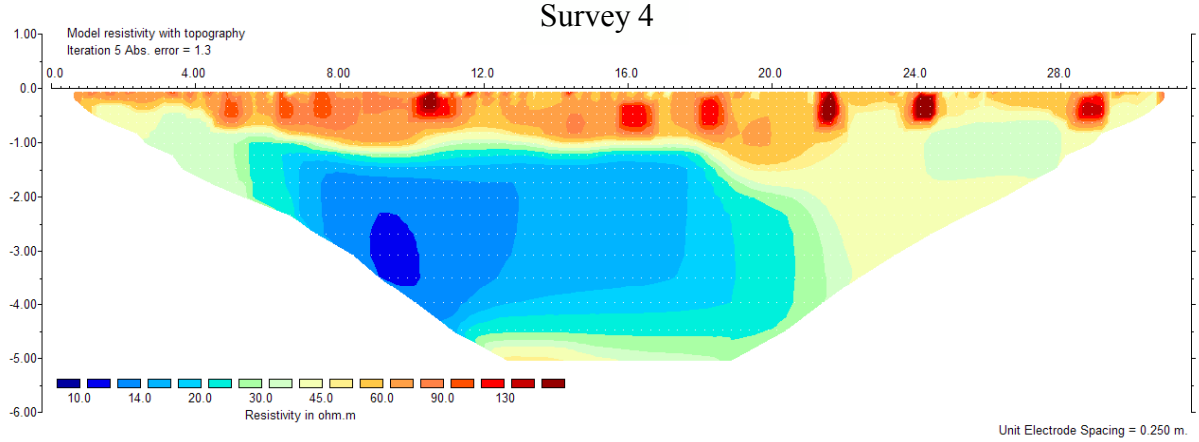

Horizontal scale is 9.52 pixels per unit spacing
Vertical exaggeration in model section display = 1.50
First electrode is located at 0.0 m.
Last electrode is located at 31.5 m.

Survey 5

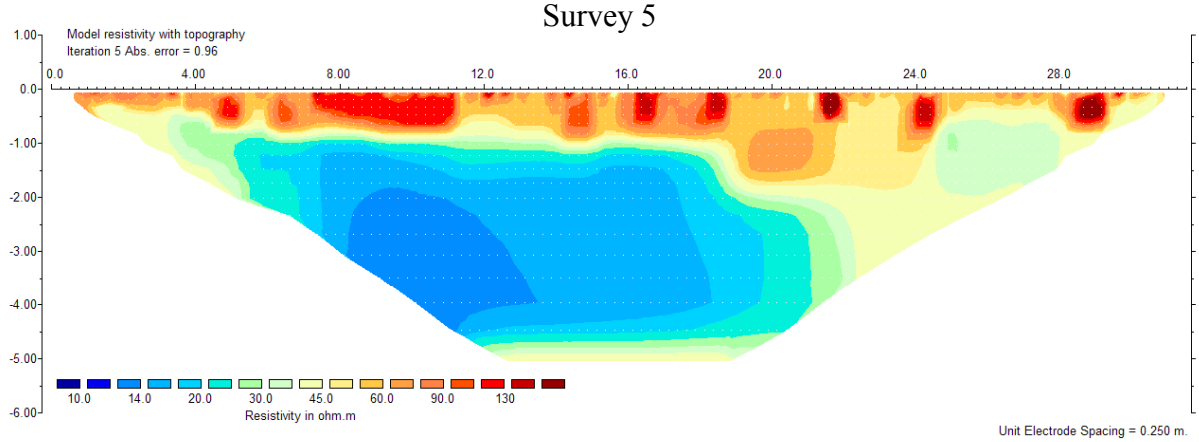

Horizontal scale is 9.52 pixels per unit spacing
Vertical exaggeration in model section display = 1.50
First electrode is located at 0.0 m.
Last electrode is located at 31.5 m.

Survey 6

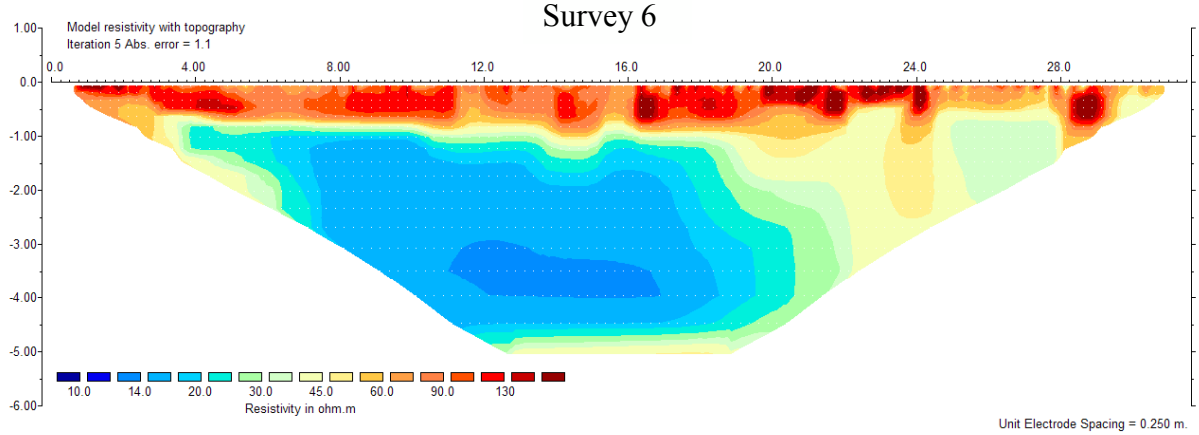

Horizontal scale is 9.52 pixels per unit spacing
Vertical exaggeration in model section display = 1.50
First electrode is located at 0.0 m.
Last electrode is located at 31.5 m.

Survey 7

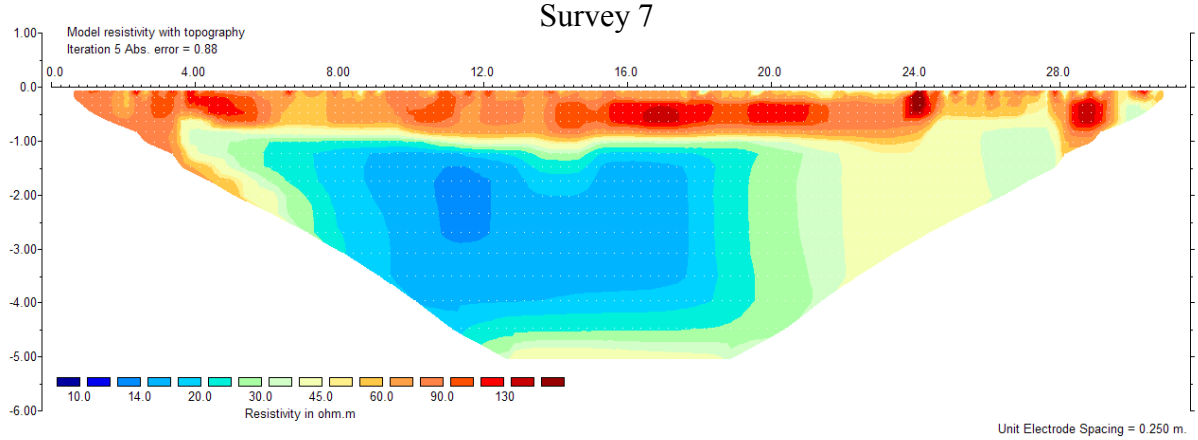

Horizontal scale is 9.52 pixels per unit spacing
Vertical exaggeration in model section display = 1.50
First electrode is located at 0.0 m.
Last electrode is located at 31.5 m.

Survey 8

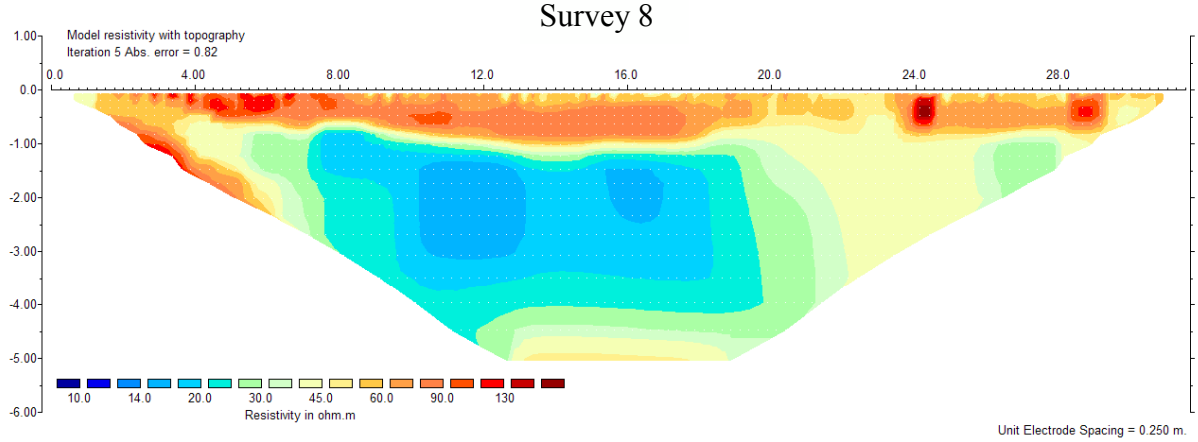

Horizontal scale is 9.52 pixels per unit spacing
Vertical exaggeration in model section display = 1.50
First electrode is located at 0.0 m.
Last electrode is located at 31.5 m.

APPENDIX B

Santa Filitica 2D ERT - SFA area

Survey 1

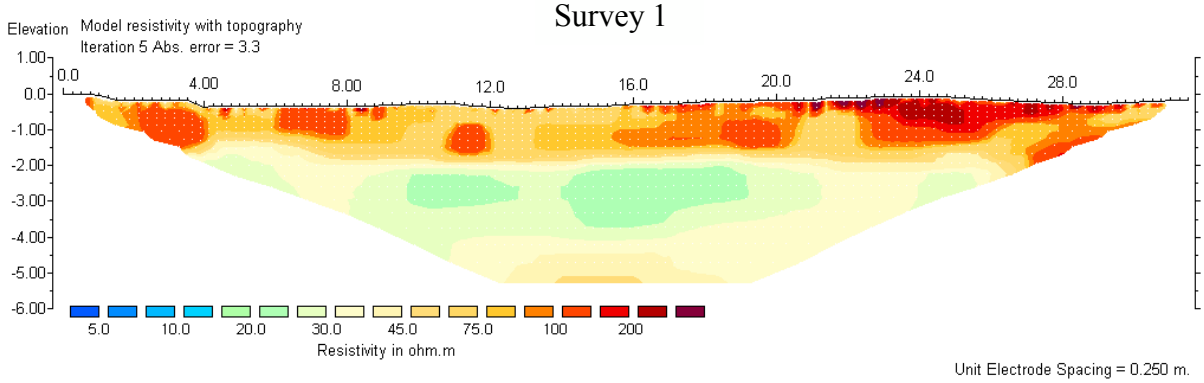

Unit Electrode Spacing = 0.250 m.

Horizontal scale is 7.57 pixels per unit spacing
Vertical exaggeration in model section display = 1.00
First electrode is located at 0.0 m.
Last electrode is located at 31.5 m.

Survey 2

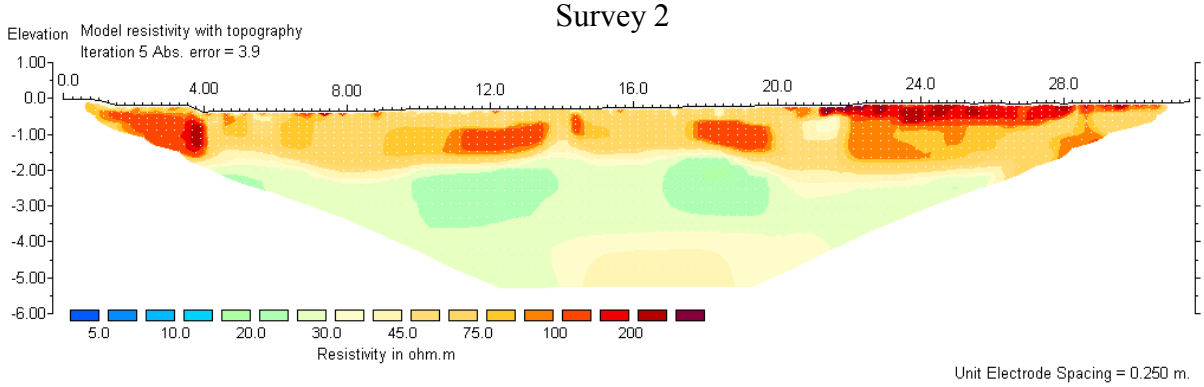

Unit Electrode Spacing = 0.250 m.

Horizontal scale is 7.57 pixels per unit spacing
Vertical exaggeration in model section display = 1.00
First electrode is located at 0.0 m.
Last electrode is located at 31.5 m.

Survey 3

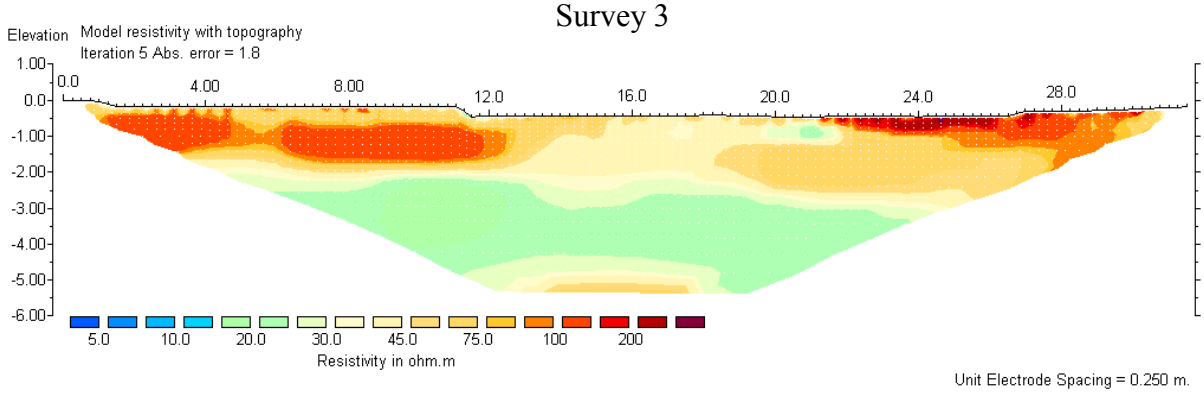

Unit Electrode Spacing = 0.250 m.

Horizontal scale is 7.57 pixels per unit spacing
Vertical exaggeration in model section display = 1.00
First electrode is located at 0.0 m.
Last electrode is located at 31.5 m.

Survey 4

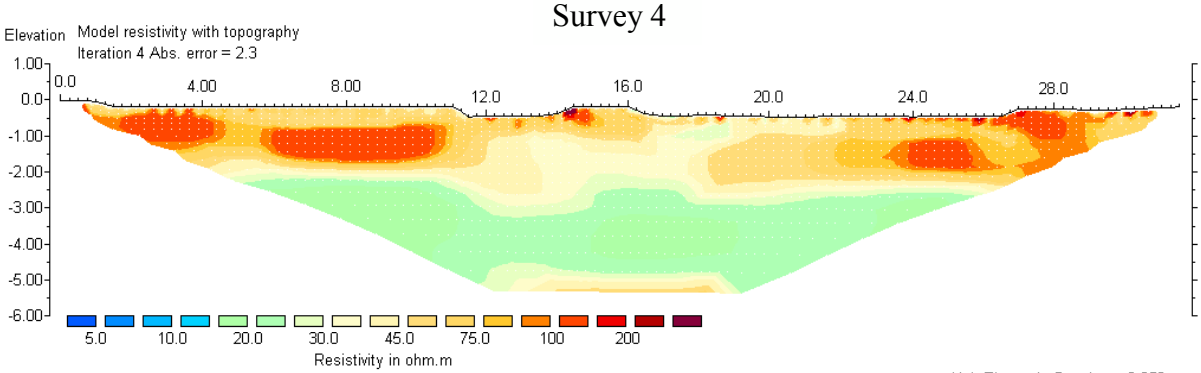

Unit Electrode Spacing = 0.250 m.

Horizontal scale is 7.57 pixels per unit spacing
Vertical exaggeration in model section display = 1.00
First electrode is located at 0.0 m.
Last electrode is located at 31.5 m.

Survey 5

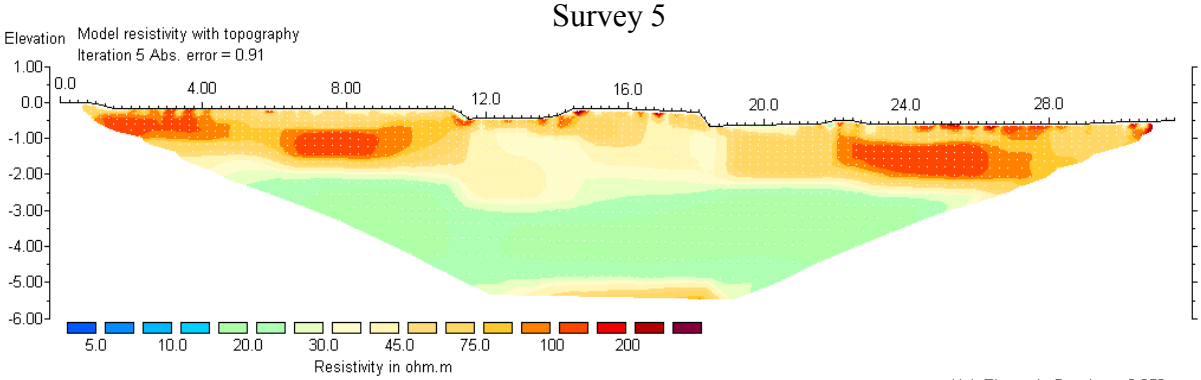

Unit Electrode Spacing = 0.250 m.

Horizontal scale is 7.57 pixels per unit spacing
Vertical exaggeration in model section display = 1.00
First electrode is located at 0.0 m.
Last electrode is located at 31.5 m.

Survey 6

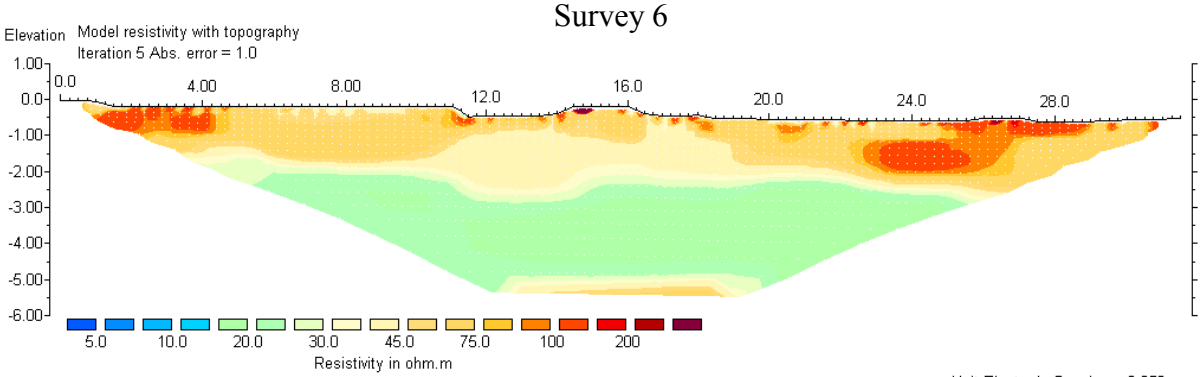

Unit Electrode Spacing = 0.250 m.

Horizontal scale is 7.57 pixels per unit spacing
Vertical exaggeration in model section display = 1.00
First electrode is located at 0.0 m.
Last electrode is located at 31.5 m.

Survey 7

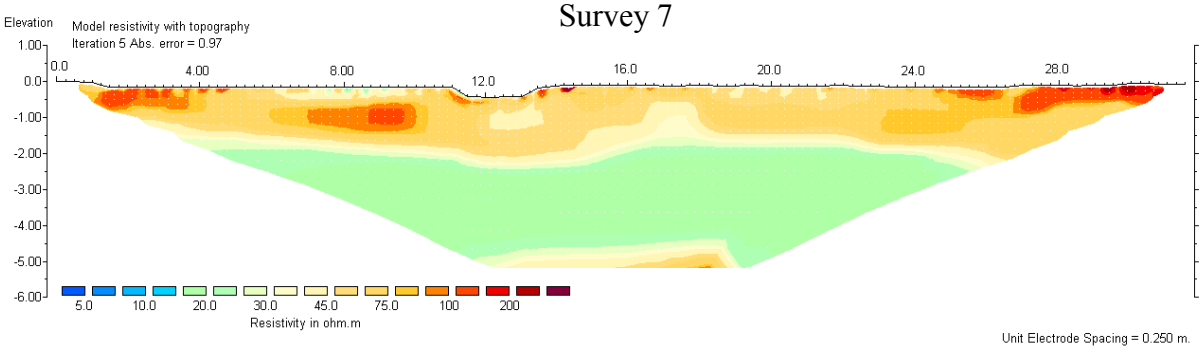

Horizontal scale is 9.52 pixels per unit spacing
Vertical exaggeration in model section display = 1.00
First electrode is located at 0.0 m.
Last electrode is located at 31.5 m.

Survey 8

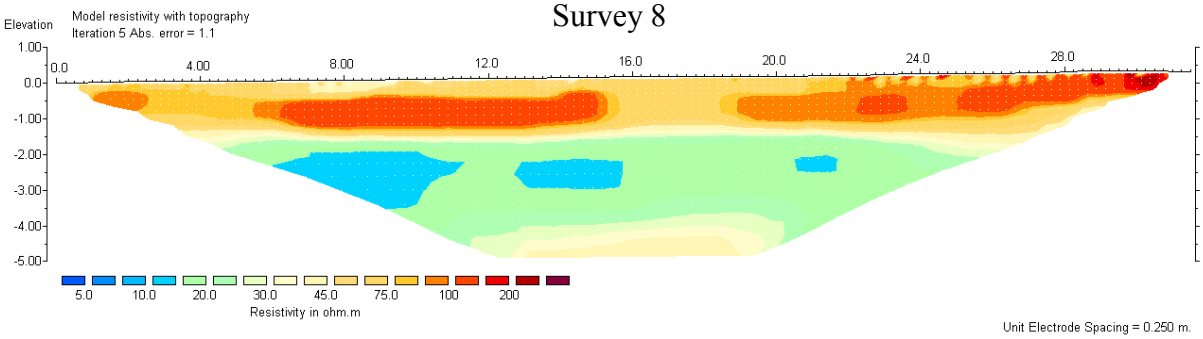

Horizontal scale is 9.52 pixels per unit spacing
Vertical exaggeration in model section display = 1.00
First electrode is located at 0.0 m.
Last electrode is located at 31.5 m.

Survey 9

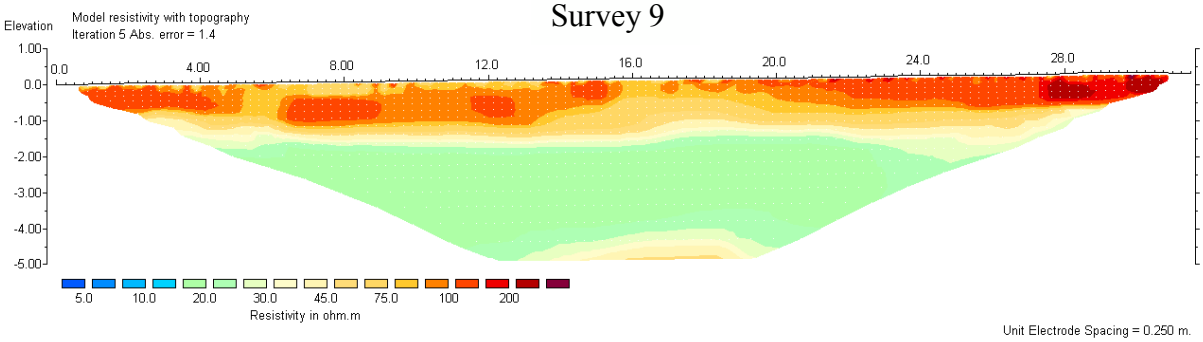

Horizontal scale is 9.52 pixels per unit spacing
Vertical exaggeration in model section display = 1.00
First electrode is located at 0.0 m.
Last electrode is located at 31.5 m.

Survey 10

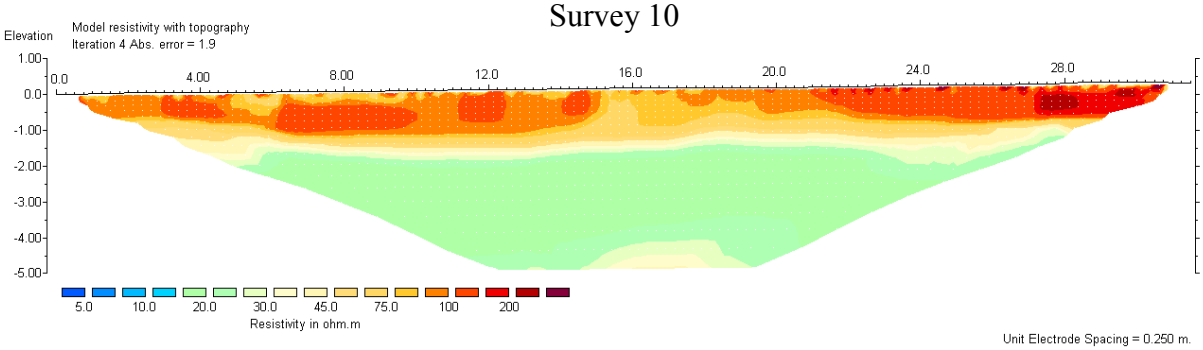

Horizontal scale is 9.52 pixels per unit spacing
Vertical exaggeration in model section display = 1.00
First electrode is located at 0.0 m.
Last electrode is located at 31.5 m.

Santa Filitica 2D ERT - SFB area

Survey 1

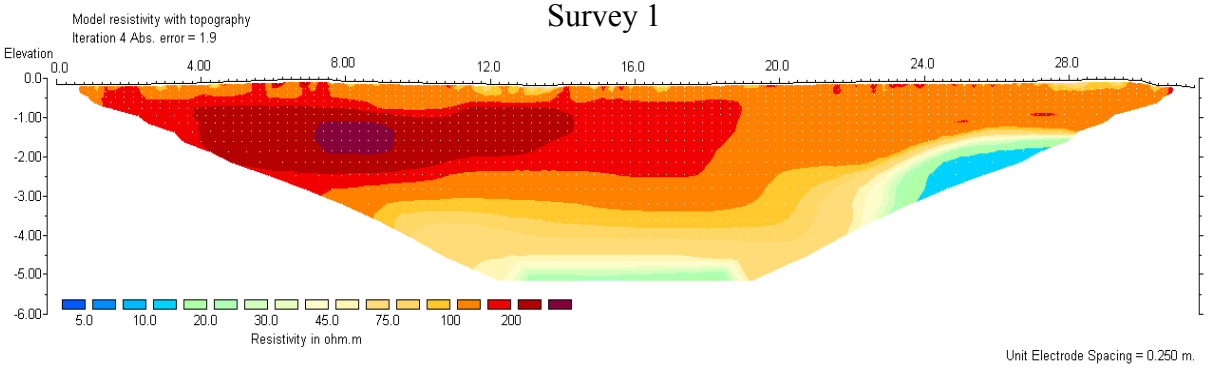

Horizontal scale is 9.52 pixels per unit spacing
Vertical exaggeration in model section display = 1.00
First electrode is located at 0.0 m.
Last electrode is located at 31.5 m.

Survey 2

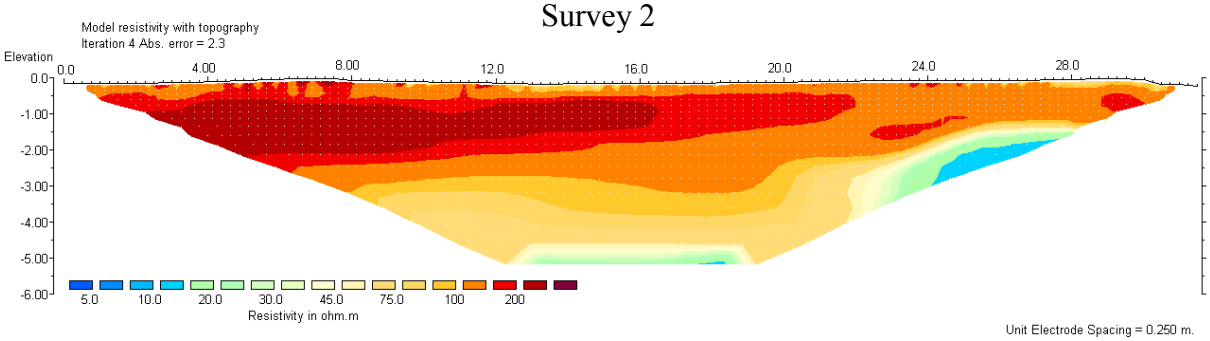

Horizontal scale is 9.52 pixels per unit spacing
Vertical exaggeration in model section display = 1.00
First electrode is located at 0.0 m.
Last electrode is located at 31.5 m.

Survey 3

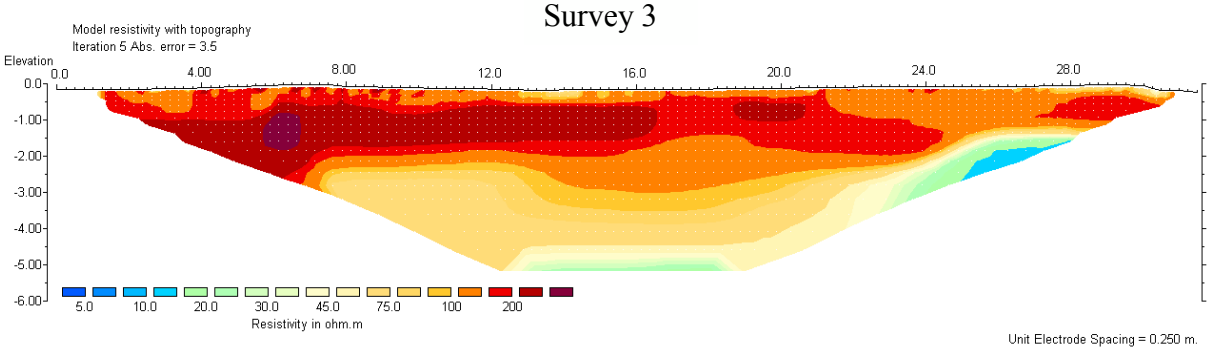

Horizontal scale is 9.52 pixels per unit spacing
Vertical exaggeration in model section display = 1.00
First electrode is located at 0.0 m.
Last electrode is located at 31.5 m.

Survey 4

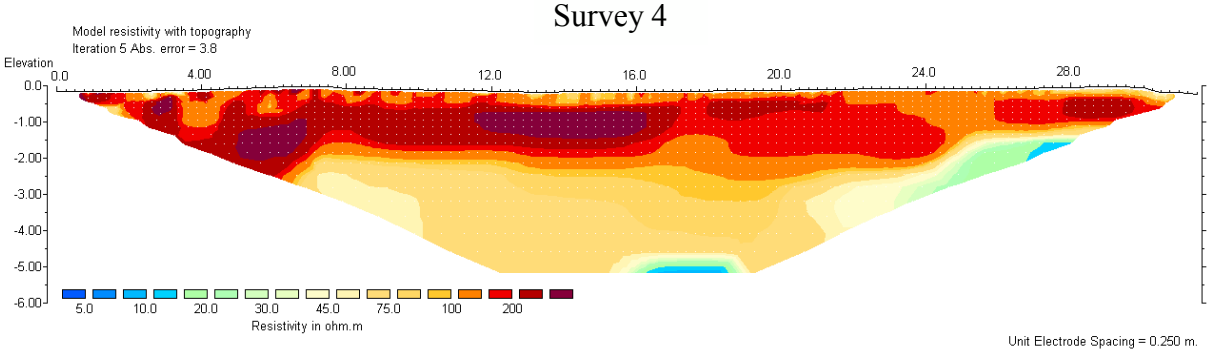

Horizontal scale is 9.52 pixels per unit spacing
Vertical exaggeration in model section display = 1.00
First electrode is located at 0.0 m.
Last electrode is located at 31.5 m.

Survey 5

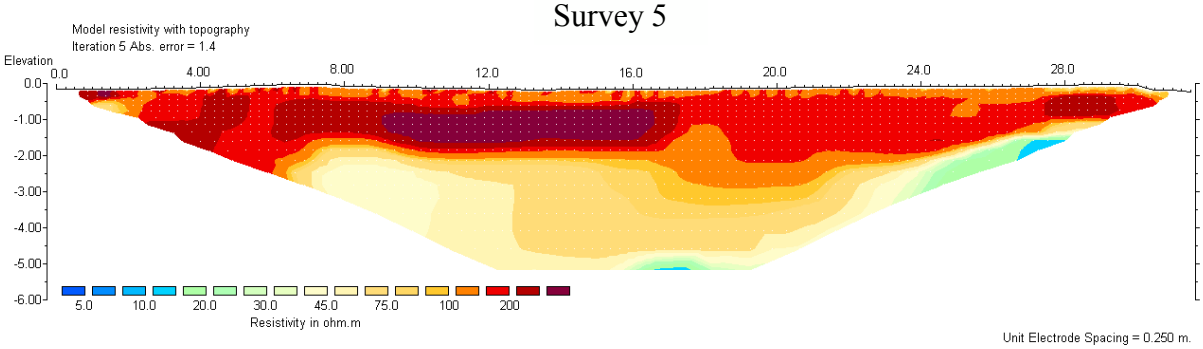

Horizontal scale is 9.52 pixels per unit spacing
Vertical exaggeration in model section display = 1.00
First electrode is located at 0.0 m.
Last electrode is located at 31.5 m.

Survey 6

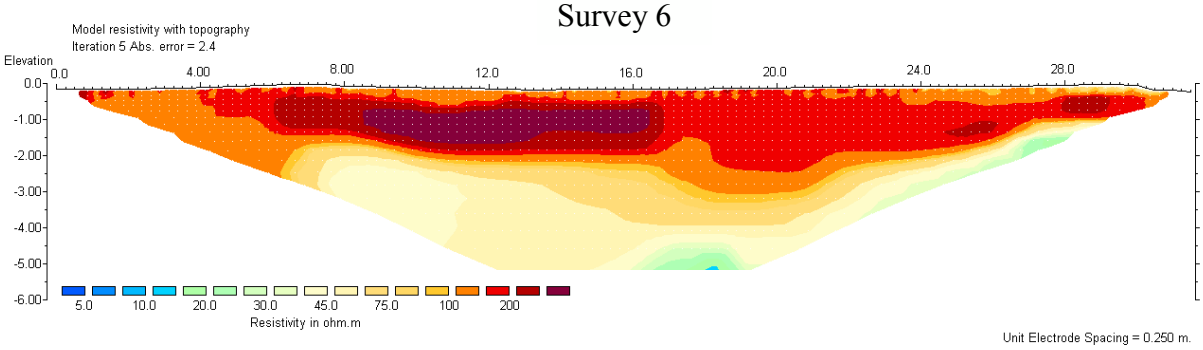

Horizontal scale is 9.52 pixels per unit spacing
Vertical exaggeration in model section display = 1.00
First electrode is located at 0.0 m.
Last electrode is located at 31.5 m.

Survey 7

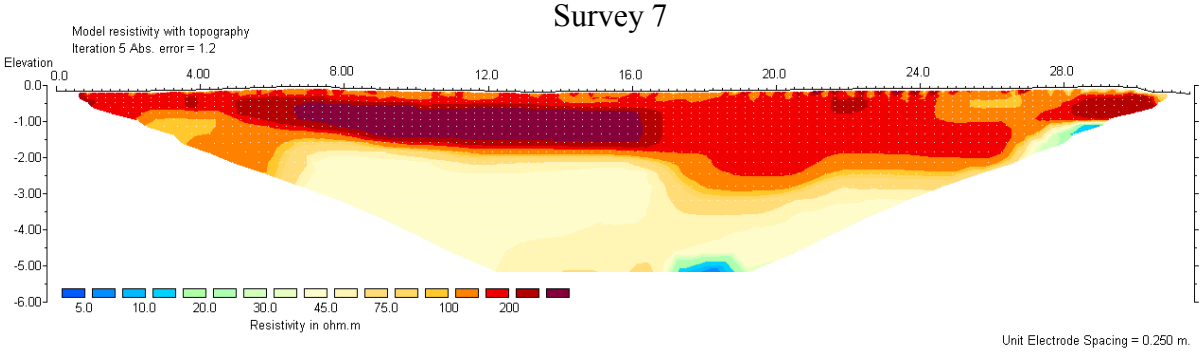

Horizontal scale is 9.52 pixels per unit spacing
Vertical exaggeration in model section display = 1.00
First electrode is located at 0.0 m.
Last electrode is located at 31.5 m.

Survey 8

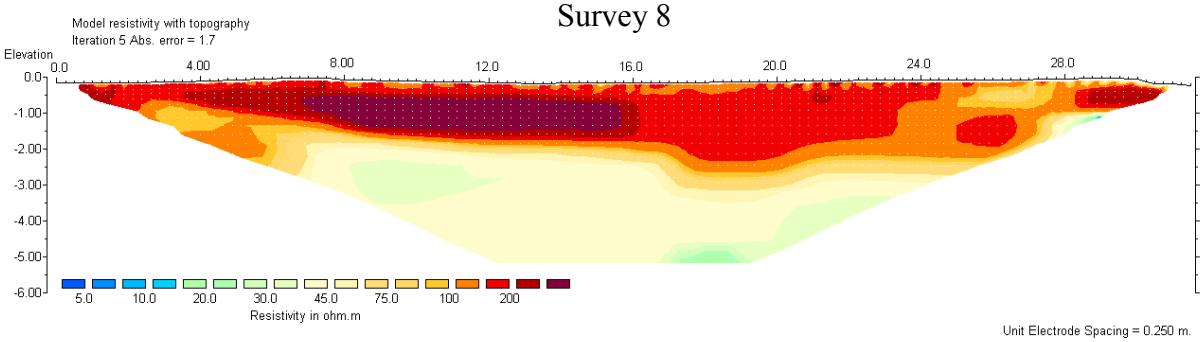

Horizontal scale is 9.52 pixels per unit spacing
Vertical exaggeration in model section display = 1.00
First electrode is located at 0.0 m.
Last electrode is located at 31.5 m.